MSc thesis in Geomatics

# Modeling tree topology effects on wind

Runnan Fu

2022

**MSc thesis in Geomatics**

# Modeling tree topology effects on wind

Runnan Fu

June 2022

A thesis submitted to the Delft University of Technology in
partial fulfillment of the requirements for the degree of Master of
Science in Geomatics

The work in this thesis was carried out in the:



3D geoinformation group
Delft University of Technology

| Supervisors: | Asst. Prof. Dr. Clara García-Sánchez |
| | Mr. Ivan Pađen |
| Co-reader: | Asst. Prof. Dr. Liangliang Nan |

# Abstract

Planting of trees is widely considered an effective way to create a good urban wind environment, to improve air quality, mitigate heat island effects, improve pedestrian wind comfort and reduce buildings energy consumption. In order to assess tree effect and find suitable tree setups in urban areas, Computational Fluid Dynamic (CFD) simulations can be used.

To handle trees in CFD simulations, the implicit tree modeling approach, i.e, porosity model, is widely used where finite volume cells that roughly account for trees are marked as porous zones. Some studies have also attempted to model trees as obstacles rather than porous zones, which can be referred to as an explicit tree modeling approach. The difference between these two approaches deserves further study. Also, for practical purposes and lack of information, the geometric features of trees are usually oversimplified or even ignored in CFD simulations.

This thesis investigates the difference between implicit and explicit tree modeling approach and analyzes the impact of tree Level of Detail (LoD) and shapes on the flow structure. For comparative analysis, several numerical test cases with different urban complexities, tree modeling approach, tree LoDs, tree shapes, Leaf Area Density (LAD) values and wind directions were used for CFD simulations.

The results show: (a) the implicit models always allow some of the wind flow into the porous cells no matter how high the LAD values are, resulting in smaller wind acceleration on the lateral sides of implicit tree models; (b) for the idealized street canyon and realistic urban geometry test cases simulated in this thesis, the velocity magnitude differences between the LoD2 cases and the LoD3 cases is rather limited, with maximum differences in the order of 0.5 m/s; (c) differences in tree shapes, LAD values and wind directions will change the effects of tree modeling approaches and tree LoDs on wind. For instance, the case using an isolated explicit LoD2 conifer tree model has a different wake flow pattern from other explicit cases. Also, with the inflow direction perpendicular to buildings, the higher the LAD values, the larger the velocity magnitude difference between cases using LoD2 tree models and those using LoD3 tree models.

# Acknowledgements

Although it is embarrassing to say this, the first person I want to thank is myself. This is the first time I have completed an English academic thesis relatively independently. I am thankful that I did not give up when I encountered difficulties and finally finished such a decent, albeit much lacking, thesis on time. In fact, before, I always thought I was not suitable for academics, and of course I dare not say I am now, but at least I have more interest and confidence. I am no longer afraid to read a lot of literature, and I am starting to feel excited about presenting my own ideas.

Of course, I couldn't have done these without the help of my TU Delft supervisors: Clara García-Sánchez and Ivan Pađen. I would like to show my appreciation to Clara for her guidance and help with all CFD and academic thesis related issues. Many thanks also to Ivan Pađen, whose academic rigor and guidance on many technical issues helped me to make further progress. I am also very grateful to Liangliang Nan, my co-reader, who provided constructive feedback. I would also like to thank Leo van den Burg for his patience in organizing several presentations. And I am also very thankful for the encouragement and praise that each of them gave me, which made me more motivated and confident.

Finally, I am very grateful to my parents who read my thesis with great enthusiasm and were very proud of me. I always feel blessed by their concern for me.

# Contents

*Contents*

# List of Figures

# List of Tables

# Acronyms

# 1. Introduction

## 1.1. Motivation

With more and more people living in urban areas, urbanisation is expanding. The rise of human activities is linked to problems such as the rising temperatures (Urban Heat Islands (UHI), specially at night) and air pollution in cities, which eventually can lead to various diseases and premature deaths [Fouillet et al., 2006; Salmond et al., 2016]. Since a good urban wind environment can ameliorate air quality, mitigate heat island effects, improve pedestrian wind comfort and reduce buildings energy consumption, this field of research is currently receiving more and more attention [Hsieh and Huang, 2016; Blocken et al., 2012].

A widely considered econonomical and effective way to create a good urban wind environment is planting of trees [Salmond et al., 2016; Aflaki et al., 2017; Szkordilisz and Zöld, 2016], as trees can affect the wind flow by reducing its speed and changing its direction [Szkordilisz and Zöld, 2016]. Yet, trees may also have a negative impact on local air quality because they reduce ventilation. It is worth noting that the dynamic effects of trees on urban wind environment depends not only on environmental factors such as the surrounding built environment, local climate and wind speed, but also on tree properties such as tree shape, height and foliage density [Hefny Salim et al., 2015; Manickathan et al., 2018]. In order to assess tree effects and find suitable tree layouts in urban areas, Computational Fluid Dynamics (CFD) simulations can be used.

To handle trees in CFD simulations, the implicit tree modeling approach, i.e, porosity model, is widely used where finite volume cells that roughly account for trees are marked as porous zones [Hefny Salim et al., 2015; Kang et al., 2020]. In these porous zones, the effect of trees is defined as a source and/or sink term in the momentum equation and turbulence equations. It can be seen that this approach oversights resolving tree structures. With the development of 3D tree reconstruction methods, some studies have also attempted to model trees as obstacles rather than porous zones in CFD simulations, which can be referred to as the explicit tree modeling approach. Basically, an explicit tree model has no wind passing through its interior, while the drag of an implicit tree model is able to be changed by adjusting the parameter values of the source/sink terms. This makes the implicit modeling approach typically used for tree canopies [Balczó et al., 2009; Kang et al., 2020; Vranckx et al., 2015; Gromke et al., 2012], while the explicit modeling approach tends to be used for tree trunks and branches [Hong et al., 2018b; Wang et al., 2021]. However, when the drag of an implicit tree model (corresponding to the LAD values in this thesis) are set very high, does the implicit model behave similarly to the explicit model? If so, can we use implicit models instead of explicit models for tree trunks, branches or even buildings in order to reduce the time spent on designing a good CFD grid/mesh? If not, what are the main differences? These questions deserve further study.

Also, for practical purposes and lack of information, the geometric features of trees are usually oversimplified or even ignored in CFD simulations of the wind flow in urban areas. Most studies use simple regular cylinders or prisms to represent trees, or assume that all trees within

the study area have the same shape. In this context, the question arises: what is the impact of different tree level of details (LoDs) and tree shapes on the wind flow structure?

This thesis investigates the difference between implicit and explicit tree modeling approaches and analyzes the impact of tree LoDs and shapes on the flow structure. For comparative analysis, several numerical test cases with different urban complexities, tree modeling approaches, tree LoDs, leaf area density (LAD) values and wind directions were used for CFD simulations.

## 1.2. Research questions

The main research question for this thesis is:
***What is the impact of tree topology modelling for urban flow simulations?***

To answer this, the following sub-questions will be relevant:

- How to obtain explicit tree models and implicit tree models from point cloud?

- What is the difference between the simulation results using implicit tree models and explicit tree models?

- What is the tree LoDs impact on urban wind flow simulations?

- Does changing tree shapes (broadleaf or conifer) make any difference to the impact of tree LoDs?

- Does changing the LAD value or wind direction make any difference to the impact of tree LoDs?

## 1.3. Scope of research

This thesis focuses on design numerical test cases and comparisons between simulation results, and will not work on building completely new tree reconstruction algorithms. In order to obtain tree models of different shapes and LoD from open point cloud data, this thesis will find suitable tree reconstruction algorithms among the already existing ones to be used directly or with minor changes to fit CFD applications. The algorithm introduced by de Groot [2020] will be mainly applied and adapted.

## 1.4. Thesis outline

This thesis is structured as follows:

- Chapter 2 presents the theoretical background and related work. It introduces the general background of urban wind flow simulations and the current approach to model tree effects in CFD simulations. It also presents the existing standards for tree LoDs and the existing approaches for automatic reconstruction of trees in different LoDs.

- Chapter 3 presents the methodology followed in this thesis. It first introduces the general workflow of this thesis, and then describes in detail the specific methods for important steps. It briefly describes the design and set up of test cases in different urban complexities. It also introduces the approaches used in this thesis to prepare explicit and implicit tree models for simulations. It then briefly explains the governing equations, computational domain, and boundary conditions for CFD simulations set up. Finally, it explains the quantitative analysis measures used in this thesis to better compare the CFD predictions for different test cases.

- Chapter 4 presents the implementation of the implicit tree modeling approach in Open-FOAM and the verification results of the CFD simulations.

- Chapter 5 goes over the CFD predictions for isolated tree cases, street canyon cases and realistic urban geometry cases. It presents the differences between test cases and also explains the possible reasons for these differences.

- Chapter 6 presents the conclusion of this thesis. It first summarizes the main findings and reviews the answers to the research questions. Then, it presents the limitations and recommendations for further improvements.

# 2. Theoretical background and related work

In this section, the theory and literature related to wind flow simulations and tree modeling is discussed. First, a general background of urban wind flows is given. After that, the numerical models and implicit tree modeling approach currently used to conduct flow simulations are discussed. The development of 3D tree modeling is also presented, which is useful for this thesis to find an explicit tree modeling approach suitable for urban wind flow simulations.

## 2.1. Urban wind flows

As an atmospheric phenomenon, winds occur in a range of spatial and temporal dimensions, from a few tens of meters to thousands of kilometers, and from seconds to weeks (figure 2.1). In general, they can be grouped into three different scale categories [Blocken, 2015]:

1. Macroscale or synoptic scale: includes phenomena such as migrating cyclones that control daily weather changes, ranging from a few hundred to a few thousand kilometres.

2. Mesoscale: includes phenomena such as mountain waves, sea and land breezes, thunderstorms, which range from a dozen to several hundred kilometres and have a lifetime of one day or less.

3. Microscale: includes phenomena such as building wakes and turbulence, which have spatial scales of 2 km or less.

In the field of the built environment, research is mainly focused on the meteorological microscale and building scale. At these scales, in order to understand the transport and distribution of fluids, such as wind or pollutants, three methods can be used: 1) field measurements, 2) wind tunnel measurements, and 3) numerical simulations, mainly Computational Fluid Dynamics (CFD) [Blocken, 2015].

The fundamental consideration of CFD is how to deal with continuous fluids in a discrete manner on a computer. One approach is to discretize the computational domain into finite volumes (figure 2.2), and then apply suitable algorithms to solve the transport equations such as mass, momentum, and energy equations for each finite volume. The general formulation of the transport equations for compressible flow in differential form [Moukalled et al., 2016] is

$$\frac{\partial}{\partial t}(\rho\phi) + \nabla \cdot (\rho\mathbf{v}\phi) = \nabla \cdot (\Gamma^\phi \nabla\phi) + Q^\phi \tag{2.1}$$

where the four components, from left to right, are unsteady term, convection term, diffusion term and source/sink term; $\rho$ is the fluid density, $\phi$ is the quantity of interest, $\mathbf{v}$ is velocity, $\Gamma$ is the diffusion coefficient and $Q^\phi$ is the generation/destruction of $\phi$ within the control volume per unit volume.
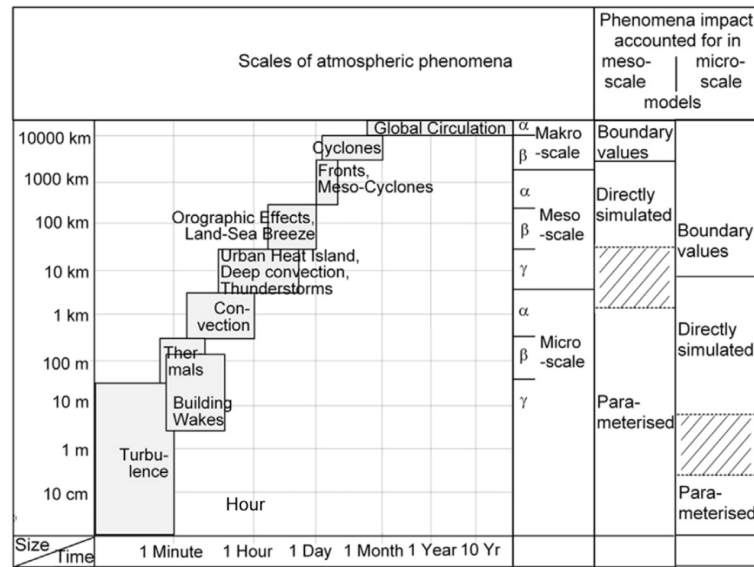
Figure 2.1.: Spatial and temporal scales of atmospheric phenomena (Source: Blocken, 2015)
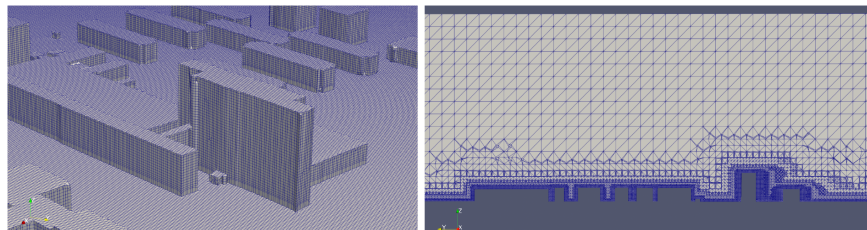


Figure 2.2.: Finite volume mesh for a 3D city model

The computational grid/mesh is one of the key aspects to accurate CFD predictions. A high quality computational mesh not only reduces discretization errors, but also promotes convergence [Blocken, 2015; Tominaga et al., 2008]. It is worth noting that complex meshes may lead to a decrease in mesh quality and a significant increase in the number of mesh cells, resulting in errors and long processing times. However, computational meshes are often complex due to the presence of complicated 3D geometries, such as buildings and trees with detailed features. Therefore, an acceptable degree of simplification of geometries in CFD simulations is recommended [Tominaga et al., 2008]. Such simplifications include using parameters in place of geometry, for example, using porosity or roughness length, or adding additional terms in the transport equations. In addition, reducing the Level of Detail (LoD) of geometric objects and removing small geometric features are also common simplifications. Indeed, simplifications may affect simulation results and introduce some uncertainty, so finding an acceptable level of simplification and investigating the effect of LoDs on urban wind flow simulations will also be goals of this work.

## 2.2. Current numerical simulations of tree drag on wind

There has been a lot of interest in using CFD models to study tree effects. Current studies have focused on the effects on air quality [Vos et al., 2013; Santiago et al., 2019; Balczó et al., 2009; Moradpour et al., 2017], pedestrian wind comfort [Kang et al., 2020; Hong and Lin, 2015] and thermal urban environment [Manickathan et al., 2018; Hong and Lin, 2015; Gromke et al., 2015]. Although the above numerical simulation studies have demonstrated the importance of trees, in these studies trees were usually reduced to circular or rectangular porous zones (figure 2.3) rather than geometrically modeled as objects. That is, these studies have chosen to implicitly model trees. This is mainly due to the fact that such implicit approach reduces computational complexity and the general lack of data that can be used to explicitly model trees.
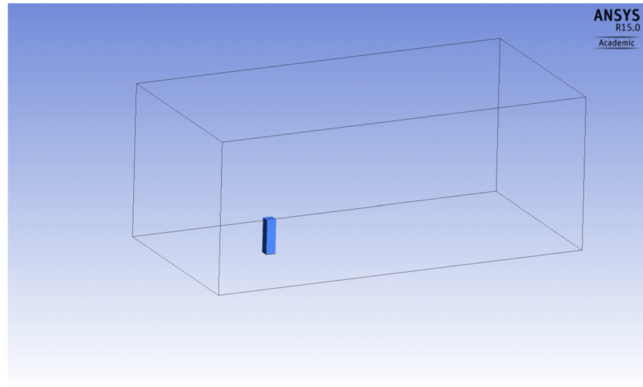


Figure 2.3.: A single conifer modeled as a blue rectangular block, which was set as a porous zone (Source: Mohamed and Wood, 2015)

In this implicit tree modeling approach, tree drag is represented by adding a sink term ($S_{u_i}$) in the momentum equation and source terms ($S_k$ and $S_\varepsilon$) in the turbulence equations. Note that these sink/sources are only considered in porous zones that represent trees.

$$S_{u_i} = - \rho \, C_d \, LAD \, U_i \, \mathbf{U} \left[ \frac{N}{m^3} \right] \tag{2.2}$$

$$S_k = \rho \, C_d \, LAD \left( \beta_p \mathbf{U}^3 - \beta_d \mathbf{U}k \right) \left[ \frac{W}{m^3} \right] \tag{2.3}$$

$$S_\varepsilon = \rho \, C_d \, LAD \, \frac{\varepsilon}{k} \left( C_{\varepsilon4} \beta_p \mathbf{U}^3 - C_{\varepsilon5} \beta_d \mathbf{U}k \right) \left[ \frac{W}{m^3} \right] \tag{2.4}$$

Equation (2.2) is the sink term for the momentum equation, (2.3) is the source term for the turbulence kinetic energy equation, and (2.4) is the source term for the turbulent dissipation rate equation; $\rho$ is the air density, $C_d$ is the leaf drag coefficient, LAD is the leaf area density, $U_i$ is the velocity component in direction i, $\mathbf{U}$ is the wind speed magnitude, $\beta_p$ is the fraction of mean kinetic energy converted into turbulent kinetic energy, $\beta_d$ is the dimensionless coefficient

for the short-circuiting of turbulent cascade, $C_{\varepsilon4}$ and $C_{\varepsilon5}$ are model constants. Depending on the studied cases, several values for $\beta_p$, $\beta_d$, $C_{\varepsilon4}$ and $C_{\varepsilon5}$ could be found in the literature [Hong et al., 2018a; Hefny Salim et al., 2015; Santiago et al., 2019; Buccolieri et al., 2018; Liang et al., 2006]. Usually, $\beta_p$ is assumed equal to 1 and the values for $\beta_d$, $C_{\varepsilon4}$ and $C_{\varepsilon5}$ range between 4–6.5, 0.9–2 and 0.9–1.8, respectively [Buccolieri et al., 2018]. In this thesis, the values of $\beta_p$, $\beta_d$, $C_{\varepsilon4}$ and $C_{\varepsilon5}$ are set to 1, 5.1, 0.9 and 0.9, respectively.

$C_d$ is known to depend on tree species. In the literature, the values for $C_d$ vary between 0.1 and 0.3, with 0.2 being the most commonly used [Gromke et al., 2015]. LAD, defined as the one-side leaf surface area per unit volume ($m^2\,m^{-3}$) (2.5), also depends on tree species and varies with height over the tree crown. The values used in CFD simulations range from 0.1 to 4, with an average value in the literature about 1 [Buccolieri et al., 2018]. For deciduous trees, the effect of seasons can also lead to variation in LAD values. Lalic and Mihailovic [2004] reported LAD values for deciduous trees ranging from 0.2 to 2.2, where 1.6, 2.0 and 2.2 are the respective maximum values of LAD for the canopy of full grown oak, silver birch and maple trees.

$$LAD = \frac{A_{leaf}}{V} \tag{2.5}$$

The Leaf Area Index (LAI), the ratio of the leaf area to the ground area ($m^2\,m^{-2}$), describes the tree density and its relationship with LAD is defined as:

$$LAI = \int_z^h LAD(z)\,dz \tag{2.6}$$

where $h$ is the height of the tree.
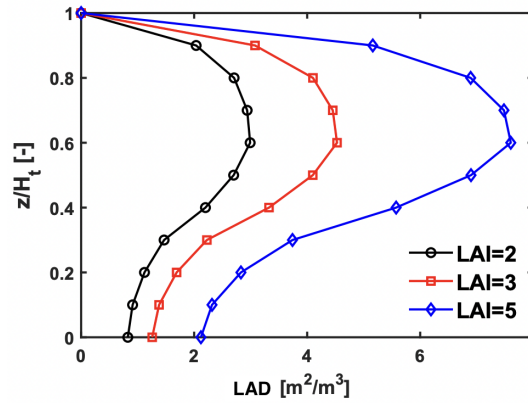


Figure 2.4.: Profiles of LAD over the dimensionless tree height $H_t$ for different $LAI$. (Source: Von Der Grün et al., 2020)

$LAI$ values of several types of trees are discussed in Parker [2020]. The mean values for $LAI$ of broadleaf and conifer trees are 4.02($\pm$2.44) and 5.18($\pm$3.22), respectively [Parker, 2020]. For trees with known $LAI$, the LAD values can be obtained from the generalised canopy

density curves defined in the literature [Shaw and Schumann, 1992; Von Der Grün et al., 2020]. Figure 2.4 shows the $LAD - LAI$ model defined by Von Der Grün et al. [2020], where $LAI = 2$ represents a sparsely covered tree canopy in winter and $LAI = 5$ a very dense tree canopy in summer.

In addition, there have been studies that provide methods to acquire LAD and $LAI$ values from airborne LiDAR data [Oshio et al., 2015; Kamoske et al., 2019]. These methods usually voxelize LiDAR point clouds, and then estimate LAD and $LAI$ values based on the information of each voxel, e.g., number of returns. Yet the applicability of these methods in CFD simulations remains to be investigated.

## 2.3. Automatic reconstruction of trees

With the development of 3D tree reconstruction methods, some studies have also attempted to use real tree models instead of porous zones in CFD simulations. For example, Wang et al. [2021] used a deciduous tree model with tree trunks and branches to simulate the dispersion of pollutants in an street canyon. However, even though the model contained only one tree, the mesh contains more than two million cells. This means that a detailed tree model like this is too demanding for a street or city scale application covering multiple buildings and trees. For such larger scale applications, it is necessary to reduce LoDs of tree models.

There are existing standards or proposed standards for LoDs of 3D tree models. Liang et al. [2016] introduced 5 LoDs for single tree reconstruction, as shown in figure 2.5. Based on this, Ortega-Córdova [2018] further proposed 14 LoDs (figure 2.6) to meet the requirements of different research cases and scales.



(a) LoD 1    (b) LoD 2    (c) LoD 3    (d) LoD 4    (e) LoD 5
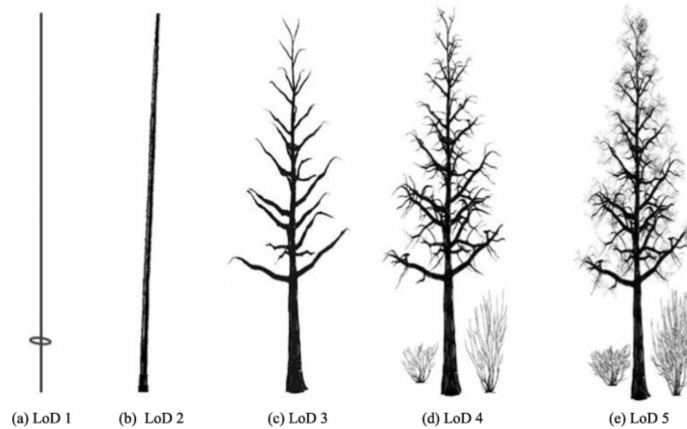
Figure 2.5.: Levels of details of a single 3D tree model. (Source: Liang et al., 2016)

Making use of the proposed LoD specifications by Ortega-Córdova [2018], de Groot [2020] offered an automatic reconstruction of trees in different LoDs, as shown in figures 2.8 and 2.7. The LoD1 models obtained by this method are cylindrical or prismatic, which are similar in shape to the tree models used to obtain porous zones in many current studies (figure 2.3). Tree models in LoD2 or higher are mainly composed of a crown and a trunk, and they differ mainly in the fineness of the crown. It is worth mentioning that de Groot [2020] also classified
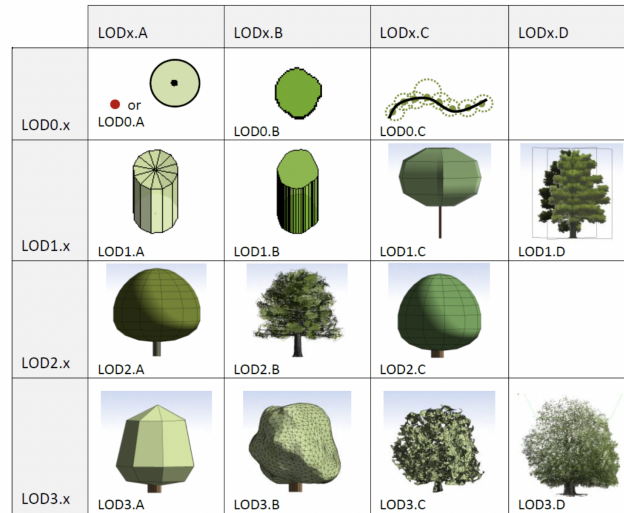
Figure 2.6.: Levels of details of a single 3D tree model. (Source: Ortega-Córdova, 2018)

trees into two groups, *Coniferae* (conifer) and *Angiospermae* (broadleaf), and this information is stored as an attribute in each tree model.



Figure 2.7.: LoD2 tree models by de Groot [2020]. (Source: [de Groot, 2020])

Other works have focused on providing highly detailed tree reconstruction methods [Du et al., 2019; Livny et al., 2011], which results in tree models that include not only trunks and crowns, but also fine branches and leaves. However, such models are usually too complex to be applicable to CFD simulations. Moreover, as presented by Du et al. [2019], highly detailed tree reconstruction models often require LiDAR point cloud data from mobile scanning or static scanning, which are difficult to obtain, so they are therefore not applicable to most urban wind environment studies. Hence, it can be safely concluded that these highly detailed tree models are beyond the scope of this thesis.

García-Sánchez et al. [2021] have demonstrated that different LoDs lead to diverse local numerical wind predictions by comparing CFD simulations results with building models in different LoDs. However, to my knowledge, few studies have given extensive consideration to the tree LoD impact on urban wind flow simulations, which will be one of the research focuses of this thesis.

| | 3D view | Front View | Top View |
|---|---|---|---|
| **LOD0** | | | |
| **LOD1** | | | |
| **LOD2** | | | |
| **LOD3.0** | | | |
| **LOD3.1** | | | |
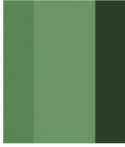
Figure 2.8.: Tree models with different LoDs by de Groot [2020].

# 3. Methodology

This chapter first introduces the general workflow of this thesis, and then describes in detail the specific methods for test cases design and set up, CFD simulations set up, and quantitative analysis.

## 3.1. Research workflow

Figure 3.1 displays a general workflow of this thesis.
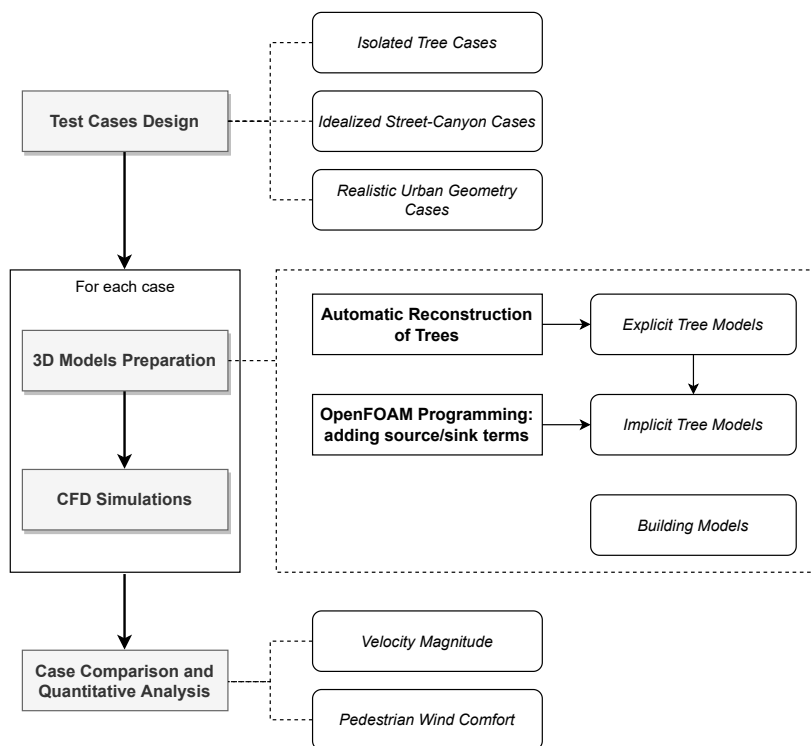


Figure 3.1.: Research workflow

First, a series of ideal numerical test cases with different urban complexities, tree modeling approaches, tree LoDs (LoD2 or 3), tree shapes (Broadleaf or Conifer), leaf area density (LAD) values and wind directions will be designed. Based on these designs, 3D building models need to be prepared and explicit tree models will be generated using open point cloud data and automatic reconstruction algorithm. Then, the corresponding implicit tree models are obtained by marking the volume cells that roughly account for the explicit tree models as

porous cells. In order to implement tree drag for those implicit tree models, i.e., considering $S_{u_i}$, $S_k$ and $S_\varepsilon$ in porous cells, OpenFOAM programming is necessary. Finally, the simulation results of different test cases will be compared in terms of velocity magnitude and pedestrian wind comfort.

## 3.2. Test cases design and set up

It is necessary to design suitable test cases in order to cover the different geometrical complexity of urban areas and better analyze impact of tree topology modeling for urban flow simulations. Illuminating cases settings can be found in some literature [Hefny Salim et al., 2015; Vos et al., 2013]. Four commonly considered morphologies and their settings can be found in literature [Hefny Salim et al., 2015; Vos et al., 2013]: an isolated tree, an idealized street canyon, a simplified urban geometry (array of buildings), and a realistic urban geometry.

Considering the research objectives of this thesis, three scales of test cases are believed to be necessary: an isolated tree, an idealized street canyon and a realistic urban geometry (corresponding to a region of a real city). Tree models are reconstructed in LoD 2 and 3. For tree shapes, broadleaf and conifer trees will be considered.

### 3.2.1. Isolated tree

The isolated tree test cases are mainly used to investigate the difference between the explicit and the implicit tree modeling approach. Figure 3.2 shows the LoD2 and 3 broadleaf and conifer explicit tree models used in cases, which have relatively standard shapes. These explicit models were obtained using the automatic reconstruction algorithm and the input Algemeen Hoogtebestand Nederland (AHN)3 point cloud dataset example provided by de Groot [2020].
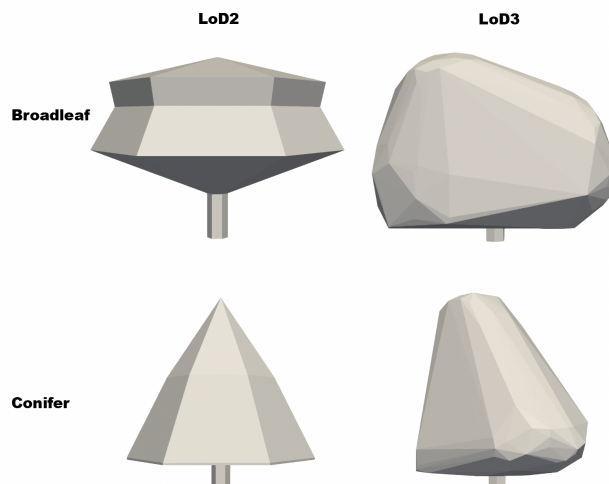


Figure 3.2.: Broadleaf (UP) and Conifer (DOWN) explicit tree models

Value of the drag coefficient $C_d$ for the corresponding implicit tree models is defined as a constant (0.2), which is consistent with most of the literature. For LAD, two values are needed: a very high value (e.g. 5e10) to investigate whether the explicit and the implicit models behave similarly, and a lower common value (e.g. 1.4) as a reference.

For each test case, the same meteorological conditions are used: the inlet wind speed is 4.97 m/s at 10 m above the ground. The flow is considered incompressible and the Atmospheric Boundary Layer (ABL) stratification is assumed to be neutral.

### 3.2.2. Idealized street canyon
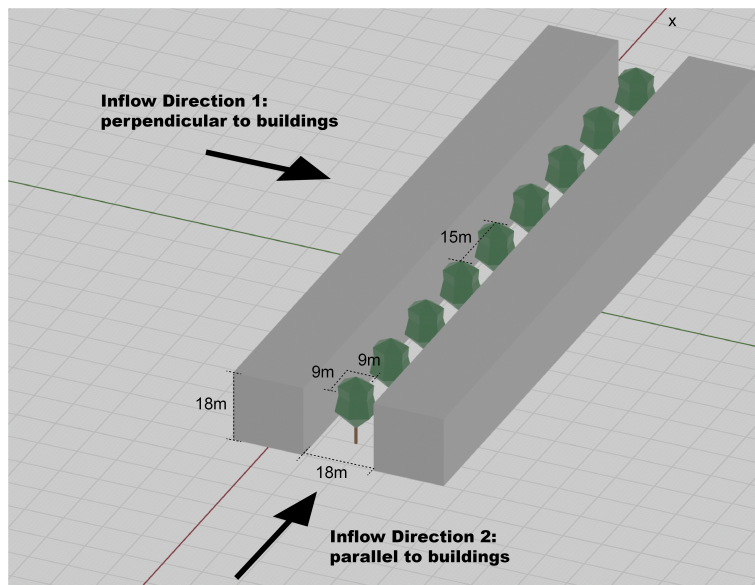


Figure 3.3.: Wind directions, buildings arrangements and tree configurations of the street canyon cases.

The idealized street canyon cases focus on analyzing the tree LoDs and shapes impact. The insights obtained can be used to analyze the further effects of tree topography on pollutant dispersion and heat exchange.

The street canyon representation of each case consists of two parallel-aligned building blocks (length L = 180 m, height H = 18 m, width W = 18 m, aspect ratio W/H = 1) and a row of tree models placed in the middle with a gap of 15 m. Two wind directions are used: perpendicular and parallel to buildings, both with the same meteorological conditions as the isolated tree cases.

Similar to isolated tree cases, four types of tree models are used, namely LoD2 broadleaf, LoD3 broadleaf, LoD2 conifer, and LoD3 conifer models. To ensure consistent tree density, all tree models have a uniform bounding box size, i.e., 8 m in length and width and 18 m in height. Also, since the difference between the implicit and explicit tree modeling approaches can be explained by the isolated tree test cases, tree canopies in the street canyon cases are modeled implicitly and tree trunks are modeled explicitly.

The wind directions, building arrangements, and tree configuration are shown in Figure 3.3.

### 3.2.3. Realistic urban geometry



Figure 3.4.: Noordereiland (red line) shown in the 3D BAG database



Figure 3.5.: Locations of Noordereiland and the weather stations (Photos source: RainGain website)

Test cases for the realistic urban geometry are mainly used to simulate more complex tree effects on the airflow. Complicated street and tree configurations and variations in building shapes result in more complicated flow fields, which allow the effects of tree LoDs and shapes to potentially no longer be confined to local areas. The insights obtained may be important for larger-scale studies of urban wind environments.

The study area is Noordereiland in Rotterdam, which is an island with an area of about 67 hectares (Figure 3.4). The building models can be obtained through the 3D BAG database

[Dukai et al., 2021]. Trees in the domain will be obtained using the AHN3 point cloud dataset and the reconstruction algorithm adapted from [de Groot, 2020], and thus have different shapes. The differences between the test cases are the LoDs of tree models.

The appropriate wind direction and wind speed are obtained from the data provided by the RainGain project of TU Delft. The 5-minute average data in 2021 measured at the nearest weather stations (Rijnhaven), are mainly used. Data from another three nearer weather stations (Oost, Bolnes and SpaansePolder), are used as references. Figure 3.5 shows the locations of Noordereiland and the weather stations.

## 3.3. CFD simulations set up

To perform the CFD simulations, OpenFOAM, an open-source computational fluid dynamics software, is used. The flow is considered incompressible, steady and temperature stratification is neutral.

### 3.3.1. Governing equations

The Reynolds averaged Navier Stokes (RANS) approach is used for CFD simulations. The mass (3.1) and momentum conservation equations that govern the flow are the following:

$$\frac{\partial \overline{u_j}}{\partial x_j} = 0 \tag{3.1}$$

$$\overline{u_j}\frac{\partial \overline{u_i}}{\partial x_j} = -\frac{1}{\rho}\frac{\partial \overline{p}}{\partial x_i} + \nu \frac{\partial^2 \overline{u_j}}{\partial x_j \partial x_j} - \frac{\partial \overline{u_i' u_j'}}{\partial x_j} + F_i \tag{3.2}$$

where $u_i$ denotes time-averaged velocity components, $\rho$ is the density, $p$ is the pressure, $\nu$ is the kinematic viscosity and $F_i$ is the source or sink term. $F_i$ is only considered in porous zones that represents trees and is equal to Equation 2.2. In other cases, it is zero. The term $\overline{u_i' u_j'}$ represents the Reynolds stress tensor, which is unknown and needs to be closed with a turbulence model. For our case, we used the two equations $k - \epsilon$ turbulence model since it is widely used in outdoor wind simulations, and it is rather simple [García-Sánchez et al., 2021; Blocken, 2015]. In this model, $\overline{u_i' u_j'}$ is computed based on the linear eddy viscosity hypothesis:

$$\overline{u_i' u_j'} = \frac{2}{3}k\delta_{ij} - 2\mu_t S_{ij} \tag{3.3}$$

where $k$ is the turbulence kinetic energy, $S_{ij}$ the time-averaged shear stress tensor, and $\mu_t$ is the coefficient termed turbulence viscosity. $\mu_t$ is computed using following equation:

$$\mu_t = C_\mu \frac{k^2}{\epsilon} \tag{3.4}$$

where $C_\mu$ is a model constant equal to 0.09. The equations for the two turbulence variables, namely the turbulence kinetic energy $k$ and the turbulence dissipation rate $\epsilon$ are as follows:

$$\overline{u_j}\frac{\partial k}{\partial x_j} = \frac{\partial}{\partial x_j}\left[(\mu + \frac{\mu_t}{\sigma_k})\frac{\partial k}{\partial x_j}\right] + P_k - \epsilon \tag{3.5}$$

$$\overline{u_j}\frac{\partial \epsilon}{\partial x_j} = \frac{\partial}{\partial x_j}\left[(\mu + \frac{\mu_t}{\sigma_\epsilon})\frac{\partial \epsilon}{\partial x_j}\right] + C_{\epsilon 1}\frac{\epsilon}{k}P_k - C_{\epsilon 2}\frac{\epsilon^2}{k} \tag{3.6}$$

where $P_k$ is the turbulent production term and $\sigma_k$, $\sigma_\epsilon$, $C_{\epsilon 1}$ and $C_{\epsilon 2}$ are model constants, with values of 1.0, 1.3, 1.44, and 1.92, respectively.

### 3.3.2. Computational domain and mesh

For all numerical test cases, the computational domain should be chosen large enough to avoid too strong artificial acceleration of the flow due to too strong contraction of the flow by the side and top boundaries of the computational domain [Blocken, 2015]. Conforming to the best practice guidelines prescribed by Franke et al. [2011]; Blocken [2015], the inlet, lateral and top boundary are set at least $5H_{max}$ away from the group of building and tree models, where $5H_{max}$ is the height of the tallest geometry. A distance of at least $15H_{max}$ should be kept downstream of the group of building and tree models to allow for adequate wake development.

For generating the computational mesh, i.e., to discretize the space where the airflow is modelled, the automatic parallel mesh generator, snappyHexMesh, is used. An example of the computational mesh design for an isolated tree model is shown in figure 3.6. It can be seen that the cell density increases closer to the ground and to the tree model.

Note that in order to ensure the comparability of CFD predictions, the test cases to be compared should use computational mesh designs that are as similar as possible. Figure 3.7 shows the computational meshes for a test case using an isolated implicit tree models and a test case using an isolated explicit tree models, respectively. It can be found that the two meshes are overall consistent, except that the explicit case has no cells within the tree model, while in the implicit case these cells are still present but marked as porous medium.

### 3.3.3. Boundary conditions

The inflow boundary condition will be modelled as a fully developed neutral boundary condition with the following equations for the velocity, turbulence kinetic energy, and dissipation:
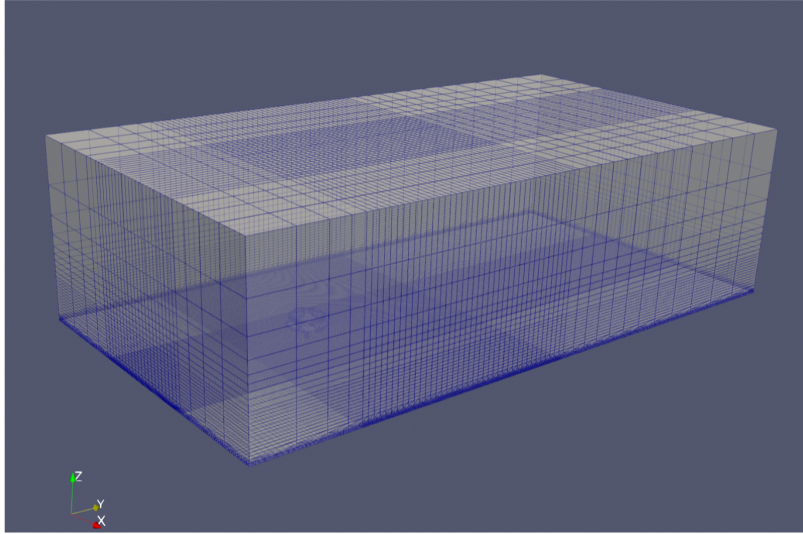
Figure 3.6.: Planning overview
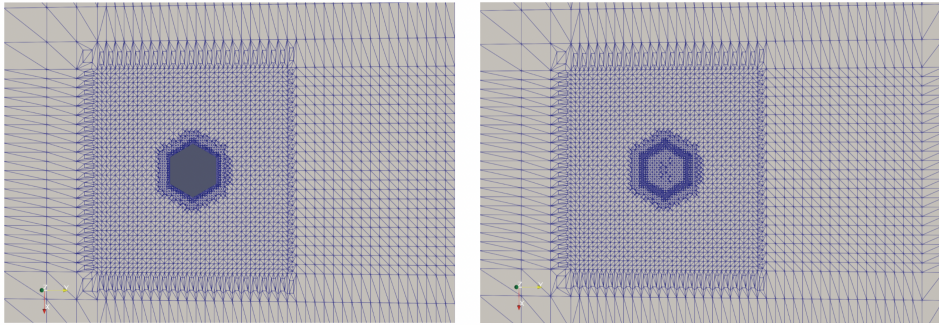


Figure 3.7.: the computational mesh designs (Horizontal cross-section) for a test case using the explicit approach for tree modelling (left) and a test case using the implicit approach (right).

$$U = \frac{u_*}{\kappa} \ln \frac{z + z_0}{z_0} \tag{3.7}$$

$$k = \frac{u_*^2}{\sqrt{C_\mu}} \tag{3.8}$$

$$\epsilon = \frac{u_*^3}{\kappa(z + z_0)} \tag{3.9}$$

where $u_*$ denotes the friction velocity and $\kappa$ is the von Karman constant with a value of 0.41. $z_0$ is the aerodynamic roughness length. The $z_0$ value used for terrain in this thesis is 0.2 m,

which corresponds to a 'rough area' according to the updated Davenport-Wieringa roughness classification [Blocken, 2015]. For water, 0.0002 m is used.

To run the simulation, the standard $k - \epsilon$ turbulence model and the *simpleFoam* solver in OpenFOAM need to be modified to add the sink/source terms ($S_{u_i}$, $S_k$ and $S_\varepsilon$).

## 3.4. Measures for quantitative analysis

### 3.4.1. Non-dimensional velocity magnitude difference

To better compare the velocity magnitude difference between explicit cases and implicit cases, CFD prediction data of two cases can be subtracted and normalized to obtain the non-dimensional velocity magnitude difference $U_{ex-im}$:

$$C_{ex-im} = \frac{(U_{ex} - U_{im})}{U_{ref}} \qquad (3.10)$$

where $U_{ex}$ and $U_{im}$ represent the velocity magnitude predictions of an explicit case and an implicit case, respectively. The value is normalized by $U_{ref}$, the inflow velocity magnitude at 1.75 m height.

The same method can be used to obtain the non-dimensional velocity magnitude difference between LoD2 and LoD3 cases $C_{l2-l3}$:

$$C_{l2-l3} = \frac{(U_{lod2} - U_{lod3})}{U_{ref}} \qquad (3.11)$$

where $U_{lod2}$ and $U_{lod3}$ represent the velocity magnitude predictions of a case using LoD2 tree models and a case using LoD3 tree models, respectively.

Note that in this thesis, the values of non-dimensional velocity magnitude differences are expressed as percentages.

### 3.4.2. Pedestrian wind comfort criteria

Wind speed affects whether an outdoor environment is comfortable for pedestrians. The use of tree models at different LoDs can result in different wind speed predictions for certain locations, which in turn may lead to different evaluations of the pedestrian wind comfort at that location.

A variety of different wind comfort criteria can be found in the literature. Table 3.1 shows the extended Land Beaufort scale provided by Blocken and Carmeliet [2004]; Lawson and Penwarden [1975], which is considered generally suitable for use in the Netherlands [Janssen et al., 2013; Bottema, 2000]. This criteria has detailed descriptions of people's perception of wind for each category.

In comparison, the wind comfort criteria used in the City of London [of London Corporation, 2019] (table 3.2) summarizes the wind effect on pedestrians as acceptable activities, which are good references for urbanized areas. Note that not only the average wind speed affects pedestrian comfort, but also the gust wind speed, so their combined effect, i.e. Gust Equivalent Mean (GEM) wind speed, is also used as a basis for the criteria. The GEM wind speed is obtained by diving the maximum mean wind speed or the gust wind speed by 1.85.

In this thesis, the criteria provided by Blocken and Carmeliet [2004]; Lawson and Penwarden [1975] is mainly used, but with the added distinction between acceptable outdoor activities as described in the City of London wind comfort criteria [of London Corporation, 2019]. Table 3.3 shows the final criteria used in this thesis.

Table 3.1.: Extended Land Beaufort Scale showing wind effects on people (Source: [Blocken and Carmeliet, 2004; Lawson and Penwarden, 1975]).

| Category | Description | Mean wind speed at 1.75 m height (m/s) | Effect |
|---|---|---|---|
| A | Calm | 0.0–0.1 | |
| B | Light air | 0.2–1.0 | No noticeable wind |
| C | Light breeze | 1.1–2.3 | Wind felt on face; |
| D | Gentle breeze | 2.4–3.8 | Hair disturbed, clothing flaps, newspaper difficult to read; |
| E | Moderate breeze | 3.9–5.5 | Raises dust and loose paper, hair disarranged; |
| F | Fresh breeze | 5.6–7.5 | Force of wind felt on body, danger of stumbling when entering a windy zone; |
| G | Strong breeze | 7.6–9.7 | Umbrellas used with difficulty, hair blown straight, difficult to walk steadily, sideways wind force about equal to forwards walking force, wind noise on ears unpleasant; |
| H | Near gale | 9.8–12.0 | Inconvenience felt when walking |
| I | Gale | 12.1–14.5 | Generally impedes progress, great difficulty with balance in gusts |
| J | Strong gale | 14.6–17.1 | People blown over |

Table 3.2.: Wind comfort criteria for the City of London (Source: [of London Corporation, 2019])

| Category | Description | Mean and GEM wind speed at 1.75 m height (m/s) | Acceptable activities |
|---|---|---|---|
| A | Frequent Sitting | 2.5 | Frequent outdoor sitting use, e.g. restaurant, café. |
| B | Occasional Sitting | 4 | Occasional outdoor seating, e.g. general public outdoor spaces, balconies and terraces intended for occasional use, etc. |
| C | Standing | 6 | Entrances, bus stops, covered walkways or passageways beneath buildings. |
| D | Walking | 8 | External pavements, walkways |
| E | Uncomfortable | >8 | Not comfortable for regular pedestrian access |
| F | Unsafe | >15 | Unsafe for pedestrians |

Table 3.3.: Wind comfort criteria showing wind effects and acceptable activities ( based on the work by [of London Corporation, 2019; Blocken and Carmeliet, 2004; Lawson, 1978] )

| Category | Description | Mean and GEM wind speed at 1.75 m height (m/s) | Effect | Acceptable activities |
|---|---|---|---|---|
| A | Calm | 0.0–0.1 | | Frequent outdoor sitting use, e.g. restaurant, café. |
| B | Light air | 0.2–1.0 | No noticeable wind | |
| C | Light breeze | 1.1–2.3 | Wind felt on face; | |
| D | Gentle breeze | 2.4–3.8 | Hair disturbed, clothing flaps, newspaper difficult to read; | Occasional outdoor seating, e.g. general public outdoor spaces, balconies and terraces intended for occasional use, etc. |
| E | Moderate breeze | 3.9–5.5 | Raises dust and loose paper, hair disarranged; | Entrances, bus stops, covered walkways or passageways beneath buildings. |
| F | Fresh breeze | 5.6–7.5 | Force of wind felt on body, danger of stumbling when entering a windy zone; | External pavements, walkways |
| G | Strong breeze | 7.6–9.7 | Umbrellas used with difficulty, hair blown straight, difficult to walk steadily, sideways wind force about equal to forwards walking force, wind noise on ears unpleasant; | Not comfortable for regular pedestrian access |

# 4. Implementation and Verification

This section will present the modified source code of OpenFOAM used in this thesis for adding source/sink terms for tree drag. The verification results of CFD simulations will also be introduced.

## 4.1. OpenFOAM programming to add source/sink terms

As it was said before, to implement the tree drag in implicit tree modeling approach, it is required to add a sink term ($S_{u_i}$) in the momentum equation and source terms ($S_k$ and $S_\varepsilon$) in the turbulence equations. This can be achieved by implementing a new porosity model and using fvOptions, or creating a new turbulence model and solver based on the source code of the standard $k - \epsilon$ turbulence model and the *simpleFoam* solver in OpenFOAM. The latter was chosen for this thesis as it is simple and not prone to problems due to mishandling of dependency libraries. The implementation is based on the work of [Maldonado, 2012; Segersson, 2017].

The new turbulence model is named "*treekEpsilon*", which includes the source terms for the kinetic energy equation and the dissipation rate equation defined in the *treekEpsilon.C* and *treekEpsilon.H* file. The new solver is named "*treeFoam*" and it includes the sink term for the momentum equation defined in the *UEqn.H* and *createFields.H* files. The codes can be found in Appendix B.

## 4.2. Explicit and implicit tree models preparation

The explicit tree models (e.g. those shown in figure 3.2) are triangulated edge mesh models, which can be in formats such as **stl**, **obj**, **vtk**, and so on. Since the format of the tree models obtained by the reconstruction algorithm introduced by [de Groot, 2020] is CityJSON, it is also necessary to convert the format.

Each tree model obtained after the reconstruction and format transformation steps described above has only one mesh object. Tree trunk and canopy are not distinguished as two different objects, but are defined with different materials. This thesis uses Blender software to split the mesh into separate mesh objects by material and to export the tree trunk and canopy as separate files. This is because there are needs to use different modeling approaches or different LAD values for tree trunks and canopies; for instance, the tree trunks will be solid while the canopies will be porous in all street canyon and realistic urban geometry cases.

To insert an explicit tree model as an input geometry in a CFD grid/mesh, the tree model file should be included and defined in the 'geometry' and 'castellatedMesh' sections in the snappyHexMeshDict dictionary file. After generating a good CFD grid/mesh with the explicit tree model, the corresponding implicit tree model can be obtained with the following steps:

Step 1:  Use the same snappyHexMeshDict file but exclude the tree model from the 'refinementSurfaces' of 'castellatedMesh' dictionary. In this way, the case using the explicit model and the case using the corresponding implicit model can have as similar a CFD grid/mesh design as possible, which can avoid the influence of the CFD grid/mesh on simulations.

Step 2:  Select all finite volume cells that are inside or very near to the surface of the explicit tree model and mark them as porous zones. This can be achieved with a topoSetDict dictionary file.

## 4.3. Performing CFD simulations

After the codes have been compiled and the models have been prepared, CFD simulations can be performed. In order for the solver to take into account the values of LAD and $C_d$ for implicit tree models, there should be a *leafAreaDensity* and a *plantCd* file in the '0' folder. In order to make sure LAD and $C_d$ are only considered in porous zones, their default values defined in the *leafAreaDensity* and *plantCd* file should be set to 0, and a setFieldsDict dictionary file can be used to set specific values of LAD and $C_d$ for each porous zone prior the start of the simulation.

For the cases using explicit tree models, since there are no needs to add source/sink terms for tree drag, the standard $k - \epsilon$ turbulence model and *simpleFoam* solver can be used directly. *treekEpsilon* and *treeFoam* can also be used, but the values of LAD and $C_d$ need to be set to 0. These two methods have been compared and proven to have identical results. For the sake of a simpler case setup and running, this thesis uses *simpleFoam* and $k - \epsilon$ model for explicit cases.

## 4.4. Residuals convergence

As CFD problems are generally nonlinear, CFD solvers will iterate continuously to find a solution, until convergence is reached. We can say that one solution reaches convergence when the following three conditions are met:

1. The residuals have reduced to an acceptable threshold ($10^{-4}$ is used in this thesis for all fields of interest, i.e., $p, U, k, \varepsilon$);

2. The change in residuals between iterations is zero or very small;

3. The monitoring points of our variables of interest have achieved a stable values.

Figure 4.1 shows an example from a realistic urban geometry test case (case 22). It clearly shows that residuals for $U$, $k$ and $\varepsilon$ have dropped below $10^{-4}$ and that the change in residuals between iterations tends to zero after roughly the 1500th iteration. Although residuals for $p$ have not reduced to $10^{-4}$, they are close and this is somewhat expected with complex geometries. Also, figure 4.2 shows that the velocity magnitude values of the probes have stabilised. Thus, we can consider that this solution reaches residuals convergence at the 1500th iteration.
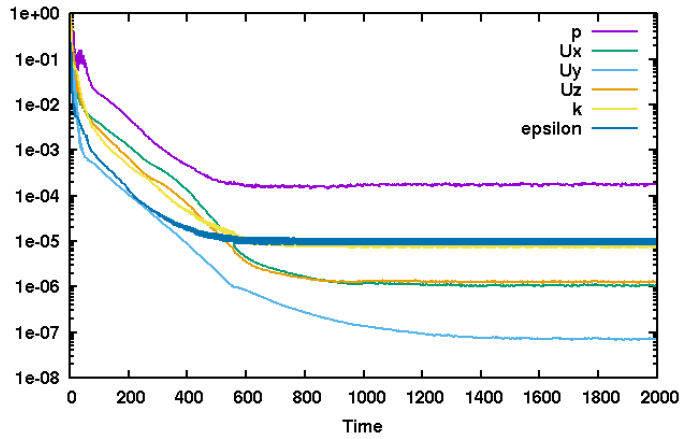
Figure 4.1.: Residuals of fields of a realistic urban geometry test case
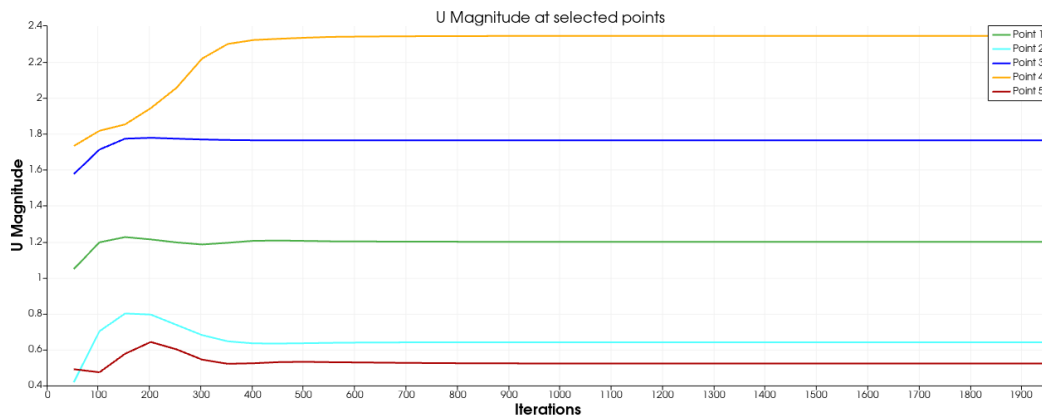


Figure 4.2.: Velocity magnitude values over time for five monitoring points

## 4.5. Mesh independence verification

To ensure that a solution is also independent of the mesh resolution, it is necessary to do mesh independence verification. The way to do mesh independence verification can be summarized in the following three steps:

Step 1: Design a relatively coarse mesh to run the initial simulation. Ensure that the residuals converge;

Step 2: Refine the initial mesh at a constant ratio (1.3 is used in this thesis) to obtain at least two new meshes: medium mesh and fine mesh. Run simulations on these two meshes and ensure that the residuals converge.

Step 3: Mesh independence can be considered achieved when the relative difference between the solutions of the fine mesh and the medium mesh is a certain margin smaller than that of the medium mesh and the coarse mesh. This means that a finer mesh does not significantly change the solution anymore and that using the medium mesh for final

simulations is sufficient, which allow us to make a compromise in terms of time and computational resources. If not, continue refining the mesh and repeat.

Table 4.1 introduces the three generated meshes for a realistic urban geometry test case. And figure 4.3 to 4.8 shows that, for all fields of interest, the gap between the medium mesh and the fine mesh is generally smaller than that between the medium mesh and the coarse mesh. Notably, although the rate of change in cell size was 1.3, the increase in the total number of cells was approximately twofold. This highlights the need to use the medium mesh rather than the fine mesh for final simulations, since a larger total number of cells also means a larger computational time.

Table 4.1.: Properties of the meshes with different resolutions

| Mesh | Smallest cell size (m) | Total number of cells |
|------|------------------------|------------------------|
| Coarse | 0.52 | 3038617 |
| Medium | 0.4 | 5710610 |
| Fine | 0.3 | 11390599 |
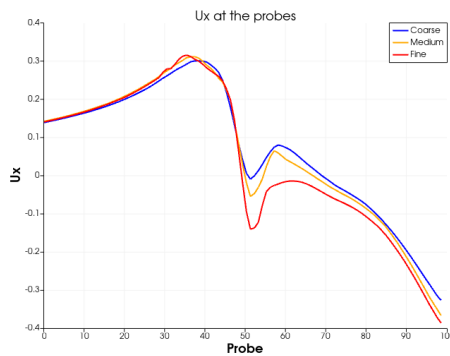


Figure 4.3.: $U_x$ plot for all three meshes
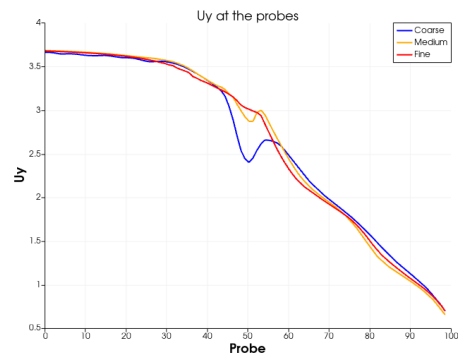


Figure 4.4.: $U_y$ plot for all three meshes
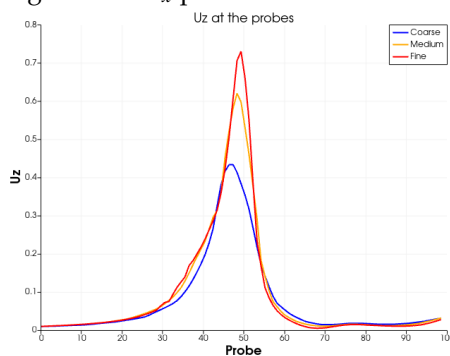


Figure 4.5.: $U_z$ plot for all three meshes
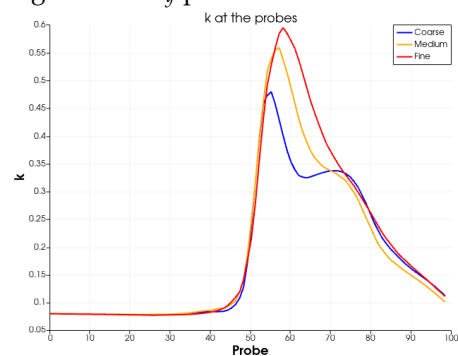


Figure 4.6.: $k$ plot for all three meshes
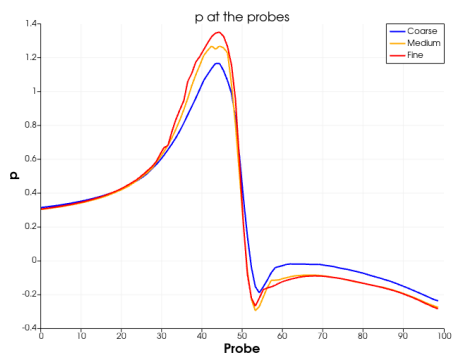
Figure 4.7.: $p$ plot for all three meshes
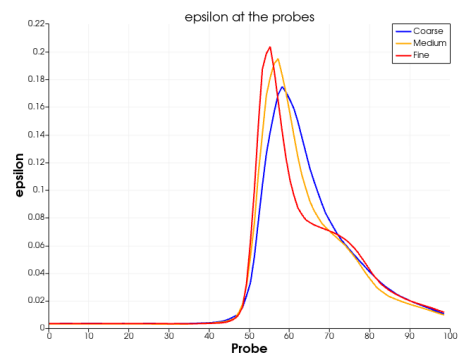


Figure 4.8.: $\varepsilon$ plot for all three meshes

# 5. Results and Analysis

This section will go over the CFD prediction results for isolated tree cases, street canyon cases and realistic urban geometry cases. Findings of the difference between test cases will be enumerated, and the possible reasons for these differences will be explained.

When discussing the results related to wind features and vortex at specific locations, the names used within thesis are referenced in figure 5.1.
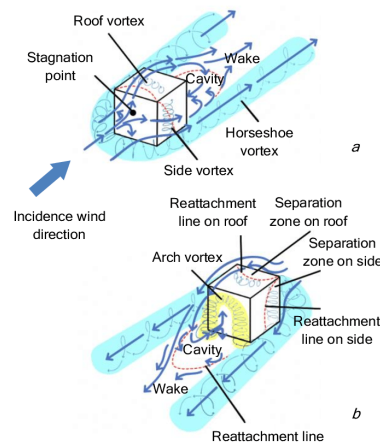


Figure 5.1.: Wind features and and vortex naming at specific locations (Source: Pourteimouri et al., 2020)

## 5.1. CFD predictions: Isolated tree

Table 5.1 shows the test cases using only an isolated tree model. Two LAD values are considered for the tree canopy, 1.4 and 5e10, of which the first value is commonly used in the literature for tree canopies. 5e10 is set to make the implicit models as similar as possible to the explicit models, i.e., models with no wind flow inside, so that the difference between the explicit and implicit tree modeling approach in terms of their effects on wind could be better compared.

Table 5.1.: Isolated tree test cases

| Case ID | Tree shape | Tree modeling approach | LoD of tree | LAD value ($m^2 \, m^{-3}$) |
|---|---|---|---|---|
| 1 | Broadleaf | Explicit | 2 | - |
| 2 | | | 3 | - |
| 3 | | Implicit | 2 | 1.4 |
| 4 | | | 3 | 1.4 |
| 5 | | | 2 | 5e10 |
| 6 | | | 3 | 5e10 |
| 7 | Conifer | Explicit | 2 | - |
| 8 | | | 3 | - |
| 9 | | Implicit | 2 | 1.4 |
| 10 | | | 3 | 1.4 |
| 11 | | | 2 | 5e10 |
| 12 | | | 3 | 5e10 |

Table 5.2.: Overview of $C_{ex-im}$ plots for isolated-tree cases.

| $C_{ex-im}$ ID | Tree shape | LoD of tree | Explicit case ($U_{ex}$) | Implicit case ($U_{im}$) | Measurement Height |
|---|---|---|---|---|---|
| A-1′ | Broadleaf | 2 | Case 1 | Case 3 (LAD = 1.4) | Canopy |
| A-1 | | | | Case 5 (LAD = 5e10) | |
| A-2 | | | | | Trunk |
| B-1′ | | 3 | Case 2 | Case 4 (LAD = 1.4) | Canopy |
| B-1 | | | | Case 6 (LAD = 5e10) | |
| B-2 | | | | | Trunk |
| C-1′ | Conifer | 2 | Case 7 | Case 9 (LAD = 1.4) | Canopy |
| C-1 | | | | Case 11 (LAD = 5e10) | |
| C-2 | | | | | Trunk |
| D-1′ | | 3 | Case 8 | Case 10 (LAD = 1.4) | Canopy |
| D-1 | | | | Case 12 (LAD = 5e10) | |
| D-2 | | | | | Trunk |
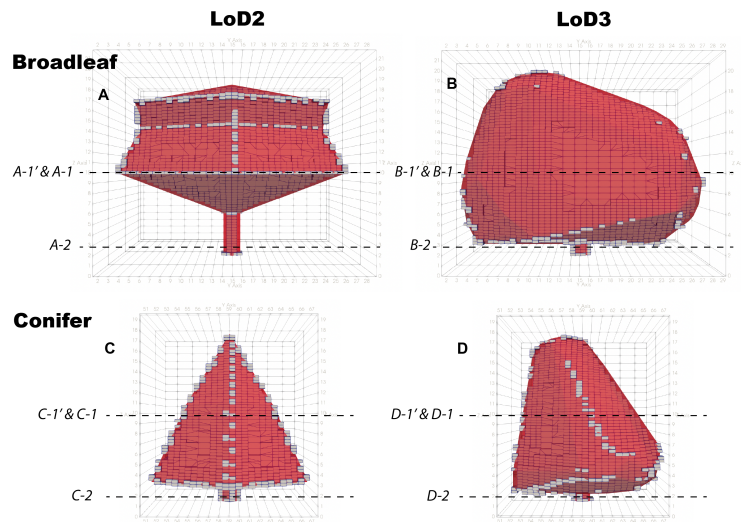


Figure 5.2.: The explicit (RED) and implicit (WHITE) tree models used in test cases

As suggested in section 3.4, test cases need to be compared in pairs to get the non-dimensional velocity magnitude difference ($C_{ex-im}$ or $C_{l2-l3}$). Since isolated tree cases focus on comparing the difference between the implicit and explicit tree modeling approach, the velocity magnitude predictions of the explicit cases and the corresponding implicit cases are subtracted and normalized to get $C_{ex-im}$. The overview of the $C_{ex-im}$ plots for isolated-tree cases are presented in table 5.2.

Figure 5.2 shows the explicit tree models (meshes in red color) and the corresponding implicit tree models (porous cells in white color) used in test cases. The subplots A and B show the LoD2 and LoD3 models of the broadleaf tree, respectively, while C and D show the LoD2 and LoD3 models of the conifer tree. The dashed lines suggest the locations of the horizontal planes used for computing $C_{ex-im}$.

### 5.1.1. Broadleaf tree

In order to improve readability, the flow velocity magnitude predictions for case 1-6 are displayed in figure C.1 in Appendix C, and figure 5.3 here only introduces the predictions for the test case 1 and 5.
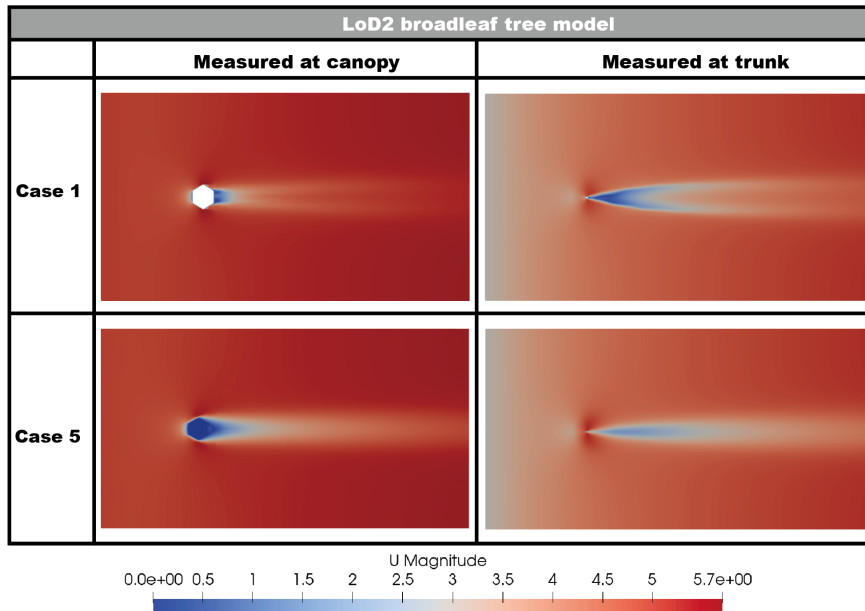


Figure 5.3.: Velocity magnitude for test case 1 (LoD 2 explicit) and test case 5 (LoD 2 implicit) with LAD = $5 \times 10^{10}\,\mathrm{m^2\,m^{-3}}$)

The relative velocity magnitude differences $C_{ex-im}$ at height of tree trunk as well as canopy for broadleaf tree models are shown in figure 5.4, where the red color indicates that the magnitude of wind flow velocity is higher in the explicit case than in the implicit case. Figure 5.5 shows the stream trace for some of the test cases, which reveals more details on the differences between the explicit and implicit tree modeling approach. Observing the characteristics of the figures and the differences between subplots, we can enumerate some findings and possible reasons:
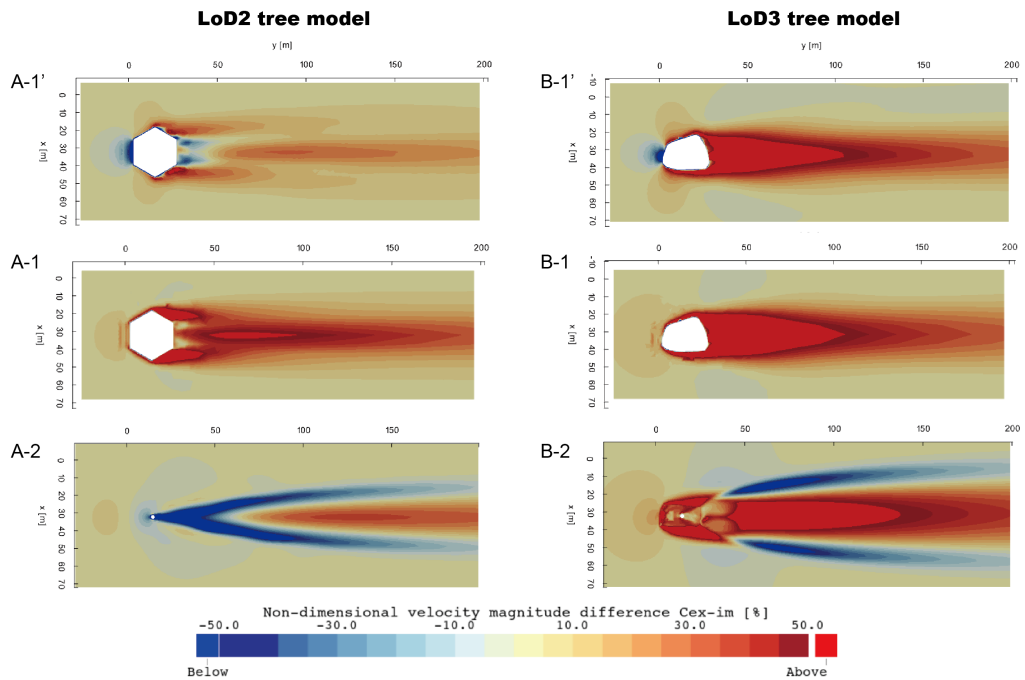
Figure 5.4.: $C_{ex-im}$ for broadleaf tree models. (A-1') difference between LoD2 explict broadleaf & LoD2 implicit broadleaf with LAD = 1.4, measured at canopy; (B-1') difference between LoD3 explict broadleaf & LoD3 implicit broadleaf with LAD = 1.4, measured at canopy; (A-1) difference between LoD2 explict broadleaf & LoD2 implicit broadleaf with LAD = 5e10, measured at canopy; (B-1) difference between LoD3 explict broadleaf & LoD3 implicit broadleaf with LAD = 5e10, measured at canopy; (A-2) difference between LoD2 explict broadleaf & LoD2 implicit broadleaf with LAD = 5e10, measured at trunk; (B-2) difference between LoD3 explict broadleaf & LoD3 implicit broadleaf with LAD = 5e10, measured at trunk;

## 1. Characteristics of $C_{ex-im}$ at canopy:

When using a lower LAD value ($1.4\,\mathrm{m^2\,m^{-3}}$) for the canopy, the explicit cases have lower velocity than the implicit cases on the upstream windward (leftmost) side of the tree models, and the explicit cases are faster on both lateral sides of the tree models. This is expected, because the explicit tree models will block the wind from entering their interior and promote a rapid flow of the wind to their lateral sides, which will create a stagnant zone at the very front of the models. In contrast, when the wind approaches the implicit models with a lower LAD value, most of the flow will not be blocked and will enter inside of the models instead of turning to the lateral sides, so the wind speed in the stagnant zone will be relatively fast.

It is worth noting that, as shown in subplots A-1 and B-1, when the LAD value of the tree canopy is set very high ($5 \times 10^{10}\,\mathrm{m^2\,m^{-3}}$), the difference between the explicit and implicit cases is still evident. It can be found that explicit cases still have higher velocity than the implicit cases on the lateral sides and also on the wake flow. This is probably because no matter how high the LAD value is set, the implicit models always allow some of the wind flow into the porous cells, which results in less acceleration of the wind on the lateral sides of the models

as the volume flow rate must remain constant. The volume flow rate is the volume of fluid that passes through a certain cross-sectional face per unit time, which can be calculated by multiplying the area of the cross-sectional face by the average velocity of flow perpendicular to the face. For the explicit cases, the velocity inside the explicit tree models is zero as no volumes used for simulation exist there, and therefore the wind around the models is accelerated to keep the volumetric flow rate constant. Figure 5.5 indicates the stream trace for test case 1 (LEFT) and test case 5 (RIGHT), where the subplot (f) clearly shows the implicit model with LAD $= 5 \times 10^{10} \, \mathrm{m^2 \, m^{-3}}$ still have flow inside while the explicit model (c) does not.
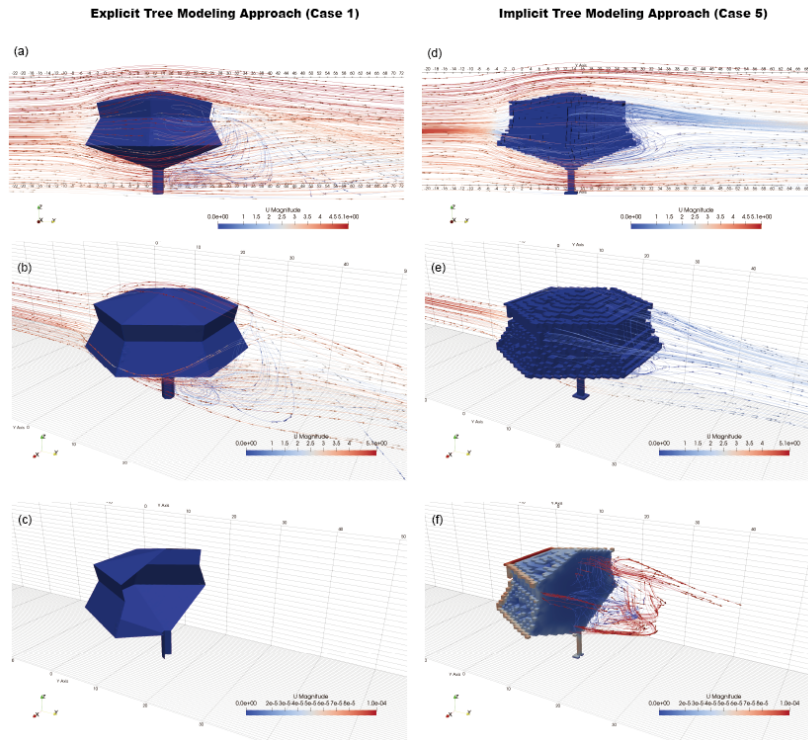


Figure 5.5.: Stream trace for test case 1 (LEFT) and test case 5 (RIGHT)

**2. Characteristics of $C_{ex-im}$ at trunk:**

In the upper and lower part of the wake of tree trunk, where the horseshoe vortex often occurs, the explicit cases have lower velocity than the implicit cases, while the opposite is true in the middle of the wake. By looking separately at the $U_{ex}$ and $U_{im}$ plots used to obtain the $C_{ex-im}$ plots (figure 5.3, and case 2 and 6 in figure C.1), it can be found that this is because the horseshoe vortex of the explicit cases spreads up and down and the low velocity region is concentrated near the horseshoe vortex, while the horseshoe vortex of the implicit cases spreads less up and down and the low velocity region is more concentrated in the middle part of the wake. This may be related to the fact that the explicit trunk model has sharper edges, and it prevents wind from entering the interior of it, resulting in higher velocity and stronger shear force of its side vortex. This is actually present in tree canopy as well, as shown in figure 5.3.

One unexpected observation is the lateral sides of trunk models in the subplot A-2 in figure

5.4 are shown in blue, meaning the explicit case has lower velocity than the implicit case here. This is not consistent with the previous analysis of volume flow rate. In fact, this situation only occurs in A-2, but not in B-2 in figure 5.4, nor in C-2 or D-2 in figure 5.6. Observing figure 5.2, we can find that other models (B, C, D) have a wider canopy bottom and lower trunk height compared to LoD2 broadleaf models (A), which may be one of the reasons for the above situation. Another possible reason could be the difference between the explicit mesh models and the corresponding implicit porosity models. Observing the trunk parts in the four subplots, we can find the size of the implicit trunk model in (A) is smaller than that of the explicit trunk model, while others (B, C, D) have the exact opposite situation.

**3. Difference between LoD2 and LoD3:**

The most obvious differences occur in the leeward cavity and the middle of the tree wake, where the red areas are relatively more and larger in LoD3 cases. This may be related to the representation of the model surface, where the LoD3 models are more rounded and has fewer rough and sharp edges compared to the LoD2 models.

**4. Characteristics of stream trace:**

In addition, more interesting information can be seen in figure 5.5. As showns in subplots (a), (b), (d) and (e), the explicit case has a recirculation vortex in the leeward cavity and there is some downward wind flow in the wake; on the contrary the implicit case does not have a clear recirculation vortex and its wake flows upward.

## 5.1.2. Conifer tree

The flow velocity magnitude predictions for case 7-12 are displayed in figure C.2 in Appendix C. Figure 5.6 illustrates the $C_{ex-im}$ obtained from case 7-12.
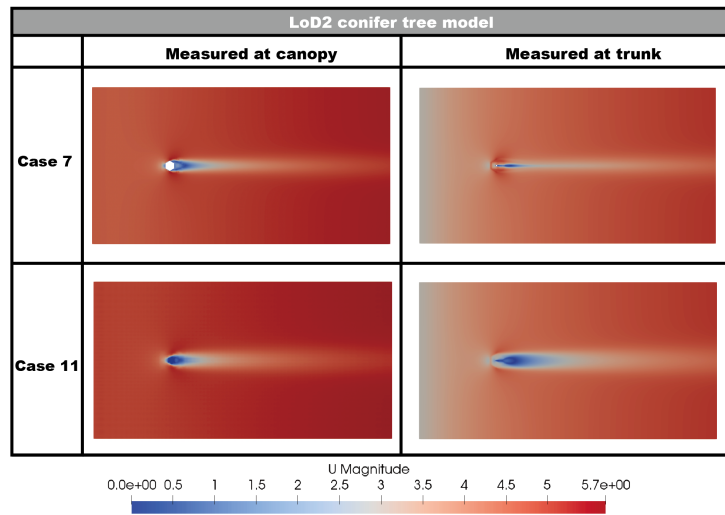


Figure 5.7.: Velocity magnitude for test case 7 and test case 11

**1. Characteristics of $C_{ex-im}$ at canopy:**
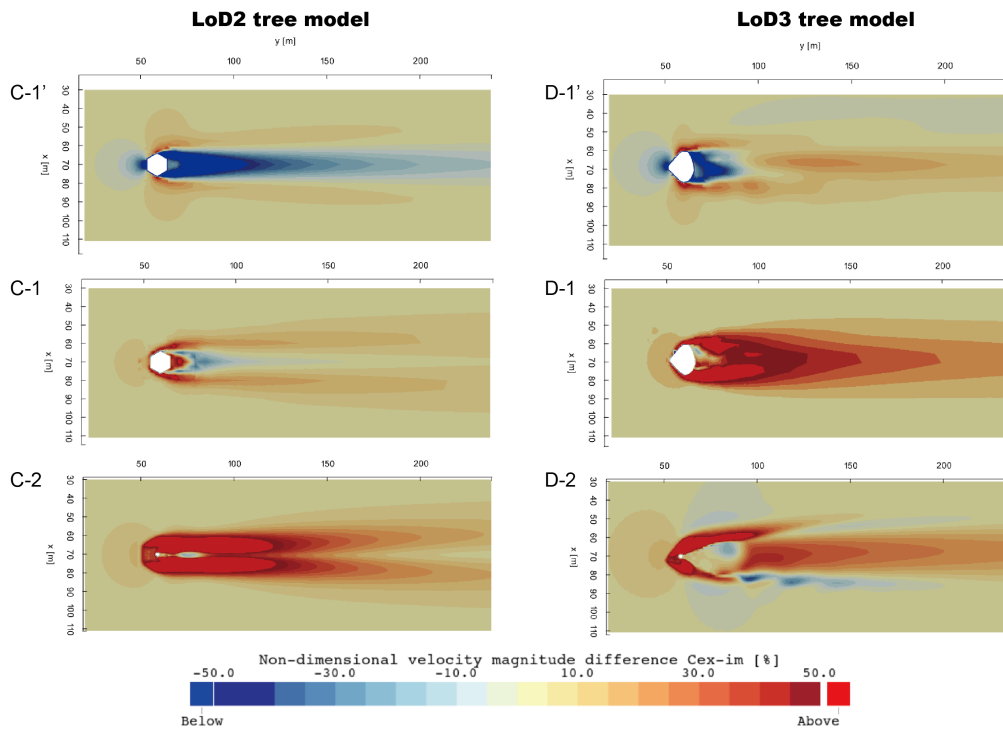
Figure 5.6.: $C_{ex-im}$ for conifer tree models. (C-1') difference between LoD2 explict conifer & LoD2 implicit conifer with LAD = 1.4, measured at canopy; (D-1') difference between LoD3 explict conifer & LoD3 implicit conifer with LAD = 1.4, measured at canopy; (C-1) difference between LoD2 explict conifer & LoD2 implicit conifer with LAD = 5e10, measured at canopy; (D-1) difference between LoD3 explict conifer & LoD3 implicit conifer with LAD = 5e10, measured at canopy; (C-2) difference between LoD2 explict conifer & LoD2 implicit conifer with LAD = 5e10, measured at trunk; (D-2) difference between LoD3 explict conifer & LoD3 implicit conifer with LAD = 5e10, measured at trunk;

The maximum difference from the $C_{ex-im}$ plots for broadleaf tree models occurs in C-1' and C-1, both using LoD2 models. Contrary to A-1' and A-1, the middle part of the tree wake in C-1' and C-1 shows that the explicit cases have a slower wind speed than the implicit cases here.

Looking at the $U_{ex}$ (figure 5.7 LEFT) plot and the $U_{im}$ plot (figure 5.7 RIGHT) used to obtain the C-1 plot in figure 5.6 and compare them with figure 5.3, it can be found that this is because the case 7 does not have a clear horseshoe/wake vortex spreading up and down at canopy but have a low velocity region concentrated in the middle of the tree wake similar to that of case 11.

**2. Characteristics of $C_{ex-im}$ at trunk:**

Compared C-2 and D-2 in figure 5.6 with A-2 and B-2 in figure 5.4, we can find the maximum difference occurs in C-2. It shows that the explicit case have higher velocity in the upper and lower part of the wake of tree trunk, while the opposite is true in the middle of the wake. Similar to the characteristics of $C_{ex-im}$ at canopy, this is because the case 7 does not have a

clear horseshoe/wake vortex spreading up and down at trunk either.

**3. Difference between LoD2 and LoD3:**

The characteristics of LoD3 conifer cases ( figure 5.6 RIGHT ) at the middle of tree wake are almost opposite to LoD2 conifer cases ( figure 5.6 LEFT ). However, although the characteristics of LoD2 conifer cases differs significantly from that of broadleaf cases (figure 5.4), the difference between LoD3 conifer cases and broadleaf cases is not significant.

**4. Characteristics of stream trace:**

Figure 5.8 and 5.9 show the stream trace for LoD2 cases and LoD3 cases, respectively. It can be found that cases 7,8,11 and 12 all form a clear recirculation vortex in the leeward cavity.
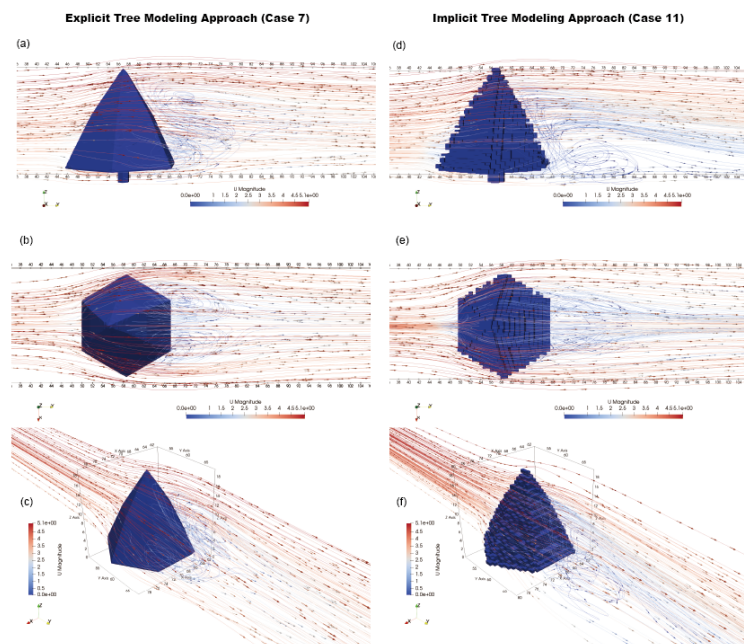


Figure 5.8.: Stream trace for test case 7 (LEFT) and test case 11 (RIGHT)
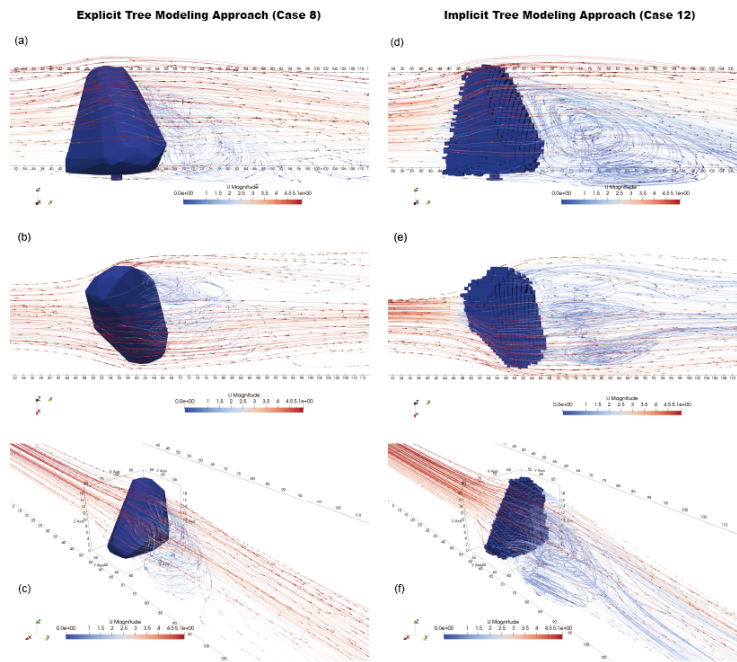
Figure 5.9.: Stream trace for test case 8 (LEFT) and test case 12 (RIGHT)

### 5.1.3. Conclusion

This chapter investigates the difference between the explicit and implicit tree modeling approaches by analyzing the characteristics of $C_{ex-im}$ of the isolated tree cases. It also investigates the impact of tree LoDs and tree shapes on the characteristics of $C_{ex-im}$ by comparing the difference of $C_{ex-im}$ between cases using a LoD2 / broadleaf tree model and those using a LoD3 / conifer tree model. The following conclusions can be summarized:

- No matter how high the LAD value is set, the implicit models always allow some of the wind flow into the porous cells, which results in smaller wind acceleration on the lateral sides of tree models.

- The size of an explicit tree model and the corresponding implicit tree model, especially for tree trunks, are hardly to be identical, which is related to the fineness of the CFD computational mesh. This may lead to abnormal simulation results. For instance A-2 in figure 5.4 shows the higher wind acceleration on the lateral sides of the trunk of the explicit tree model, which may be due to the smaller size of porous cells marked as trunk compared to the explicit trunk geometry.

- The implicit models tend to form a low velocity region concentrated in the middle of the wake while the explicit models tend to form a horseshoe/wake vortex that spreads up and down from the wake.

- Different LoD leads to different characteristics of $C_{ex-im}$ in the leeward cavity and the middle of the tree wake.

37

- Cases using a LoD2 conifer tree model have the most different characteristics of $C_{ex-im}$. This is mainly because case 7 that has the LoD2 conifer tree modeled explicitly does not form a horseshoe/wake vortex spreading up and down from the wake, unlike the cases using a broadleaf tree model or a LoD3 conifer model. This may be related to the shape features of the LoD2 conifer tree model, the details of which need to be further investigated.

## 5.2. CFD predictions: idealized street canyon

To understand whether the impact of LoDs on wind flow within the street canyon is influenced by canopies LAD values, seven LAD values were considered: $0.2, 0.6, 1.0, 1.4, 1.6, 1.8$ and $2.2$. Also, velocity magnitude is measured on horizontal planes at heights of $z = 1.75, 6, 9, 12, 15$ and $18$ m. Table 5.3 summarizes the configurations of street canyon cases. The relationship between these measured heights and the tree models is shown in Figure 5.10.

Table 5.3.: Idealized street canyon test cases

| Case ID | Inflow direction | Tree shape | LoD of tree | LAD value ($m^2\,m^{-3}$) | Measurement Height |
|---|---|---|---|---|---|
| 13 | Perpendicular to buildings | Broadleaf | 2 | 0.2, 0.6, 1.0, 1.4, 1.8, 2.2 | 1.75m, 6m, 9m, 12m, 15m, 18m |
| 14 | | | 3 | | |
| 15 | | Conifer | 2 | | |
| 16 | | | 3 | | |
| 17 | Parallel to buildings | Broadleaf | 2 | | |
| 18 | | | 3 | | |
| 19 | | Conifer | 2 | | |
| 20 | | | 3 | | |
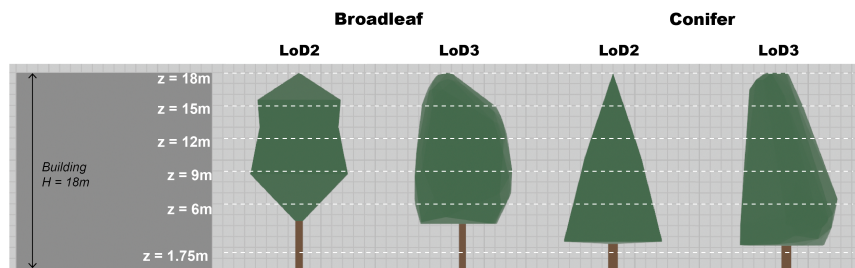


Figure 5.10.: Tree models and the measurement heights

Similar to isolated cases, cases listed in table 5.3 need to be compared in pairs to obtain the non-dimensional velocity magnitude difference ($C_{ex-im}$ or $C_{l2-l3}$). Since the difference between the implicit and explicit tree modeling approaches has been explained by the isolated tree cases, the street canyon cases focus on investigating the impact of tree LoDs, and thus $C_{l2-l3}$ is used here (e.g. case 13 minus 14 then normalized by $U_{ref}$). There are 144 $C_{l2-l3}$ plots in total (Appendix D). We can see that for most cases, the absolute values of $C_{l2-l3}$ are below 15%, which means that the velocity magnitude differences between LoD2 and LoD3 cases are below $0.5$ m/s.

The differences between them are difficult to distinguish clearly with the naked eye and need to be described in a more quantitative way. Thus, the following two sections will analyze the characteristics of $C_{l2-l3}$ within the street canyon by comparing the mean, confidence interval, distribution and values on probe lines for different wind directions.

## 5.2.1. Inflow direction perpendicular to buildings

Figure 5.11 shows the mean and 95 % confidence interval of $C_{l2-l3}$ for the broadleaf and conifer tree models, respectively. To understand the distribution of $C_{l2-l3}$ at different heights, figure D.5 in Appendix D also introduces violin plots that reveal medians, interquartile range, outliers, and kernel density estimates. In order to improve readability, figure D.5 below displays several examples of the violin plots.

Both of the above plots are summary analyses of $C_{l2-l3}$ within the street canyon at each measurement height and cannot show the characteristics of $C_{l2-l3}$ at different locations. Therefore, three probe lines were used to obtain sample data of $U$ at different locations for each measurement height. The locations of these probe lines and the corresponding $C_{l2-l3}$ sample values are presented in figure D.8 in Appendix D and several examples can be found in figure 5.13.

Looking at these figures, the following information can be found:

**1. Mean and 95 % confidence interval:**
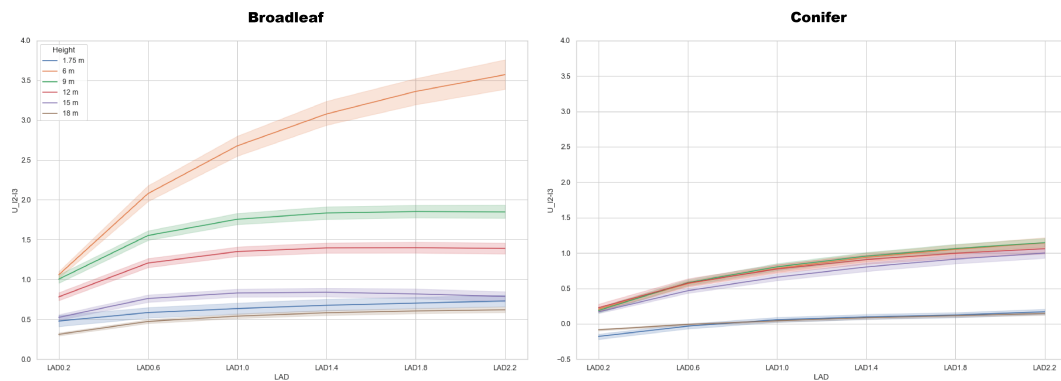


Figure 5.11.: Mean and 95% confidence interval for $C_{l2-l3}$ within the street canyon (perpendicular inflow direction)

In most cases, the averaged velocity magnitude of LoD2 cases ($U_{lod2}$) within the street canyon is greater than that of LoD3 cases ($U_{lod3}$).

The higher the LAD, the larger the mean and the wider the confidence interval. This shows that the higher the LAD, the more significant the difference between $U_{lod2}$ and $U_{lod3}$. When looking at the slope/steepness of each line, we can see that the rate of change of $U_{lod2}$ is greater when the LAD value is below 1.4. This can also be observed in figure D.8, where the differences between LAD 2.2 and 1.8 $m^2\,m^{-3}$ are clearly smaller than the differences between LAD 1.2 and 0.6 $m^2\,m^{-3}$ (the same is true for the parallel inflow direction cases shown in figure D.10). These imply that changing the LAD values does make difference to the impact

of tree LoDs, and the influence of LAD can be more noticeable when its value is lower than $1.4\,\text{m}^2\,\text{m}^{-3}$.

For broadleaf cases, the most obvious difference between $U_{lod2}$ and $U_{lod3}$ occurs at the height of $z = 6\,\text{m}$, especially with LAD $= 2.2\,\text{m}^2\,\text{m}^{-3}$, while the minimum difference happens at the height of $z = 18\,\text{m}$. The difference between $U_{lod2}$ and $U_{lod3}$ in conifer cases was overall weaker than in broad leaf cases. The smallest $C_{l2-l3}$ means and standard deviations happen at the height of $z = 1.75\,\text{m}$ and $18\,\text{m}$, while there is little difference in $C_{l2-l3}$ at other measurement heights.

**2. Violin plots:**
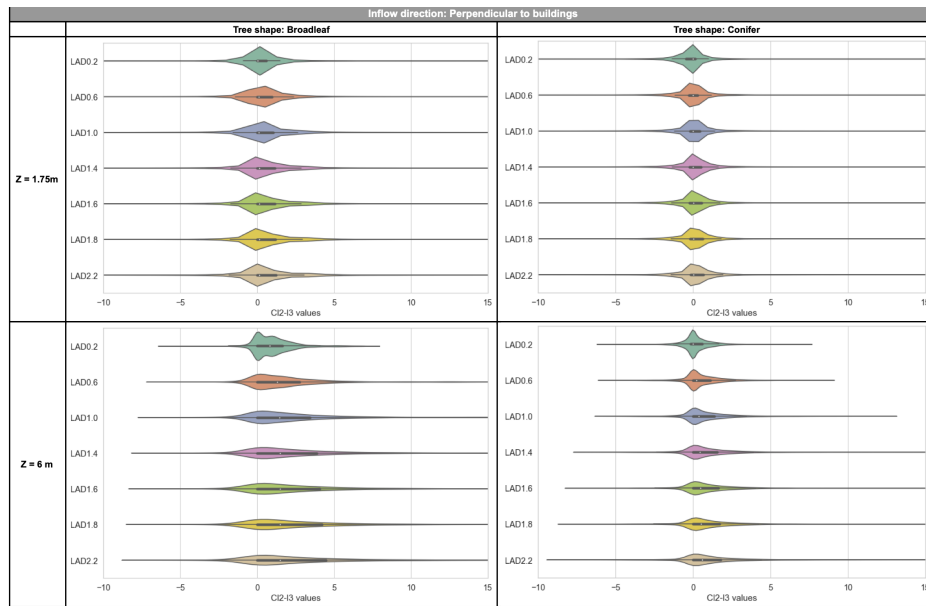


Figure 5.12.: Examples of violin plots for $C_{l2-l3}$ within the street canyon at different height (perpendicular inflow direction)

Observing the violin plots, we can find the larger the LAD, the more spread out the distribution of $C_{l2-l3}$ values within the street canyon. Compared with broadleaf cases, conifer cases have a more concentrated distribution of $C_{l2-l3}$ values. Also, most of the subplots show that the distribution of $C_{l2-l3}$ has only one peak. At the measurement height of $z = 9\,\text{m}$ and $12\,\text{m}$, broadleaf cases tend to have two peaks.

**3. Sample values on probe lines:**

We can find the value of $C_{l2-l3}$ is higher at locations closer to tree models. Note that at $z = 1.75\,\text{m}$, the probe C-D cuts to explicit trunk models, and around these models CFD grid/mesh and predicted values change rapidly, which leads to some outliers.

The E-F probe located on the windward side of the downstream building seems to have more variation in $C_{l2-l3}$ values than the A-B probe.

Figure 5.13.: $C_{l2-l3}$ values on three probe lines at 6 m height within the street canyon (perpendicular inflow direction)

## 5.2.2. Inflow direction parallel to buildings

The mean and confidence interval plots of $C_{l2-l3}$ for the cases where inflow wind direction parallel to buildings are shown in figure 5.14. Figure D.9 and D.10 in Appendix D present the violin plots and plots over lines, respectively.

**1. Mean and 95 % confidence interval:**

Similarly, the slope of each line is greater when LAD value is below $1.4\,\mathrm{m^2\,m^{-3}}$. However, it is no longer the case that the larger the LAD, the larger the mean and the wider the interval. Moreover, the conifer and broadleaf cases suffered opposite patterns in the slope variation of the lines.

Compared to the cases with perpendicular inflow, the means and confidence intervals of $C_{l2-l3}$ are higher and wider. This means the relative velocity magnitude differences between LoD2 cases and LoD3 cases are more significant when the inflow direction is parallel to buildings. It is also worth noting that there are some instances where $C_{l2-l3}$ is negative which is not common in the cases with perpendicular inflow, such as the conifer cases at the measurement height of $z = 1.75\,\mathrm{m}$.

**2. Violin plots:**
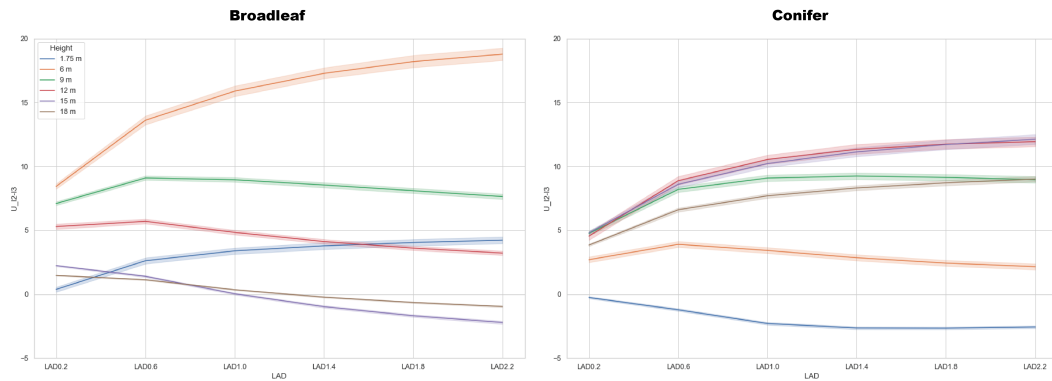
Figure 5.14.: Mean and 95% confidence interval for $C_{l2-l3}$ within the street canyon (parallel inflow direction)

The violin plots show the distribution of $C_{l2-l3}$ is more dispersed than that of the cases with an inflow perpendicular to buildings. Also, the larger the LAD, the more spread out the distribution. And we can find there are two peaks of the probability density, while there is only one peak for cases with a perpendicular inflow.

**3. Sample values on probe lines:**

Similarly, the differences between LAD 2.2 & 1.8 $\mathrm{m^2\,m^{-3}}$ are clearly smaller than the differences between LAD 1.2 & 0.6 $\mathrm{m^2\,m^{-3}}$. However, the value of $C_{l2-l3}$ is higher almost everywhere in the probe lines, not only closer to tree mode.

## 5.2.3. Conclusion

This chapter investigates the difference between the LoD2 and LoD3 tree models on wind flow within an idealized street canyon by analyzing the characteristics of the mean, confidence interval, distribution, and values on probe lines of $C_{l2-l3}$. It also investigates the impact of LAD values, tree shapes and inflow direction on the characteristics of $C_{l2-l3}$. The following conclusions can be summarized:

- For most scenarios, the velocity magnitude differences between the cases using LoD2 tree models and those using LoD3 are below 0.5 m/s.

- Generally, the average velocity magnitude of the cases using the LoD2 model is faster than those using the LoD3 model. As the mean values of $C_{l2-l3}$ shown in figure 5.11 and 5.14 are positive in most scenarios.

- The impact of tree LoDs on wind flow structure within the street canyon is generally more significant in the cases where the inflow direction is parallel to the buildings than in the case where the inflow direction is perpendicular to the buildings. As the mean values of $C_{l2-l3}$ shown in figure 5.14 are generally higher than those in figure 5.11.

- Changing the LAD values does make difference to the impact of tree LoDs, and the influence of LAD can be more noticeable when its value is lower than 1.4 $\mathrm{m^2\,m^{-3}}$. Also, the larger the LAD, the more spread out the distribution of $C_{l2-l3}$ values within the street canyon.

- With the inflow direction perpendicular to buildings, the higher the LAD, the larger the values of $C_{l2-l3}$. However, this is not true in the cases where the inflow direction is parallel to the building.

- The difference between $U_{lod2}$ and $U_{lod3}$, i.e. the absolute magnitude of $C_{l2-l3}$ values, is generally weaker in cases using conifer tree models than those using broadleaf tree models. This might be related to the geometry of tree canopy. Canopies of conifer trees are wider near the trunks, while canopies of broadlead trees are wider in the middle.

- The maximum or minimum values of $C_{l2-l3}$ appear at different heights for cases using broadleaf models and those using conifer models. For the measurement heights where the maximum values of $C_{l2-l3}$ happens, the higher the LAD, the higher the values of $C_{l2-l3}$.

## 5.3. CFD predictions: realistic urban geometry

### 5.3.1. Test cases setting

Since all four weather stations show the average wind direction of SSW in 2021 (figure 5.15), SSW is thus used as the inflow wind direction for the study area in this thesis. For the choice of inflow wind speed, as mentioned in section 3.4.2, it is better to use GEM wind speed rather than mean wind speed in order to take into account the effect of the gust wind speed on pedestrian wind comfort. The maximum 5-minute average wind speed from SSW direction measured at the nearest weather station (Rijnhaven) is used to calculate the GEM wind speed, which is around 3.7 m/s at 2 m height above the terrain.

With the wind direction of SSW, the bottom boundary of the CFD computational domain can be assumed to be water surface, except for the study area. The building models are obtained through the 3D BAG database [Dukai et al., 2021], and the LoD2 and LoD3 tree models are generated using the automatic reconstruction algorithm and the filtered AHN3 point cloud dataset provided by de Groot [2020]. For terrain, to reduce complexity, it is assumed to have a flat ground surface with 2 m height above the water surface. However, this left the bottom of some trees and buildings above the flat ground surface, creating gaps which the wind could pass through. In this thesis, Blender is used to manually align the models to solve this problem, and the final models can be found in figure 5.16.

According to the updated Davenport-Wieringa roughness classification [Blocken, 2015], values of the roughness length $z_0$ for water and terrain are set to 0.0002 m and 0.2 m respectively.
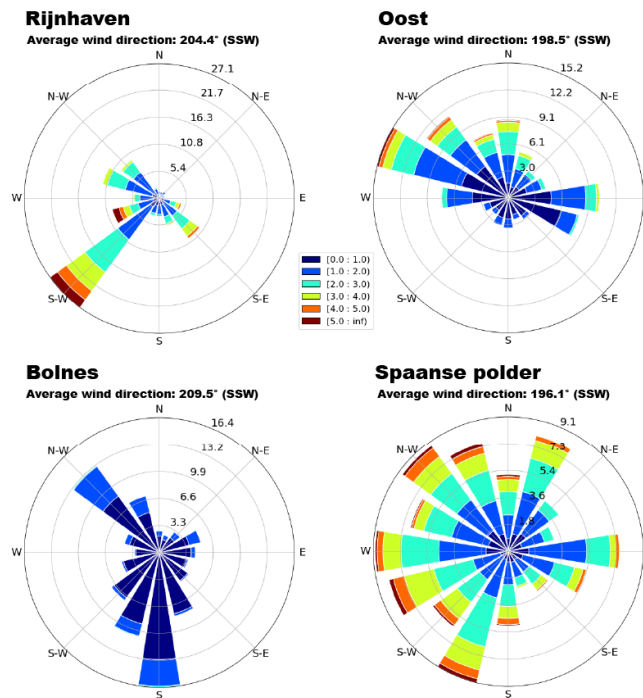
Figure 5.15.: Windrose plots and annual average wind direction data for 2021

## 5.3.2. Pedestrian wind comfort classification

Table 5.4.: Realistic urban geometry test cases.

| ID | *Inflow wind speed at* 2 m *height (*$\mathrm{m\,s^{-1}}$*)* | *LoD of trees* | *Tree modeling approach* | *LAD values (*$\mathrm{m^2\,m^{-3}}$*)* |
|----|----|----|----|----|
| 21 |  | without trees |  |  |
| 22 | 3.7 | LoD2 | Canopy: implicit; Trunk: explicit; | Broadleaf: 1.6; Conifer: 1.4; |
| 23 |  | LoD3 |  |  |
| 24 | 7.4 | LoD2 |  |  |
| 25 |  | LoD3 |  |  |

Table 5.4 summarizes the setting of the realistic urban geometry test cases. Case 21 uses only the building and terrain models for simulation, and the result can be used to compare with case 22 and 23 so that the impact of the trees on wind flow can be revealed. Apart from the calculated GEM wind speed, 3.7 m/s, 7.4 m/s is also used in the simulations (case 24 and 25), so that we can see if a higher inflow wind speed will change the impact of tree LoDs on pedestrian wind comfort. For each test case, tree trunks are modeled explicitly while tree canopies are modeled implicitly with LAD values of 1.6 and 1.4 $\mathrm{m^2\,m^{-3}}$ for broadleaf trees and conifer trees, respectively.

The criteria summarized in table 3.3 is used to generate the plots of pedestrian wind comfort classification at 1.75 m height. Figure E.2 shows the results for case 22 and 23. The results for
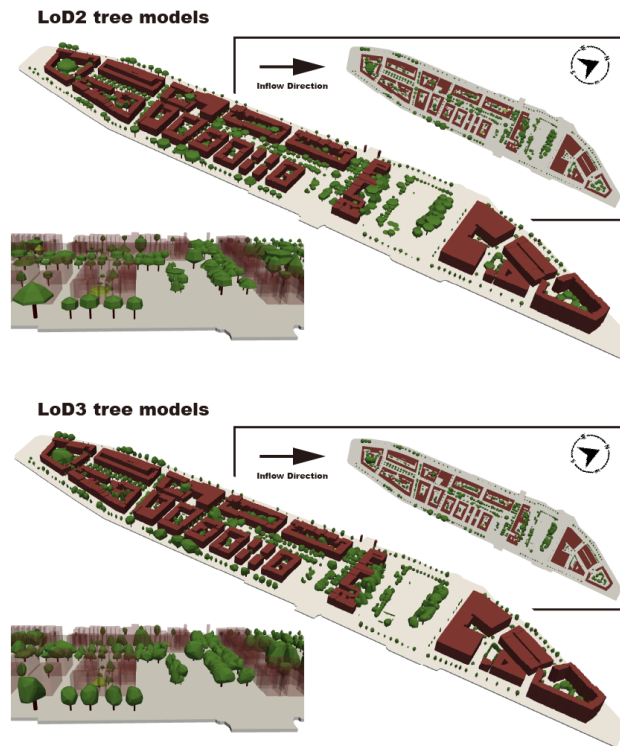
Figure 5.16.: realistic urban geometry models

the other cases can be found in appendix E.

With an inflow velocity of only 3.7 m/s at 2 m height above the terrain, the study area is mainly classified as Class A-D. Although the effect of trees is obvious when comparing figure E.2 and figure E.1, slight differences can be found between case 22 and 23. These differences between case 22 and 23 are mainly concentrated in the dense-tree areas and in some narrow passages between buildings, i.e. in the street canyons. For the open, non-tree concentrated spaces, the non-dimensional velocity magnitude differences between the two cases are around -5% to 5%.

Figure E.3 displays the pedestrian wind comfort classification at 1.75 m height for case 24 and 25, which have higher inflow velocity: 7.4 m/s. Compared figure E.3 and figure E.2, it can be found that most of the study area is still classified as A-C, i.e., good wind environment that can support frequent outdoor sitting use. It can be concluded that the overall wind environment situation in this study area is relatively good. Therefore, even though different tree LoDs result in velocity magnitude changes around the tree models, for this study area these changes do not make a great difference in the pedestrian perception of wind or acceptable activities at certain locations.

Looking at the non-dimensional velocity magnitude difference between case 22 and 23, and between case 24 and 25, we can see that there is no difference between the two $C_{l2-l3}$ plots. This indicates that increasing the inflow velocity does not change the $C_{l2-l3}$, in the other words, does not change the impact of tree LoDs on wind.
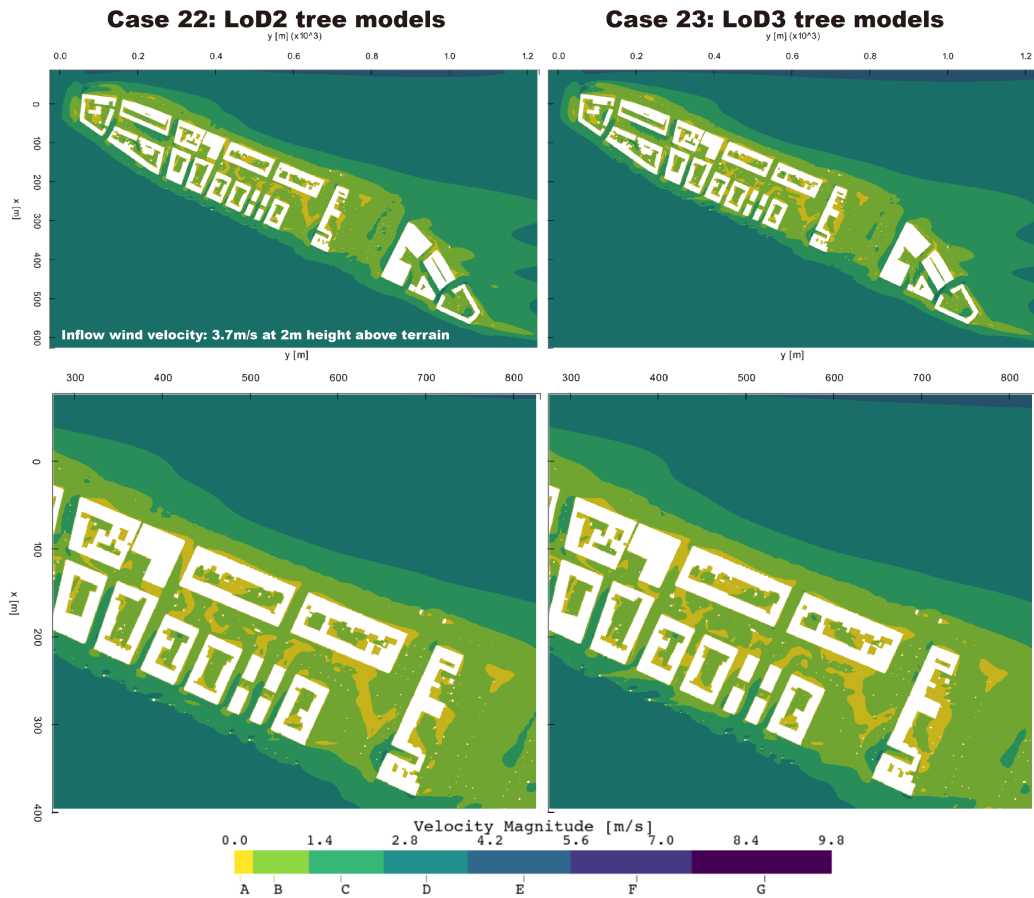
Figure 5.17.: Pedestrian wind comfort classification at 1.75 m height for Case 22 and 23

However, it is shown in figure E.4 that the differences between LoD2 case and LoD3 case are stronger in side/horseshoe vortex around some buildings and dense-tree areas, as well as in some street canyons. In these positions, the maximum and minimum values of $C_{l2-l3}$ can reach to roughly 36 and -44%, respectively. Therefore, for some urban areas with denser trees upstream, high-rise buildings and street canyons, the absolute values of $C_{l2-l3}$ could be higher and may cause greater changing in acceptable activities.

### 5.3.3. Conclusion

For Noordereiland, the study area of this thesis, the velocity magnitude differences between the LoD2 case and the LoD3 case is rather limited in most areas, with maximum differences in the order of 0.5 m/s. Thus it may be good enough to have the LoD2 tree model for wind environment studies in the region. However, the velocity magnitude differences are larger in side/horseshoe vortex around some buildings and dense-tree areas, as well as in some street canyons, where the values can reach to roughly 1.6 m/s. Therefore, for other urban areas with denser trees upstream, more high-rise buildings and street canyons, it may be better to use LoD3 tree models.
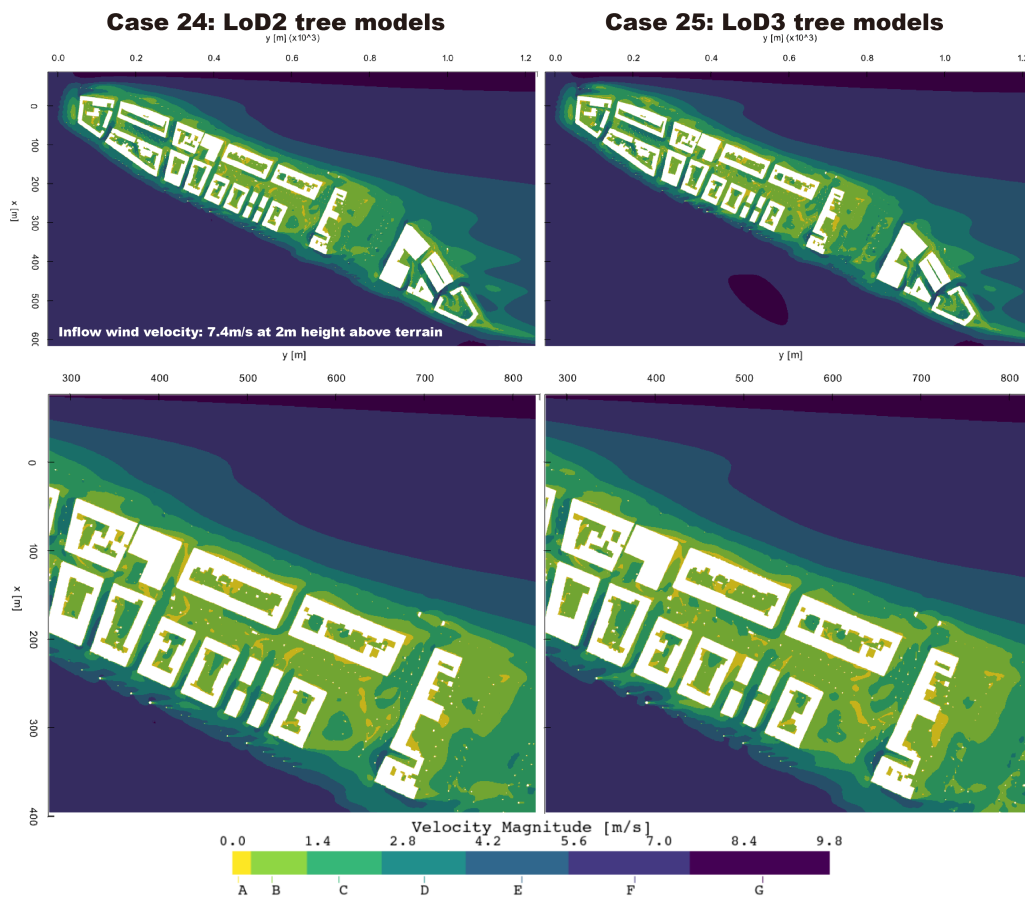
Figure 5.18.: Pedestrian wind comfort classification at 1.75 m height for case 24 and 25

# 6. Conclusion

In this chapter, the answers to the research questions of this thesis will be reviewed and the main findings will be summarized. Then, the limitations of this study will be reflected upon and corresponding suggestions for future related research are made.

## 6.1. Answers to research questions

The main research question for this thesis was:
*What is the impact of tree topology modelling for urban flow simulations?*

The focus of this thesis is on the effects of tree modeling approaches and tree LoDs on wind. However, it also explores whether differences in tree shapes, LAD values and wind directions would change the effects of tree modeling approaches and tree LoDs. Firstly, it can be concluded that different tree modeling approaches and tree LoDs lead to very diverse wind patterns. For instance, the implicit tree models always allow some of the wind flow into the porous cells. This makes the implicit models behave differently to the explicit models even if the tree drag (corresponding to values of LAD in this thesis) is set to extremely high. For LoD 2 and 3 tree models, the difference in wind velocity is mainly caused by the difference in tree geometry. Obtained by the reconstruction algorithm adapted from [de Groot, 2020], LoD2 tree models usually have a more regular and angular geometries, while the corresponding LoD3 tree models may not only have a more rounded geometries, but may also have different sizes of canopies and trunks. However, for the idealized street canyon and realistic urban geometry test cases simulated in this thesis, the velocity magnitude differences between the LoD2 cases and the LoD3 cases are rather limited. At the measurement height of 1.75 m above the terrain, the maximum velocity magnitude differences in most parts of the idealized street canyon and the realistic urban geometry are in the order of 0.5 m/s.

Secondly, it can be concluded that differences in tree shapes, LAD values and wind directions do change the effects of tree modeling approaches and tree LoDs. For instance, the case using an explicit LoD2 conifer tree model has a different wake flow pattern from other explicit cases. The following sections will focus on explaining the details.

- *How to obtain explicit tree models and implicit tree models from point cloud?*

The explicit tree models can be obtained using open point cloud datasets and automated reconstruction algorithms. In this thesis, the algorithm provided by [de Groot, 2020] is used as it can generate broadleaf and conifer tree models of different LoDs, which satisfies the research objectives. Then, it is necessary to convert the models to a format appropriate for CFD simulations, such as stl and obj. Also, since [de Groot, 2020] modeled each tree as one mesh object, for studies that require the tree canopy and trunk to be modeled separately, it might be necessary to split the mesh and to export the tree trunk and canopy as separate files.

*6. Conclusion*

With the explicit tree models prepared, they can be used to obtain the corresponding implicit tree models, i.e., marking the CFD volume cells that roughly account for the explicit tree models as porous cells. This can be done by using the snappyHexMeshDict and topoSetDict dictionary files. In order for the solver to take into account the values of LAD and $C_d$ for the implicit tree models, one needs to add the sink term ($S_{u_i}$) and source terms ($S_k$ and $S_\varepsilon$) in transport equations. This can be achieved by implementing a new porosity model and using fvOptions, or creating a new turbulence model and solver based on the existing source codes of OpenFOAM. The latter is chosen for this thesis as it is simpler and not prone to problems due to mishandling of dependency libraries. With the modified source codes compiled, LAD and $C_d$ values for each porous zone can be set using a setFieldDict dictionary file.

- **What is the difference between the simulation results using implicit tree models and explicit tree models?**

This thesis answers this question by analyzing the characteristics of $C_{ex-im}$ of isolated tree cases.

One important finding is that the implicit models always allow some of the wind flow into the porous cells no matter how high the LAD values are. This results in smaller wind acceleration on the lateral sides of implicit tree models, so that cases using an implicit tree model typically have lower velocity magnitude in tree wake than cases using an explicit tree model. In addition, for relatively small objects, such as tree trunks, insufficiently refined CFD grid/mesh may lead to abnormal simulation results. For example, higher wind acceleration on the lateral sides of trunk of an implicit tree model is found, which may be due to the smaller size of porous cells marked as trunk compared to the explicit trunk geometry. Therefore, we can conclude that it is not recommended to model tree trunks, branches or even buildings implicitly rather than explicitly in order to reduce the time spent on designing a good CFD grid/mesh. However, the above conclusions hold only for the porosity model used in this thesis ($S_{u_i}$, $S_k$ and $S_\varepsilon$); perhaps the situation would be different using other porosity definitions or immersed boundary methods.

Also, it can found that the implicit models tend to form a low velocity region concentrated in the middle of the wake while explicit models tend to form a horseshoe/wake vortex that spreads up and down.

- **What is the tree LoDs impact on urban wind flow simulations?**

This question is answered mainly by analysing the results of the idealized street canyon and realistic urban geometry cases.

Generally, cases using LoD2 tree models have higher velocity magnitude than those using LoD3 tree models.

From street canyon cases, we can see that for most scenarios, e.g. at the measurement height of 1.75 m, the absolute values of $C_{l2-l3}$ are below 15%, which means that the velocity magnitude differences between LoD2 and LoD3 cases are below 0.5 m/s. Similarly, for Noordereiland, study area of the realistic urban geometry cases, the maximum velocity magnitude differences between the LoD2 case and the LoD3 case is also in the order of 0.5 m/s. Therefore, we can conclude that the impact of tree LoDs on velocity magnitude is rather limited. For larger scale urban wind environment studies, perhaps the use of LoD2 tree model would be able to provide sufficiently accurate predictions.

However, from the Noordereiland cases, we can also find that the velocity magnitude differences between the LoD2 case and the LoD3 case can reach to roughly 1.6 m/s in side/horseshoe vortex around some buildings and dense-tree areas, as well as in some street canyons. Thus, for some urban areas with denser trees upstream, high-rise buildings and street canyons, different tree LoDs may cause greater changing in velocity magnitude and acceptable activities at certain locations. Therefore, for this type of study area where the wind environment may be more complex, perhaps the use of LoD3 tree models is a better choice.

In addition, using the algorithm from [de Groot, 2020], there is not much difference in the time to generate LoD2 and LoD3 tree models. Moreover, since both LoD2 and LoD3 tree models have only two parts, canopies and trunks, they are not particularly different in geometry, so the CFD simulation processing time is similar for both. Therefore, for studies with small study areas or relatively insensitive to computational time, LoD3 tree models can be used to obtain more accurate results.

- ***Does changing tree shapes (broadleaf or conifer) make any difference to the impact of tree LoDs?***

From the street canyon cases, we can find that the values of $C_{l2-l3}$ for conifer cases are overall lower than in broadleaf cases. This might be related to the geometry of tree canopy. Canopies of conifer trees are wider near the trunks, while canopies of broadlead trees are wider in the middle.

Also, the maximum or minimum values of $C_{l2-l3}$ appears at different heights for cases using broadleaf tree models and those using conifer models.

- ***Does changing the LAD value or wind direction make any difference to the impact of tree LoDs?***

First, changing the LAD values does make difference to the impact of tree LoDs. For instance, we can see that the larger the LAD, the more spread out the distribution of $C_{l2-l3}$ values within the street canyon. However, the influence of LAD can be more noticeable when its value is lower than $1.4\,\mathrm{m^2\,m^{-3}}$. Although the highest LAD value attempted in this thesis is $2.2\,\mathrm{m^2\,m^{-3}}$, it is conceivable from the data trend that the degree of changing of $C_{l2-l3}$ values will continue to decrease as the LAD values increase, and may eventually reach stability.

Secondly, different wind directions can also lead to difference characteristics of $C_{l2-l3}$. One obvious finding is that $C_{l2-l3}$ is generally higher in the cases where the inflow direction is parallel to the buildings. Also, with the inflow direction perpendicular to buildings, the higher the LAD, the larger the values of $C_{l2-l3}$. However, this is not true in the cases where the inflow direction is parallel to the building. Additionally, with an inflow direction perpendicular to buildings, higher values of $C_{l2-l3}$ often occur at locations closer to tree models; while with an inflow direction parallel to buildings, relatively similar values of $C_{l2-l3}$ are found at most locations along the probe lines.

## 6.2. Limitations

### 6.2.1. Limitations of preparing 3D models

The tree reconstruction algorithm used in this thesis is from [de Groot, 2020], which can automatically reconstruct tree point cloud data into tree mesh models in different LoD2. However, to save time and effort, this thesis did not adapt the algorithm for CFD simulations. Therefore, I had to rely on other software or tools to manually adapt the reconstructed tree models so that they can be used in CFD simulations, such as using Blender and FME to split the models and transform the formats.

Also, due to the limitations of the algorithm itself, most trees would be classified as broadleaf, while trees classified as conifer tend to have a strange geometry. Therefore, for the isolated tree and the idealized street canyon cases, I had to subjectively select broadleaf and conifer tree models that were relatively regular in geometry and clearly differed from each other in geometry from multiple reconstructed tree models. This also led to a lack of depth in the subsequent analysis of the impact of tree shapes.

In addition, in order to save time, I simplified the 3D models of the realistic urban geometry cases. Terrain model was assumed to have a flat ground surface, and tree and building models were manually aligned to the terrain. This made the ground too smooth compared to the real situation, and the height of the buildings and trees relative to the sea level were changed. This may led to a relatively high discrepancy between the analysis results of this thesis and the real situation.

### 6.2.2. Limitations of CFD simulations

Because of the relatively large number of test cases, I kept the definition of the conditions for achieving mesh independence relatively simple in order to make compromises in terms of time and computational resources. Moreover, I performed mesh independence verification using only one isolated tree test case (case 5) and one realistic urban geometry test case (case 22), both of which used LoD2 broadleaf tree models. Other test cases were assumed to be mesh independent since they had similar mesh designs to case 5 or 22.

Also, for some test cases, although the minimum $y^+$ values exceeded 30, the maximum $y^+$ values were too high to make the law of the wall valid. For instance, the maximum $y^+$ value for buildings in case 22 was roughly 3000. This means that mesh design could be improved further with longer time availability.

### 6.2.3. Limitations of results analysis

A relevant limitation of this study is that the results were not compared with a suitable data set from other literature or wind tunnel experiments, so the following question cannot be answered: which tree modeling approach, tree LoDs, or tree shape is closer to the 'ground truth'.

## 6.3. Recommendations and further improvements

First, additional tree models with diverse shapes and heights can be tried for simulation. In this way, we can get more knowledge about whether variations in tree features such as height, width, or canopy shape result in different characteristics of $C_{ex-im}$ or $C_{l2-l3}$.

Secondly, improvements could be made to the choice of LAD values for different trees. This thesis assumed that the LAD values for broadleaf and conifer trees in the realistic urban geometry cases were 1.6 and $1.4\,\mathrm{m^2\,m^{-3}}$, respectively. However, in theory, the LAD values should be related to tree shapes, height, and also seasons. Thus, calculating the LAD values of each tree model based on its geometry features allows the CFD predictions to more accurately reflect real world conditions.

Thirdly, besides wind velocity magnitude, cases can also be compared in terms of turbulent kinetic energy. This may further support some conclusions of this thesis.

In addition, the focus of this thesis is to investigate the effect of tree topology on wind flow, and further studies can use the results as a reference to investigate the effect of tree topology on gas/heat diffusion and numerous other concerns.

# A. Reproducibility self-assessment

## A.1. Self-reflection
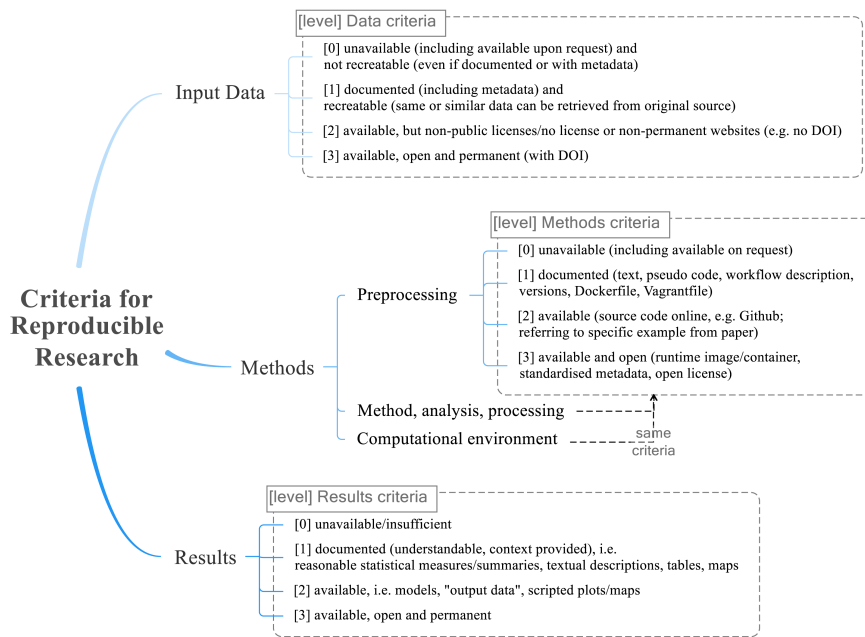


Figure A.1.: Reproducibility criteria to be assessed.

Table A.1.: Self-reflection on the reproducibility criteria

| Criteria | Grade | Reasons |
|---|---|---|
| Input data | 2 | Models are available on Github without DOI |
| Preprocessing | 3 | Available on Github |
| Methods | 3 | Available on Github |
| Computational environment | 3 | Open source software are used in this thesis |
| Results | 2 | The test cases in this study are relatively large and the simulation results take up more than 1Tb of space, so they are not stored on Github. However, the CFD setup files for each case are available on Github. The relevant plots can also be found in this thesis. |

# B. OpenFOAM implementations

## B.1. treekEpsilon.H

```
/*---------------------------------------------------------------------------*\
  =========                 |
  \\      /  F ield         | OpenFOAM: The Open Source CFD Toolbox
   \\    /   O peration     | Website:  https://openfoam.org
    \\  /    A nd           | Copyright (C) 2011-2019 OpenFOAM Foundation
     \\/     M anipulation  |
-------------------------------------------------------------------------------
License
    This file is part of OpenFOAM.

    OpenFOAM is free software: you can redistribute it and/or modify it
    under the terms of the GNU General Public License as published by
    the Free Software Foundation, either version 3 of the License, or
    (at your option) any later version.

    OpenFOAM is distributed in the hope that it will be useful, but WITHOUT
    ANY WARRANTY; without even the implied warranty of MERCHANTABILITY or
    FITNESS FOR A PARTICULAR PURPOSE.  See the GNU General Public License
    for more details.

    You should have received a copy of the GNU General Public License
    along with OpenFOAM.  If not, see <http://www.gnu.org/licenses/>.

Class
    Foam::RASModels::kEpsilon

Description
    Standard k-epsilon turbulence model for incompressible and compressible
    flows including rapid distortion theory (RDT) based compression term.

    Reference:
    \verbatim
        Standard model:
            Launder, B. E., & Spalding, D. B. (1972).
            Lectures in mathematical models of turbulence.

            Launder, B. E., & Spalding, D. B. (1974).
            The numerical computation of turbulent flows.
            Computer methods in applied mechanics and engineering,
```

```
            3(2), 269-289.

        For the RDT-based compression term:
            El Tahry, S. H. (1983).
            k-epsilon equation for compressible reciprocating engine flows.
            Journal of Energy, 7(4), 345-353.
    \endverbatim

    The default model coefficients are
    \verbatim
        treekEpsilonCoeffs
        {
            Cmu         0.09;
            C1          1.44;
            C2          1.92;
            C3          -0.33;
            sigmak      1.0;
            sigmaEps    1.3;
    betaP_       1.0;
    betaD        5.1;
    C4           0.9;
    C5           0.9;
        }
    \endverbatim

SourceFiles
    treekEpsilon.C

\*---------------------------------------------------------------------------*/

#ifndef treekEpsilon_H
#define treekEpsilon_H

#include "RASModel.H"
#include "eddyViscosity.H"


// * * * * * * * * * * * * * * * * * * * * * * * * * * * * * * * * * * * * * //

namespace Foam
{
namespace RASModels
{

/*---------------------------------------------------------------------------*\
                        Class kEpsilon Declaration
\*---------------------------------------------------------------------------*/

template<class BasicTurbulenceModel>
class treekEpsilon
```

```
:
    public eddyViscosity<RASModel<BasicTurbulenceModel>>
{
protected:

    // Protected data

        // Model coefficients
            dimensionedScalar Cmu_;
            dimensionedScalar C1_;
            dimensionedScalar C2_;
            dimensionedScalar C3_;
            dimensionedScalar sigmak_;
            dimensionedScalar sigmaEps_;

        // Canopy coefficients
            dimensionedScalar betaP_;
            dimensionedScalar betaD_;
            dimensionedScalar C4_;
            dimensionedScalar C5_;

        // Fields

            volScalarField k_;
            volScalarField epsilon_;
        //- tree canopy drag coefficient
            volScalarField plantCd_;
        //- leaf are density
            volScalarField leafAreaDensity_;


    // Protected Member Functions

        virtual void correctNut();
        virtual tmp<fvScalarMatrix> kSource() const;
        virtual tmp<fvScalarMatrix> epsilonSource() const;


public:

    typedef typename BasicTurbulenceModel::alphaField alphaField;
    typedef typename BasicTurbulenceModel::rhoField rhoField;
    typedef typename BasicTurbulenceModel::transportModel transportModel;


    //- Runtime type information
    TypeName("treekEpsilon");


    // Constructors
```

```cpp
    //- Construct from components
    treekEpsilon
    (
        const alphaField& alpha,
        const rhoField& rho,
        const volVectorField& U,
        const surfaceScalarField& alphaRhoPhi,
        const surfaceScalarField& phi,
        const transportModel& transport,
        const word& propertiesName = turbulenceModel::propertiesName,
        const word& type = typeName
    );

    //- Disallow default bitwise copy construction
    treekEpsilon(const treekEpsilon&) = delete;


//- Destructor
virtual ~treekEpsilon()
{}


// Member Functions

    //- Re-read model coefficients if they have changed
    virtual bool read();

    //- Return the effective diffusivity for k
    tmp<volScalarField> DkEff() const
    {
        return volScalarField::New
        (
            "DkEff",
            (this->nut_/sigmak_ + this->nu())
        );
    }

    //- Return the effective diffusivity for epsilon
    tmp<volScalarField> DepsilonEff() const
    {
        return volScalarField::New
        (
            "DepsilonEff",
            (this->nut_/sigmaEps_ + this->nu())
        );
    }

    //- Return the turbulence kinetic energy
    virtual tmp<volScalarField> k() const
```

```
        {
            return k_;
        }

        //- Return the turbulence kinetic energy dissipation rate
        virtual tmp<volScalarField> epsilon() const
        {
            return epsilon_;
        }

        //- Solve the turbulence equations and correct the turbulence viscosity
        virtual void correct();


    // Member Operators

        //- Disallow default bitwise assignment
        void operator=(const treekEpsilon&) = delete;
};


// * * * * * * * * * * * * * * * * * * * * * * * * * * * * * * * * * * * * * //

} // End namespace RASModels
} // End namespace Foam


// * * * * * * * * * * * * * * * * * * * * * * * * * * * * * * * * * * * * * //


// * * * * * * * * * * * * * * * * * * * * * * * * * * * * * * * * * * * * * //

#endif

// ************************************************************************* //
```

## B.2. treekEpsilon.C

```
\*---------------------------------------------------------------------------*/

#include "treekEpsilon.H"
#include "fvOptions.H"
#include "bound.H"
#include "fvMesh.H"


// * * * * * * * * * * * * * * * * * * * * * * * * * * * * * * * * * * * * * //
```

*B. OpenFOAM implementations*

```
namespace Foam
{
namespace RASModels
{

// * * * * * * * * * * * * Protected Member Functions  * * * * * * * * * * * //

template<class BasicTurbulenceModel>
void treekEpsilon<BasicTurbulenceModel>::correctNut()
{
    this->nut_ = Cmu_*sqr(k_)/epsilon_;
    this->nut_.correctBoundaryConditions();
    fv::options::New(this->mesh_).correct(this->nut_);

    BasicTurbulenceModel::correctNut();
}


template<class BasicTurbulenceModel>
tmp<fvScalarMatrix> treekEpsilon<BasicTurbulenceModel>::kSource() const
{
    return tmp<fvScalarMatrix>
    (
        new fvScalarMatrix
        (
            k_,
            dimVolume*this->rho_.dimensions()*k_.dimensions()
            /dimTime
        )
    );
}


template<class BasicTurbulenceModel>
tmp<fvScalarMatrix> treekEpsilon<BasicTurbulenceModel>::epsilonSource() const
{
    return tmp<fvScalarMatrix>
    (
        new fvScalarMatrix
        (
            epsilon_,
            dimVolume*this->rho_.dimensions()*epsilon_.dimensions()
            /dimTime
        )
    );
}


// * * * * * * * * * * * * * * * Constructors  * * * * * * * * * * * * * * * //
```

```cpp
template<class BasicTurbulenceModel>
treekEpsilon<BasicTurbulenceModel>::treekEpsilon
(
    const alphaField& alpha,
    const rhoField& rho,
    const volVectorField& U,
    const surfaceScalarField& alphaRhoPhi,
    const surfaceScalarField& phi,
    const transportModel& transport,
    const word& propertiesName,
    const word& type
)
:
    eddyViscosity<RASModel<BasicTurbulenceModel>>
    (
        type,
        alpha,
        rho,
        U,
        alphaRhoPhi,
        phi,
        transport,
        propertiesName
    ),

    Cmu_
    (
        dimensioned<scalar>::lookupOrAddToDict
        (
            "Cmu",
            this->coeffDict_,
            0.09
        )
    ),
    C1_
    (
        dimensioned<scalar>::lookupOrAddToDict
        (
            "C1",
            this->coeffDict_,
            1.44
        )
    ),
    C2_
    (
        dimensioned<scalar>::lookupOrAddToDict
        (
            "C2",
            this->coeffDict_,
            1.92
```

```
        )
    ),
    C3_
    (
        dimensioned<scalar>::lookupOrAddToDict
        (
            "C3",
            this->coeffDict_,
            0
        )
    ),
    sigmak_
    (
        dimensioned<scalar>::lookupOrAddToDict
        (
            "sigmak",
            this->coeffDict_,
            1.0
        )
    ),
    sigmaEps_
    (
        dimensioned<scalar>::lookupOrAddToDict
        (
            "sigmaEps",
            this->coeffDict_,
            1.3
        )
    ),
    betaP_
    (
        dimensioned<scalar>::lookupOrAddToDict
          (
            "betaP",
            this->coeffDict_,
            1.0
          )
    ),
    betaD_
    (
        dimensioned<scalar>::lookupOrAddToDict
          (
            "betaD",
            this->coeffDict_,
            5.03
          )
    ),
    C4_
    (
        dimensioned<scalar>::lookupOrAddToDict
```

```
            (
                "C4",
                this->coeffDict_,
                0.78
            )
    ),
    C5_
    (
        dimensioned<scalar>::lookupOrAddToDict
          (
                "C5",
                this->coeffDict_,
                0.78
          )
     ),


    k_
    (
        IOobject
        (
            IOobject::groupName("k", alphaRhoPhi.group()),
            this->runTime_.timeName(),
            this->mesh_,
            IOobject::MUST_READ,
            IOobject::AUTO_WRITE
        ),
        this->mesh_
    ),
    epsilon_
    (
        IOobject
        (
            IOobject::groupName("epsilon", alphaRhoPhi.group()),
            this->runTime_.timeName(),
            this->mesh_,
            IOobject::MUST_READ,
            IOobject::AUTO_WRITE
        ),
        this->mesh_
    ),
    plantCd_
    (
        IOobject
        (
            "plantCd",
            "2",
            this->mesh_,
            IOobject::MUST_READ,
            IOobject::AUTO_WRITE
```

```
        ),
        this->mesh_
    ),
    leafAreaDensity_
    (
        IOobject
        (
            "leafAreaDensity",
            "2",
            this->mesh_,
            IOobject::MUST_READ,
            IOobject::AUTO_WRITE
        ),
        this->mesh_
    )
{
    bound(k_, this->kMin_);
    bound(epsilon_, this->epsilonMin_);

    if (type == typeName)
    {
        this->printCoeffs(type);
    }
}


// * * * * * * * * * * * * * * * Member Functions  * * * * * * * * * * * * * //

template<class BasicTurbulenceModel>
bool treekEpsilon<BasicTurbulenceModel>::read()
{
    if (eddyViscosity<RASModel<BasicTurbulenceModel>>::read())
    {
        Cmu_.readIfPresent(this->coeffDict());
        C1_.readIfPresent(this->coeffDict());
        C2_.readIfPresent(this->coeffDict());
        C3_.readIfPresent(this->coeffDict());
        sigmak_.readIfPresent(this->coeffDict());
        sigmaEps_.readIfPresent(this->coeffDict());
        betaP_.readIfPresent(this->coeffDict());
        betaD_.readIfPresent(this->coeffDict());
        C4_.readIfPresent(this->coeffDict());
        C5_.readIfPresent(this->coeffDict());

        return true;
    }
    else
    {
        return false;
    }
```

```
}


template<class BasicTurbulenceModel>
void treekEpsilon<BasicTurbulenceModel>::correct()
{
    if (!this->turbulence_)
    {
        return;
    }

    // Local references
    const alphaField& alpha = this->alpha_;
    const rhoField& rho = this->rho_;
    const surfaceScalarField& alphaRhoPhi = this->alphaRhoPhi_;
    const volVectorField& U = this->U_;
    volScalarField& nut = this->nut_;
    fv::options& fvOptions(fv::options::New(this->mesh_));

    eddyViscosity<RASModel<BasicTurbulenceModel>>::correct();

    volScalarField::Internal divU
    (
        fvc::div(fvc::absolute(this->phi(), U))().v()
    );

    tmp<volTensorField> tgradU = fvc::grad(U);
    volScalarField::Internal G
    (
        this->GName(),
        nut.v()*(dev(twoSymm(tgradU().v())) && tgradU().v())
    );
    tgradU.clear();

    // Update epsilon and G at the wall
    epsilon_.boundaryFieldRef().updateCoeffs();

    // Dissipation equation
    tmp<fvScalarMatrix> epsEqn
    (
        fvm::ddt(alpha, rho, epsilon_)
      + fvm::div(alphaRhoPhi, epsilon_)
      - fvm::laplacian(alpha*rho*DepsilonEff(), epsilon_)
     ==
        C1_*alpha()*rho()*G*epsilon_()/k_()
      - fvm::SuSp(((2.0/3.0)*C1_ - C3_)*alpha()*rho()*divU, epsilon_)
      - fvm::Sp(C2_*alpha()*rho()*epsilon_()/k_(), epsilon_)
      + epsilonSource()
      + fvOptions(alpha, rho, epsilon_)
      + fvm::Sp(plantCd_()*leafAreaDensity_()/k_()*(C4_*betaP_*pow(mag(U()),3)
```

```
        - C5_*betaD_*k_()*mag(U())), epsilon_) //Source Term
      //+ epsilonSource()
      //+ fvOptions(alpha, rho, epsilon_)
    );

    epsEqn.ref().relax();
    fvOptions.constrain(epsEqn.ref());
    epsEqn.ref().boundaryManipulate(epsilon_.boundaryFieldRef());
    solve(epsEqn);
    fvOptions.correct(epsilon_);
    bound(epsilon_, this->epsilonMin_);

    // Turbulent kinetic energy equation
    tmp<fvScalarMatrix> kEqn
    (
        fvm::ddt(alpha, rho, k_)
      + fvm::div(alphaRhoPhi, k_)
      - fvm::laplacian(alpha*rho*DkEff(), k_)
     ==
        alpha()*rho()*G
      - fvm::SuSp((2.0/3.0)*alpha()*rho()*divU, k_)
      - fvm::Sp(alpha()*rho()*epsilon_()/k_(), k_)
      + fvm::Sp(plantCd_() *leafAreaDensity_() / k_()*(betaP_ *
        pow(mag(U()),3)- betaD_ * k_() * mag(U())), k_)//Source Term
      + kSource()
      + fvOptions(alpha, rho, k_)
    );

    kEqn.ref().relax();
    fvOptions.constrain(kEqn.ref());
    solve(kEqn);
    fvOptions.correct(k_);
    bound(k_, this->kMin_);

    correctNut();
}


// * * * * * * * * * * * * * * * * * * * * * * * * * * * * * * * * * * * * //

} // End namespace RASModels
} // End namespace Foam

// ************************************************************************* //
#include "addToRunTimeSelectionTable.H"
#include "makeTurbulenceModel.H"
#include "RASModel.H"
#include "transportModel.H"
#include "incompressibleTurbulenceModel.H"
#include "IncompressibleTurbulenceModel.H"
```

```
namespace Foam
{
    typedef IncompressibleTurbulenceModel<transportModel>
    transportModelIncompressibleTurbulenceModel;
    typedef RASModel<transportModelIncompressibleTurbulenceModel>
    RAStransportModelIncompressibleTurbulenceModel;
}

makeTemplatedTurbulenceModel(transportModelIncompressibleTurbulenceModel, RAS, treekEpsilon)
```

## B.3. UEqn.H

```
    // Momentum predictor

    MRF.correctBoundaryVelocity(U);

    tmp<fvVectorMatrix> tUEqn
    (
        fvm::div(phi, U)
      + MRF.DDt(U)
      + turbulence->divDevReff(U)
     ==
        fvOptions(U)
      - fvm::Sp(plantCd * leafAreaDensity * mag(U), U)
    );
    fvVectorMatrix& UEqn = tUEqn.ref();

    UEqn.relax();

    fvOptions.constrain(UEqn);

    if (simple.momentumPredictor())
    {
        solve(UEqn == -fvc::grad(p));

        fvOptions.correct(U);
    }
```

## B.4. createFields.H

```
Info<< "Reading field p\n" << endl;
volScalarField p
(
```

```
    IOobject
    (
        "p",
        runTime.timeName(),
        mesh,
        IOobject::MUST_READ,
        IOobject::AUTO_WRITE
    ),
    mesh
);

Info<< "Reading field U\n" << endl;
volVectorField U
(
    IOobject
    (
        "U",
        runTime.timeName(),
        mesh,
        IOobject::MUST_READ,
        IOobject::AUTO_WRITE
    ),
    mesh
);

Info<< "Reading field leafAreaDensity from time 2\n" << endl;
volScalarField leafAreaDensity
(
    IOobject
    (
        "leafAreaDensity",
        "2",
        mesh,
        IOobject::MUST_READ,
        IOobject::AUTO_WRITE
    ),
    mesh
);

Info<< "Reading field plantCd from time 2\n" << endl;
volScalarField plantCd
(
    IOobject
    (
        "plantCd",
        "2",
        mesh,
        IOobject::MUST_READ,
        IOobject::AUTO_WRITE
    ),
```

```
    mesh
);

#include "createPhi.H"


label pRefCell = 0;
scalar pRefValue = 0.0;
setRefCell(p, simple.dict(), pRefCell, pRefValue);
mesh.setFluxRequired(p.name());


singlePhaseTransportModel laminarTransport(U, phi);

autoPtr<incompressible::turbulenceModel> turbulence
(
    incompressible::turbulenceModel::New(U, phi, laminarTransport)
);

#include "createMRF.H"
#include "createFvOptions.H"
```

# C. Plots for the isolated tree cases
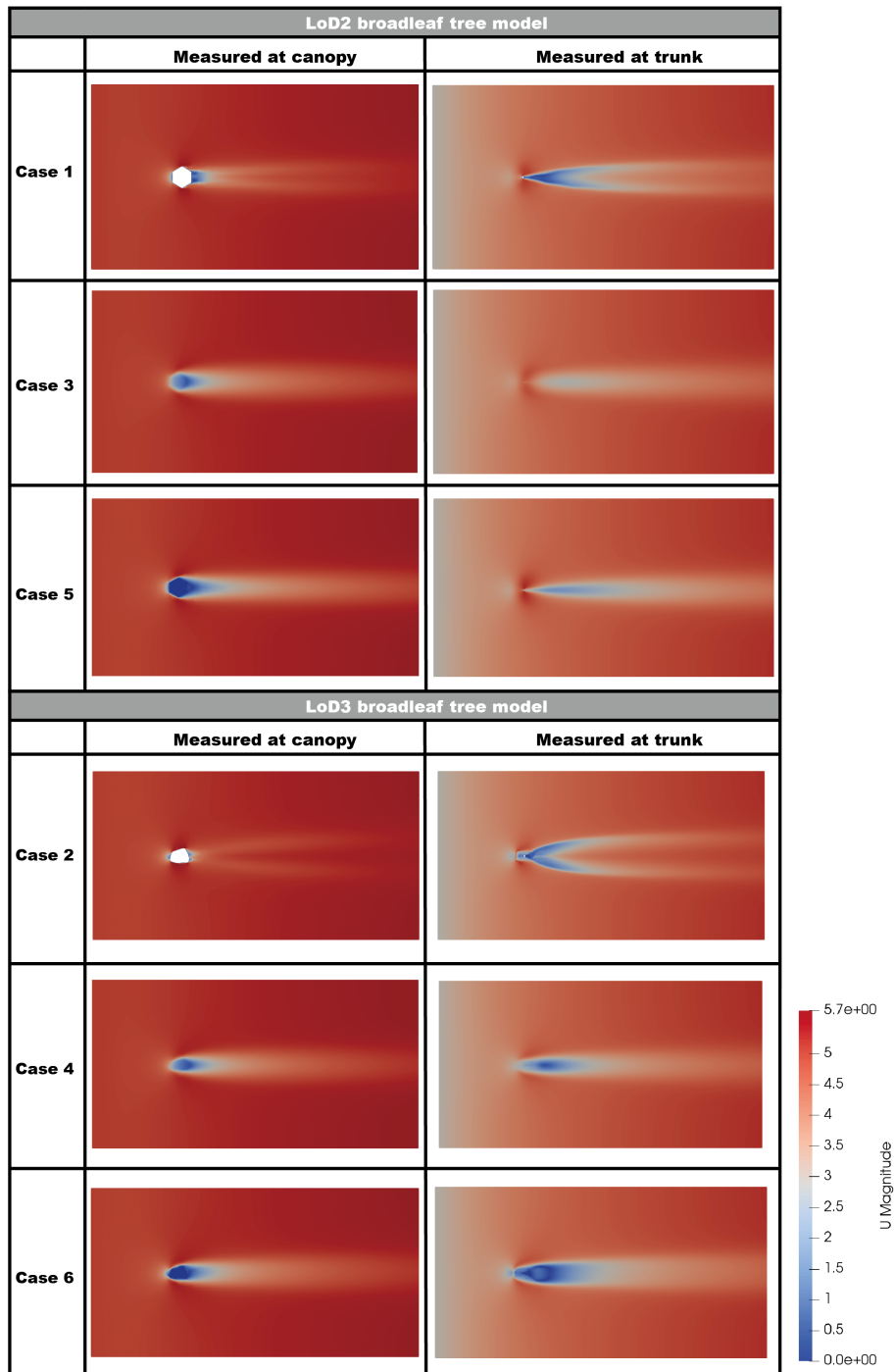


Figure C.1.: Horizontal plane results (velocity magnitude) for case 1-6.
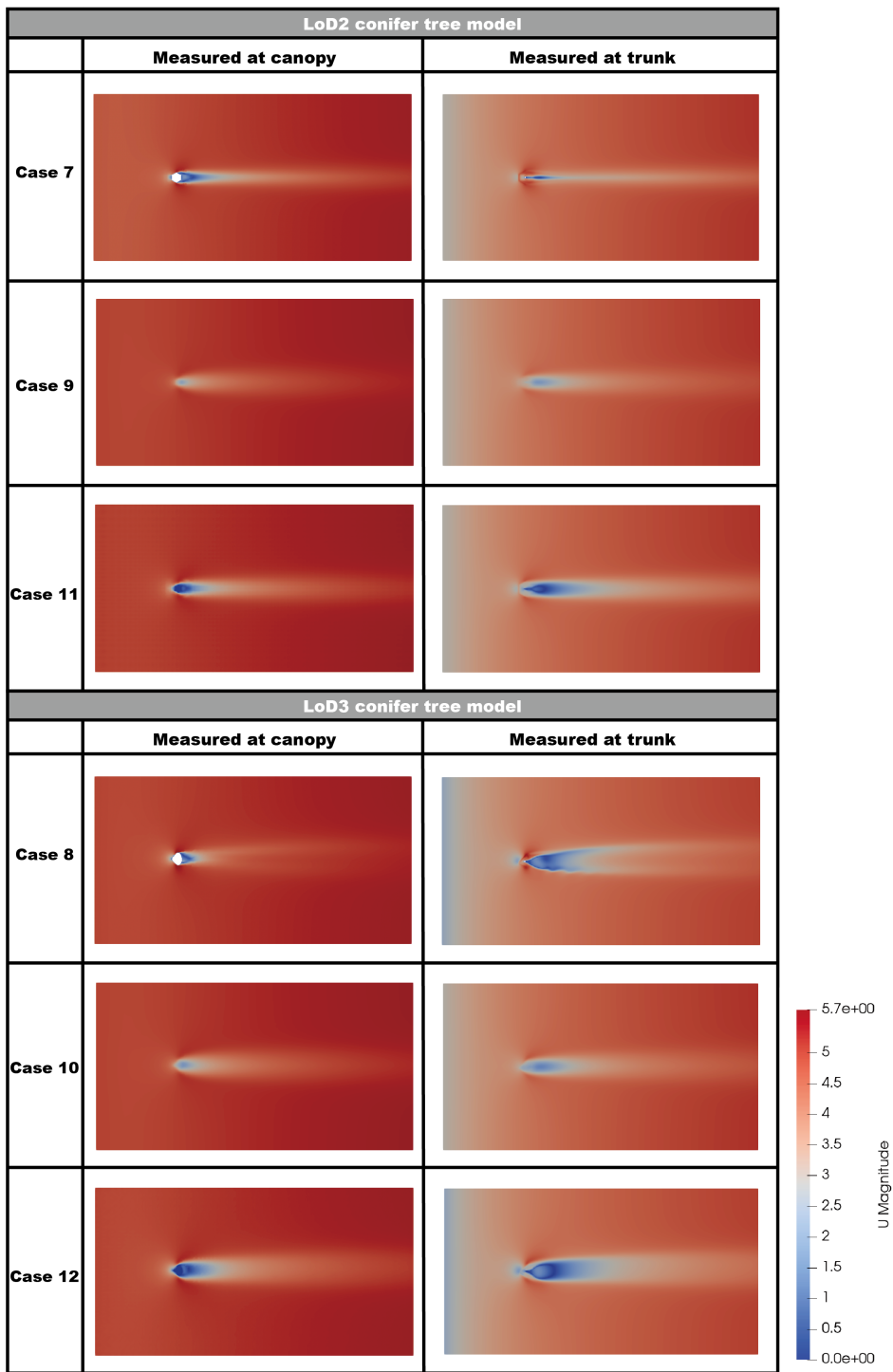
Figure C.2.: Horizontal plane results (velocity magnitude) for case 7-12.

# D. Plots for the idealized street canyon cases



Figure D.1.: $C_{l2-l3}$ plots generated from case 13 and 14

Figure D.2.: $C_{l2-l3}$ plots generated from case 15 and 16

Figure D.3.: $C_{l2-l3}$ plots generated from case 17 and 18

Figure D.4.: $C_{l2-l3}$ plots generated from case 19 and 20

## D. Plots for the idealized street canyon cases
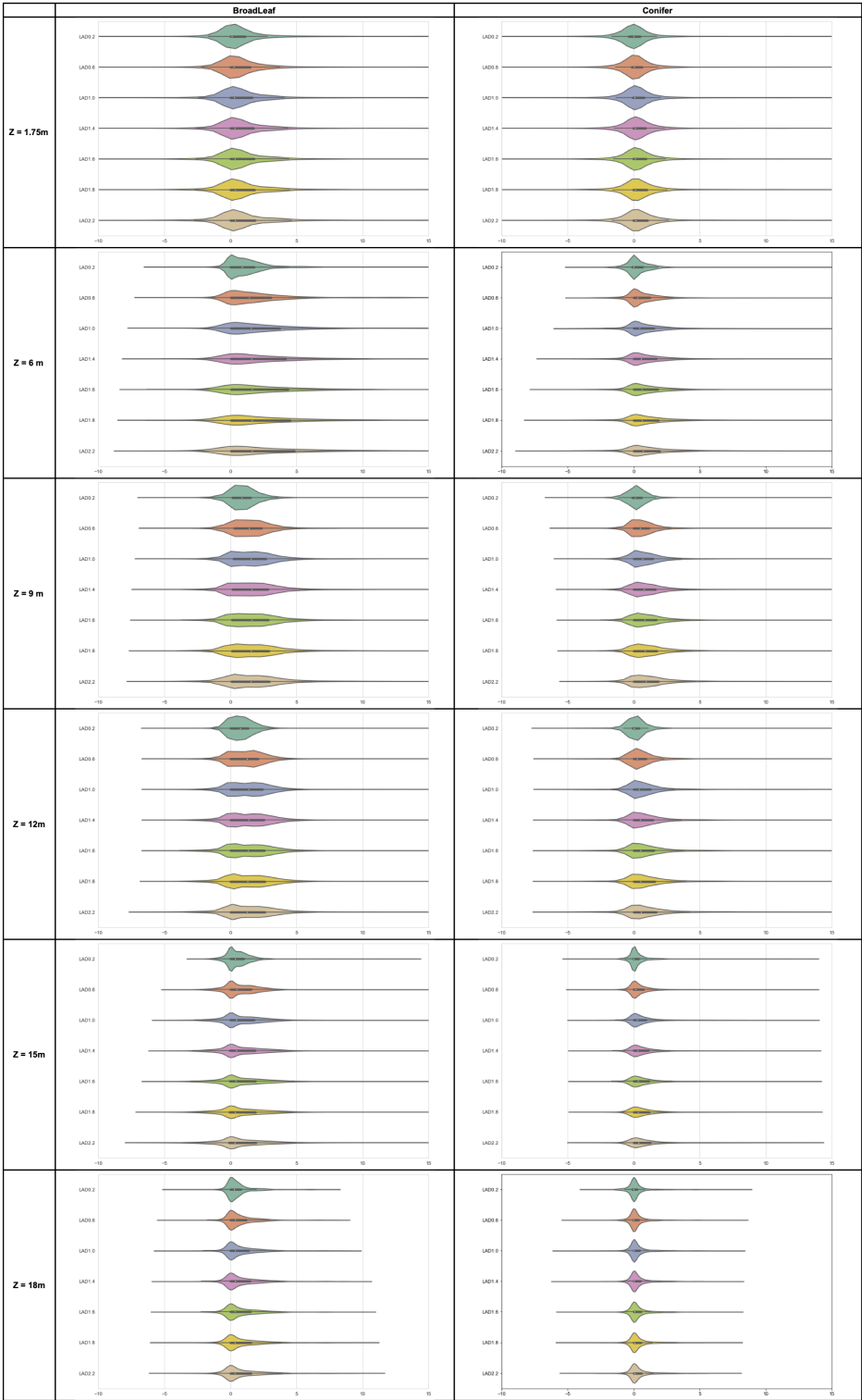


Figure D.5.: Violin plots for $C_{l2-l3}$ within the street canyon at different height (perpendicular inflow direction)

| | BroadLeaf | Conifer |
|---|---|---|



<table>
<tr><td>Z = 1.75m</td><td></td></tr>
</table>
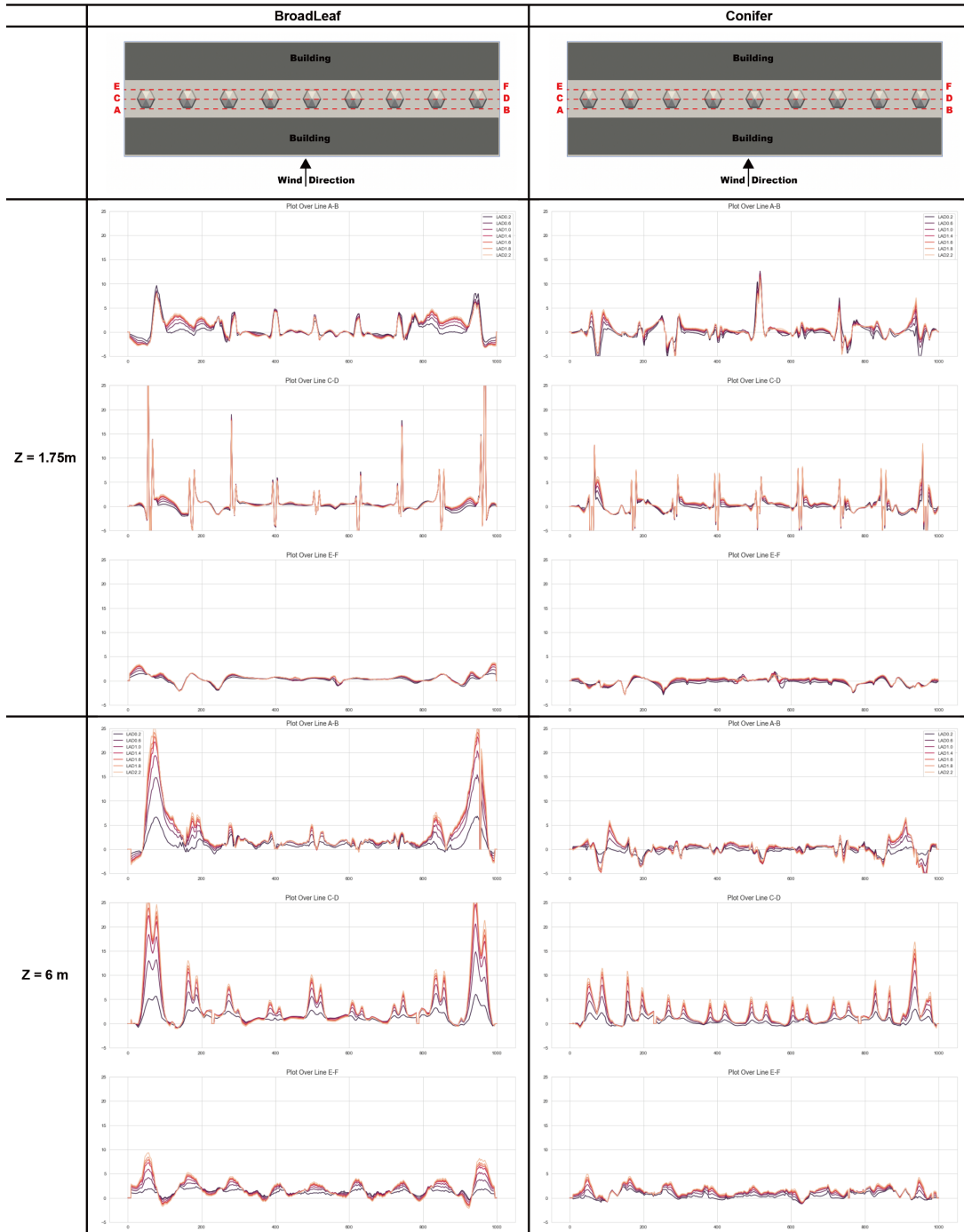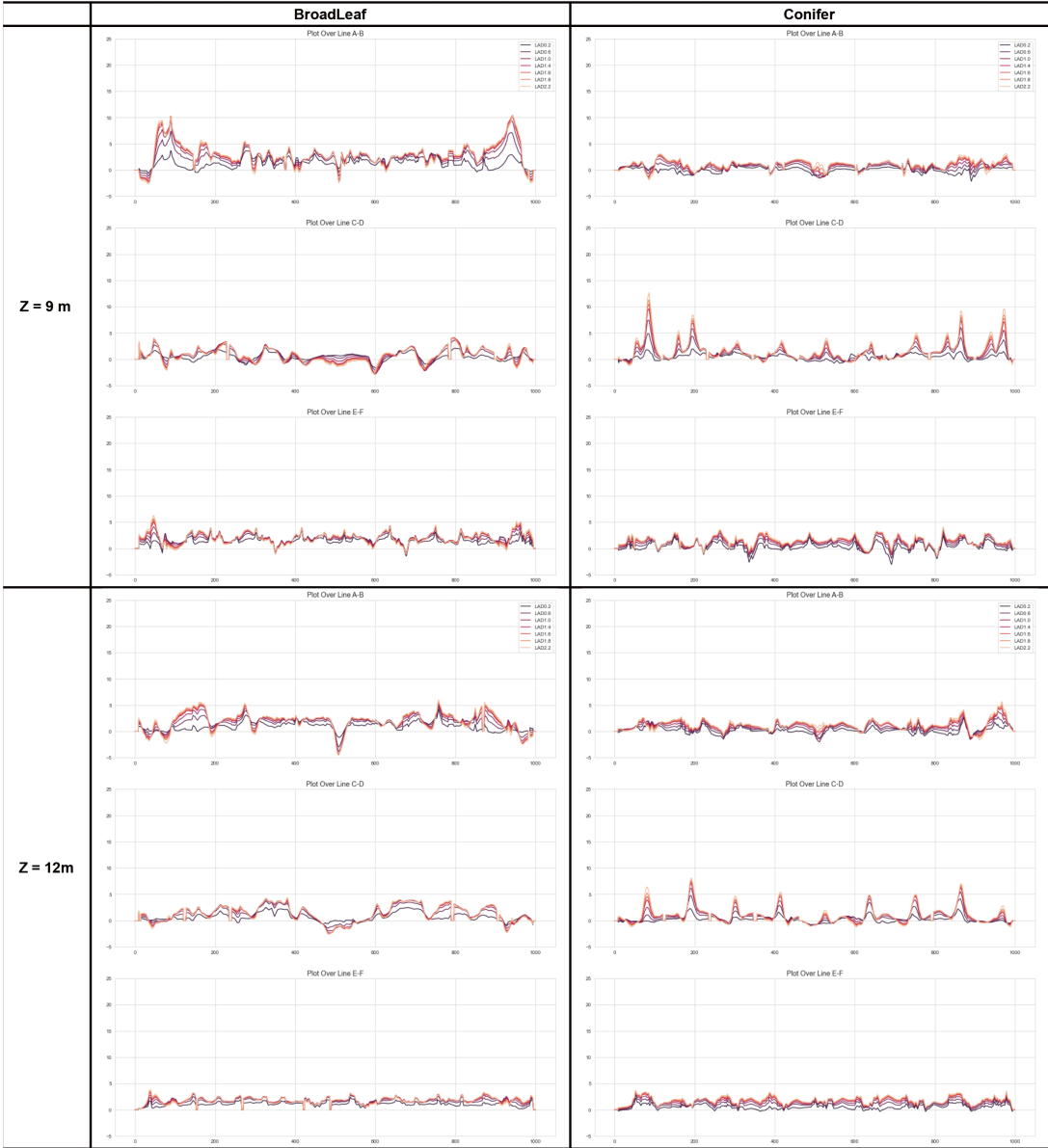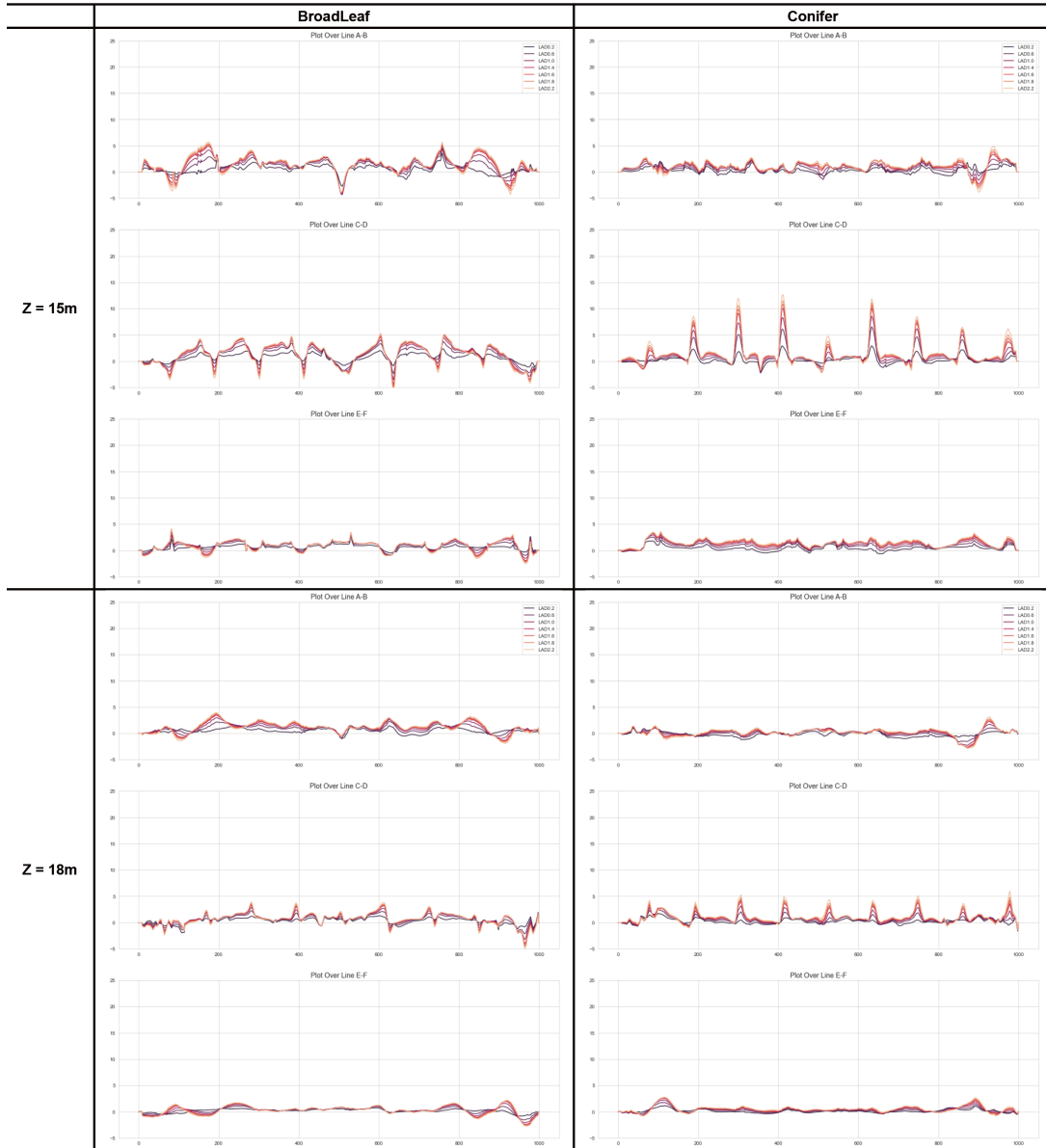
*D. Plots for the idealized street canyon cases*

Figure D.8.: $C_{l2-l3}$ values on three probe lines within the street canyon (perpendicular inflow direction)
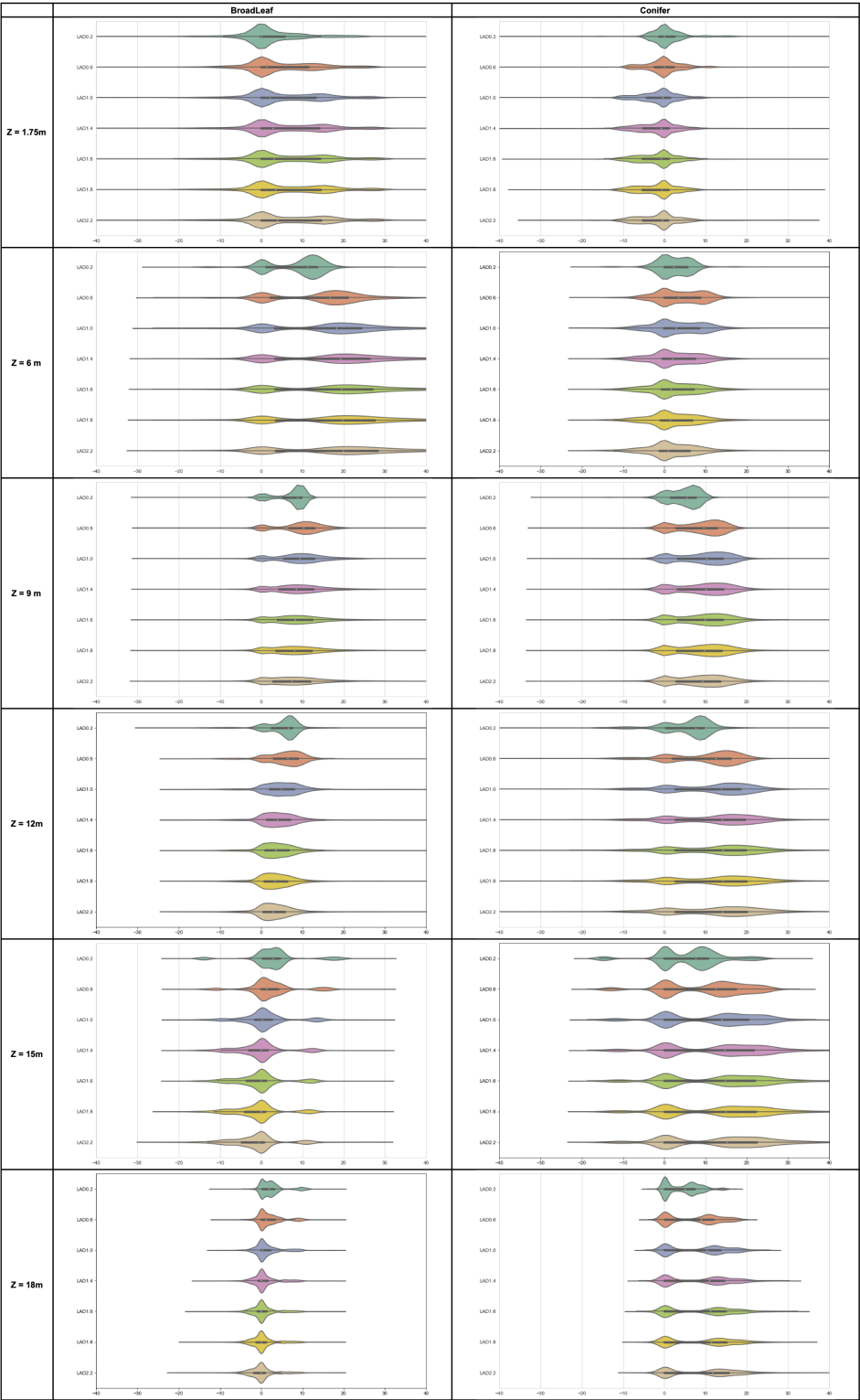
Figure D.9.: Violin plots for $C_{l2-l3}$ within the street canyon at different height (parallel inflow direction)
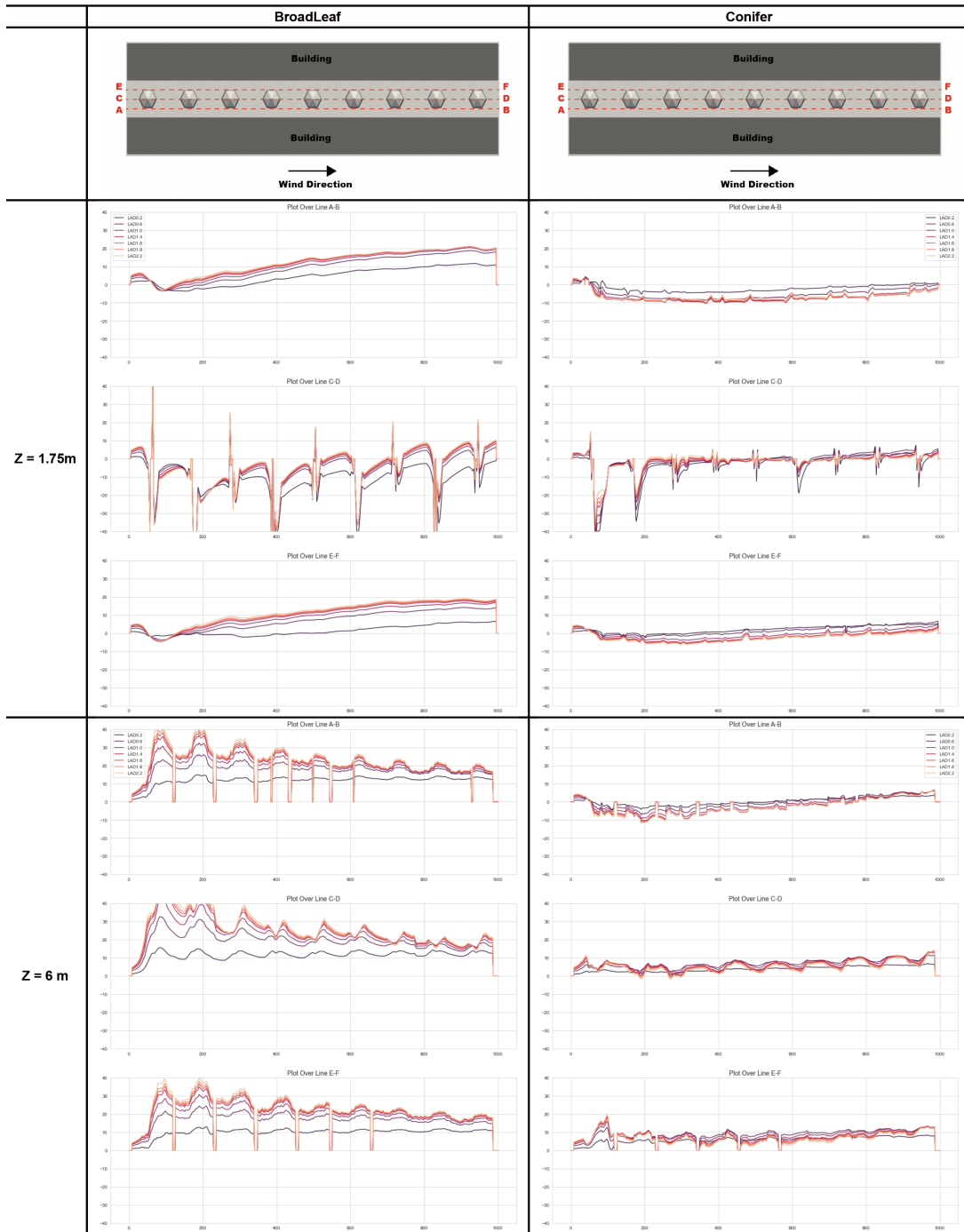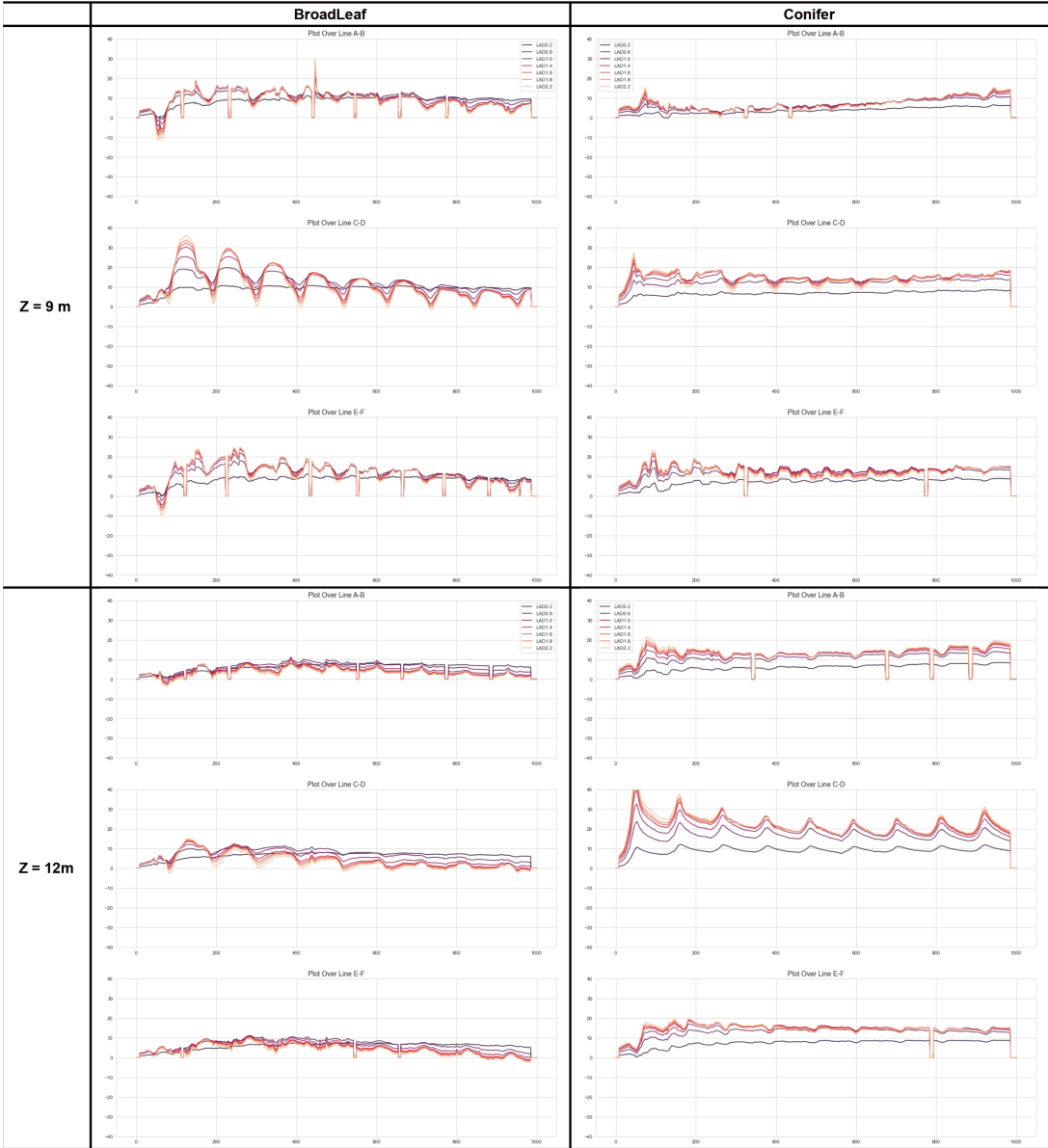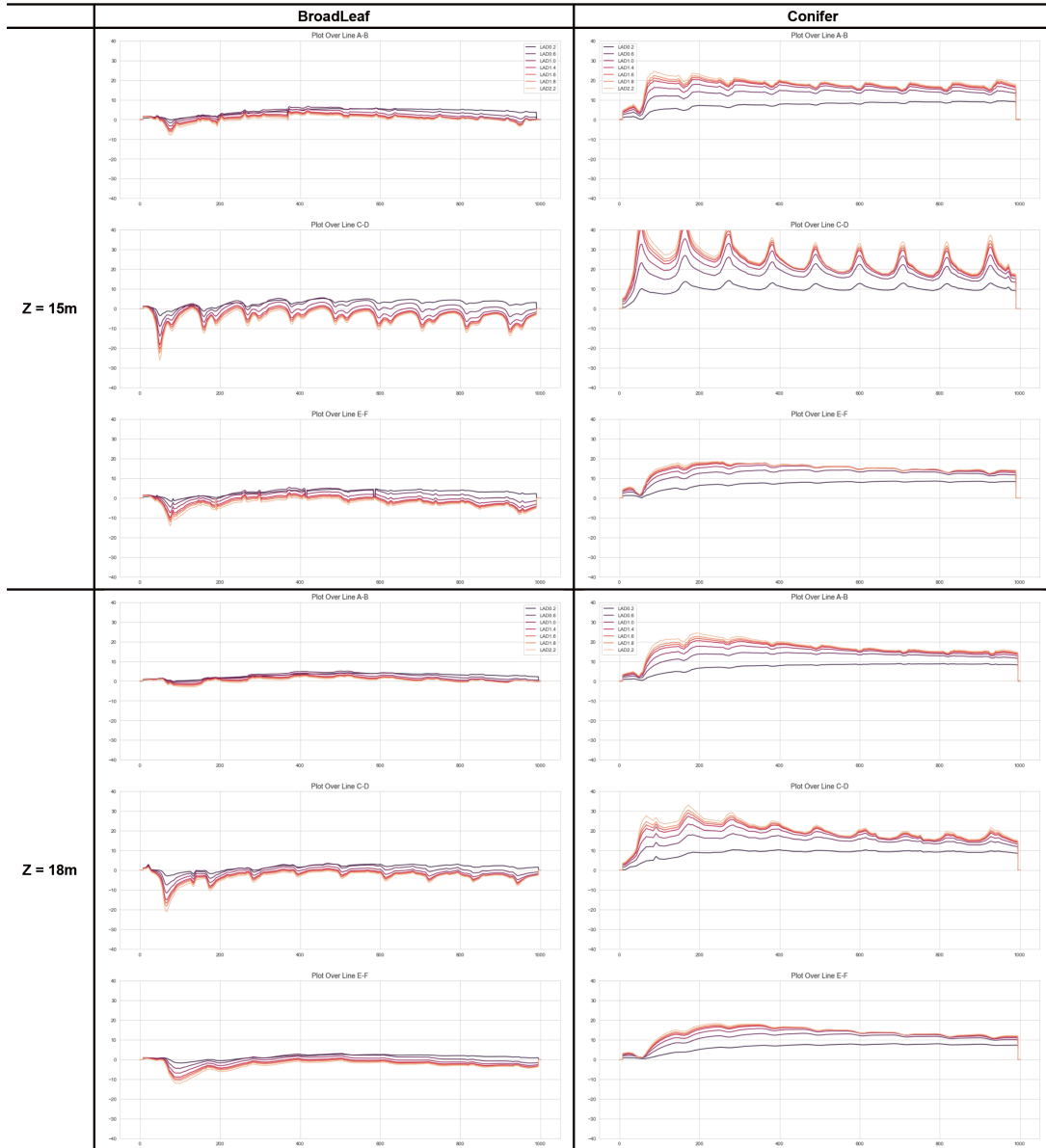
| | BroadLeaf | Conifer |
|---|---|---|



<table>
<tr><td rowspan="3"><strong>Z = 1.75m</strong></td><td>Plot Over Line A-B</td><td>Plot Over Line A-B</td></tr>
<tr><td>Plot Over Line C-D</td><td>Plot Over Line C-D</td></tr>
<tr><td>Plot Over Line E-F</td><td>Plot Over Line E-F</td></tr>
<tr><td rowspan="3"><strong>Z = 6 m</strong></td><td>Plot Over Line A-B</td><td>Plot Over Line A-B</td></tr>
<tr><td>Plot Over Line C-D</td><td>Plot Over Line C-D</td></tr>
<tr><td>Plot Over Line E-F</td><td>Plot Over Line E-F</td></tr>
</table>

87

Figure D.10.: $C_{l2-l3}$ values on three probe lines within the street canyon (parallel inflow direction)

# E. Plots for the realistic urban geometry cases
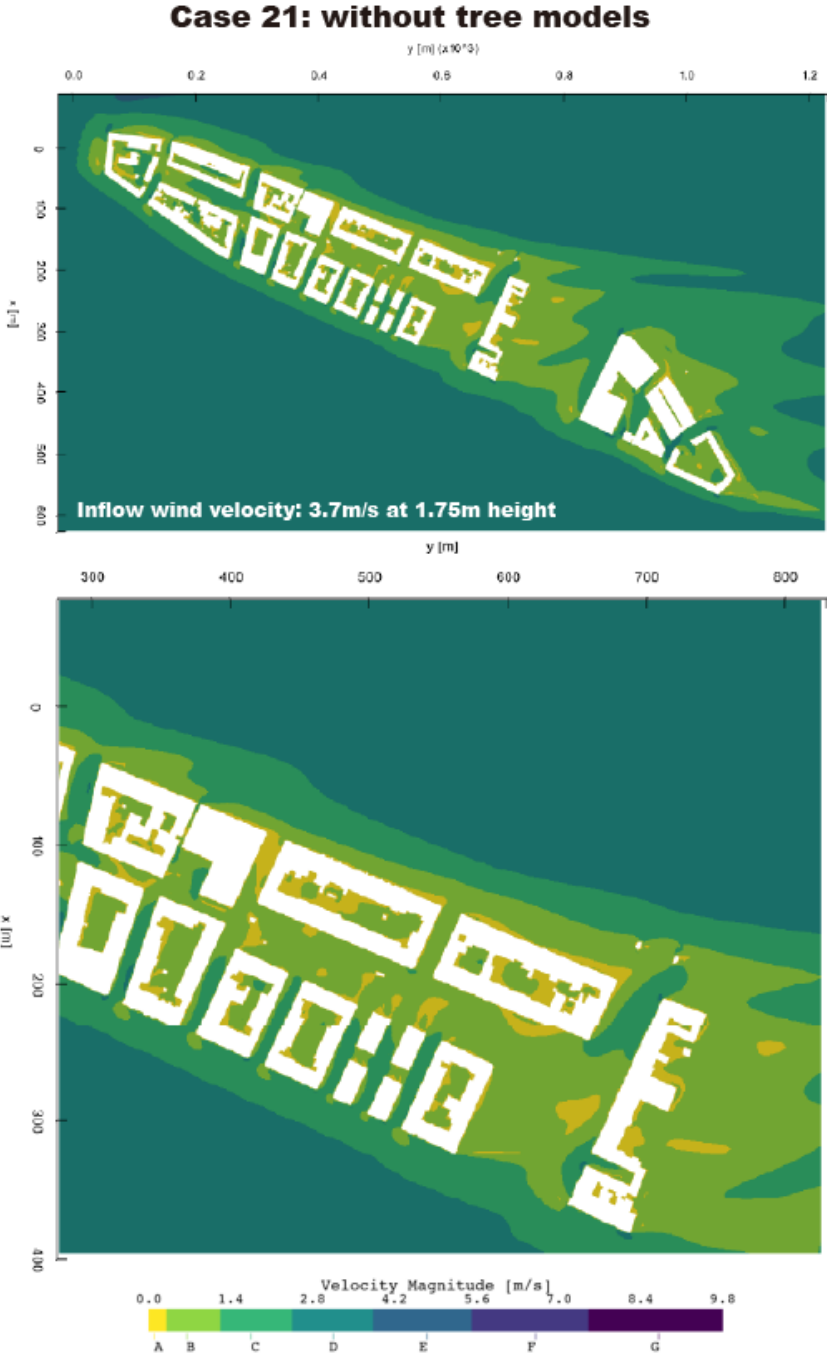


Figure E.1.: Pedestrian wind comfort classification at 1.75 m height for case 21
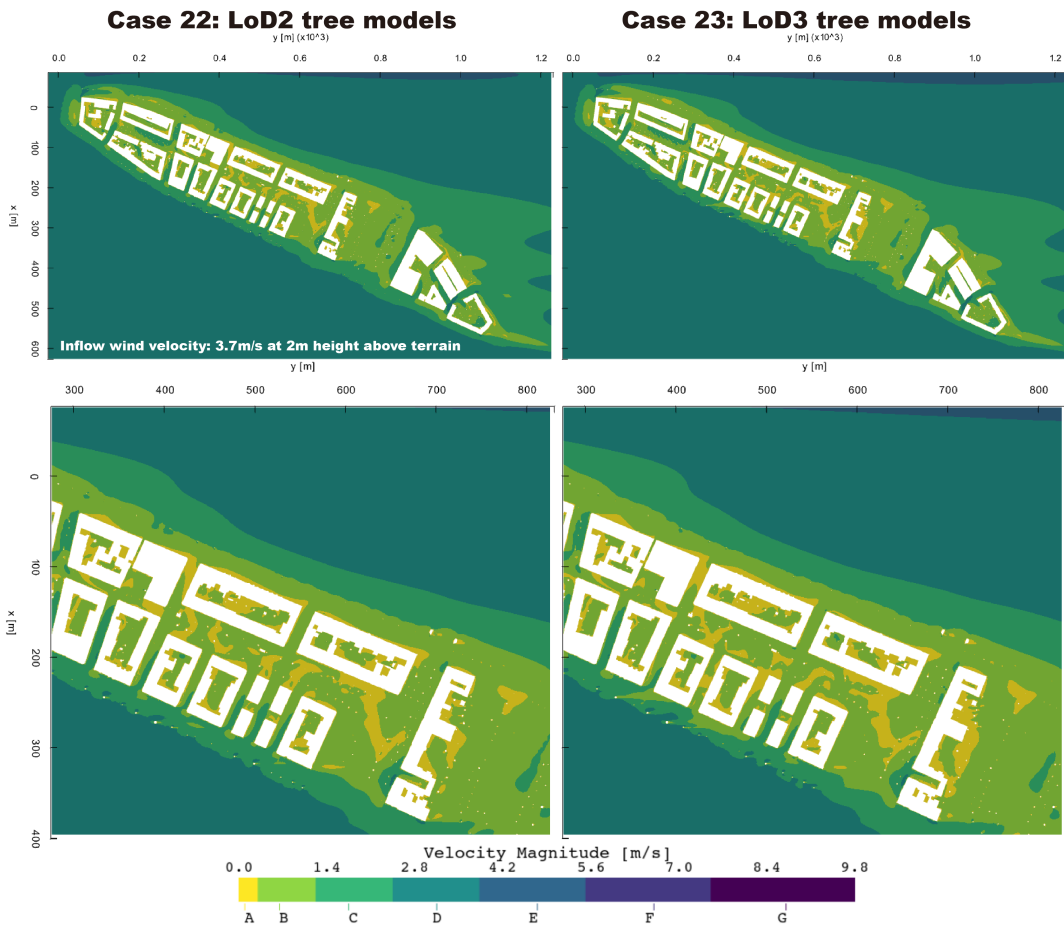
Figure E.2.: Pedestrian wind comfort classification at 1.75 m height for Case 22 and 23
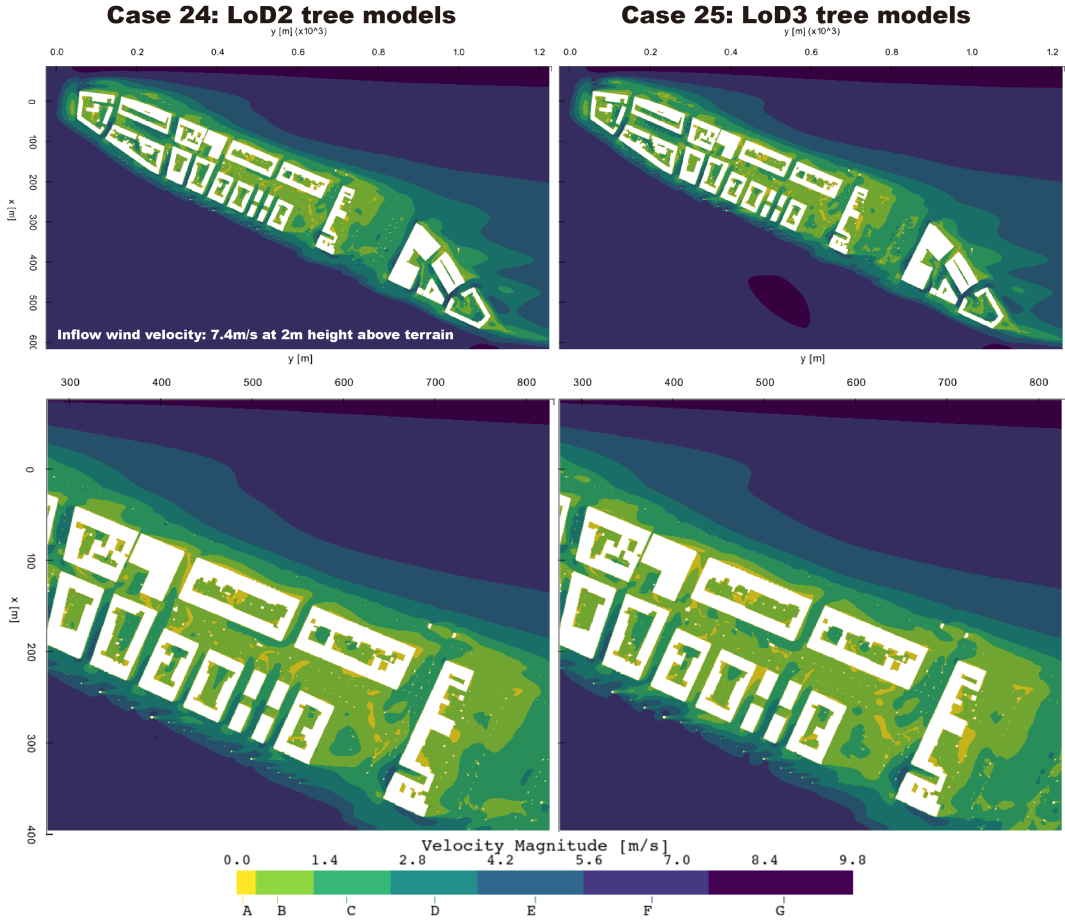
Figure E.3.: Pedestrian wind comfort classification at 1.75 m height for case 24 and 25
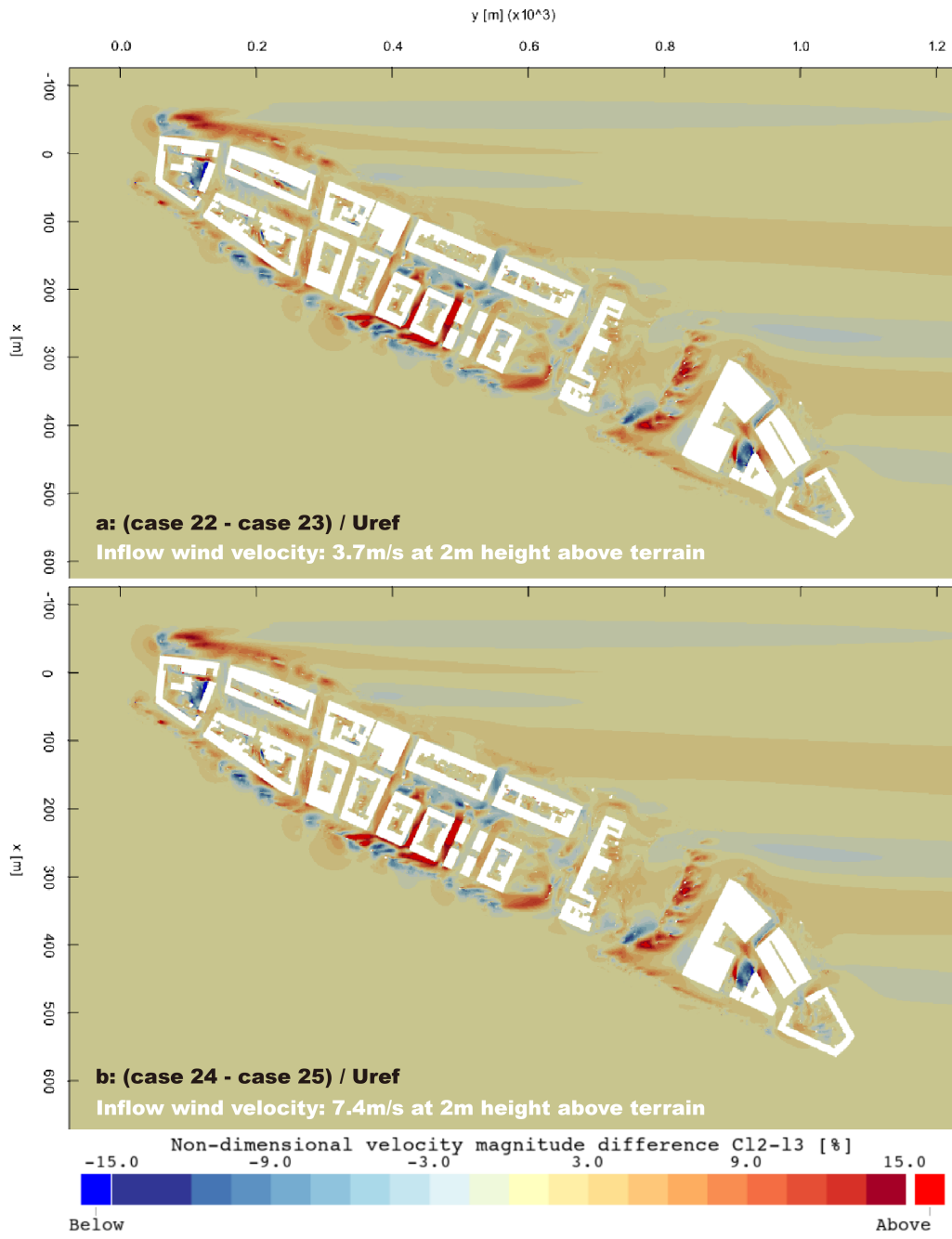
Figure E.4.: $C_{l2-l3}$ plots generated from case 22 and 23 (UP), case 24 and 25 (DOWN).

# Bibliography

Aflaki, A., Mirnezhad, M., Ghaffarianhoseini, A., Ghaffarianhoseini, A., Omrany, H., Wang, Z. H., and Akbari, H. (2017). Urban heat island mitigation strategies: A state-of-the-art review on Kuala Lumpur, Singapore and Hong Kong. *Cities*, 62:131–145.

Balczó, M., Gromke, C., and Ruck, B. (2009). Numerical modeling of flow and pollutant dispersion in street canyons with tree planting. *Meteorologische Zeitschrift*, 18(2):197–206.

Blocken, B. (2015). Computational Fluid Dynamics for urban physics: Importance, scales, possibilities, limitations and ten tips and tricks towards accurate and reliable simulations. *Building and Environment*, 91:219–245.

Blocken, B. and Carmeliet, J. (2004). Pedestrian wind environment around buildings: Literature review and practical examples. *Journal of Thermal Envelope and Building Science*, 28(2):107–159.

Blocken, B., Janssen, W. D., and van Hooff, T. (2012). CFD simulation for pedestrian wind comfort and wind safety in urban areas: General decision framework and case study for the Eindhoven University campus. *Environmental Modelling & Software*, 30:15–34.

Bottema, M. (2000). A method for optimisation of wind discomfort criteria. *Building and Environment*, 35(1):1–18.

Buccolieri, R., Santiago, J. L., Rivas, E., and Sanchez, B. (2018). Review on urban tree modelling in CFD simulations: Aerodynamic, deposition and thermal effects. *Urban Forestry & Urban Greening*, 31:212–220.

de Groot, R. (2020). Automatic construction of 3D tree models in multiple levels of detail from airborne LiDAR data.

Du, S., Lindenbergh, R., Ledoux, H., Stoter, J., and Nan, L. (2019). AdTree: Accurate, Detailed, and Automatic Modelling of Laser-Scanned Trees. *Remote Sensing 2019, Vol. 11, Page 2074*, 11(18):2074.

Dukai, B., van Liempt, J., Peters, R., Stoter, J., Vitalis, S., and Wu, T. (2021). 3D BAG Viewer.

Fouillet, A., Rey, G., Laurent, F., Pavillon, G., Bellec, S., Guihenneuc-Jouyaux, C., Clavel, J., Jougla, E., and Hémon, D. (2006). Excess mortality related to the August 2003 heat wave in France. *International Archives of Occupational and Environmental Health*, 80(1):16–24.

Franke, J., Hellsten, A., Schlunzen, K. H., and Carissimo, B. (2011). The COST 732 Best Practice Guideline for CFD simulation of flows in the urban environment: a summary. *International Journal of Environment and Pollution*, 44(1-4):419–427.

García-Sánchez, C., Vitalis, S., Paden, I., and Stoter, J. (2021). The impact of level of detail in 3d city models for cfd-based wind flow simulations. *International Archives of the Photogrammetry, Remote Sensing and Spatial Information Sciences - ISPRS Archives*, 46(4/W4-2021):67–72.

*Bibliography*

Gromke, C., Blocken, B., Janssen, W., Merema, B., van Hooff, T., and Timmermans, H. (2015). CFD analysis of transpirational cooling by vegetation: Case study for specific meteorological conditions during a heat wave in Arnhem, Netherlands. *Building and Environment*, 83:11–26.

Gromke, C., Ruck, B., Gromke, C., and Ruck, B. (2012). Pollutant Concentrations in Street Canyons of Different Aspect Ratio with Avenues of Trees for Various Wind Directions. *Boundary-Layer Meteorology 2012 144:1*, 144(1):41–64.

Hefny Salim, M., Heinke Schlünzen, K., and Grawe, D. (2015). Including trees in the numerical simulations of the wind flow in urban areas: Should we care? *Journal of Wind Engineering and Industrial Aerodynamics*, 144:84–95.

Hong, B. and Lin, B. (2015). Numerical studies of the outdoor wind environment and thermal comfort at pedestrian level in housing blocks with different building layout patterns and trees arrangement. *Renewable Energy*, 73:18–27.

Hong, B., Qin, H., and Lin, B. (2018a). Prediction of Wind Environment and Indoor/Outdoor Relationships for PM2.5 in Different Building–Tree Grouping Patterns. *Atmosphere 2018, Vol. 9, Page 39*, 9(2):39.

Hong, S. W., Zhao, L., and Zhu, H. (2018b). CFD simulation of airflow inside tree canopies discharged from air-assisted sprayers. *Computers and Electronics in Agriculture*, 149:121–132.

Hsieh, C. M. and Huang, H. C. (2016). Mitigating urban heat islands: A method to identify potential wind corridor for cooling and ventilation. *Computers, Environment and Urban Systems*, 57:130–143.

Janssen, W. D., Blocken, B., and van Hooff, T. (2013). Pedestrian wind comfort around buildings: Comparison of wind comfort criteria based on whole-flow field data for a complex case study. *Building and Environment*, 59:547–562.

Kamoske, A. G., Dahlin, K. M., Stark, S. C., and Serbin, S. P. (2019). Leaf area density from airborne LiDAR: Comparing sensors and resolutions in a temperate broadleaf forest ecosystem. *Forest Ecology and Management*, 433:364–375.

Kang, G., Kim, J. J., and Choi, W. (2020). Computational fluid dynamics simulation of tree effects on pedestrian wind comfort in an urban area. *Sustainable Cities and Society*, 56:102086.

Lalic, B. and Mihailovic, D. (2004). An Empirical Relation Describing Leaf-Area Density inside the Forest for Environmental Modeling. *Journal of Applied Meteorology - J APPL METEOROL*, 43:641–645.

Lawson, T. V. (1978). The wind content of the built environment. *Journal of Wind Engineering and Industrial Aerodynamics*, 3(2-3):93–105.

Lawson, T. V. and Penwarden, A. D. (1975). The Effects of Wind on People in the Vicinity of Buildings. In *Proceedings of Fourth International Conference on Wind Effects on Buildings and Structures*, pages 605–622. Cambridge University Press, Heathrow, UK.

Liang, L., Xiaofeng, L., Borong, L., and Yingxin, Z. (2006). Improved k–$\epsilon$ two-equation turbulence model for canopy flow. *Atmospheric Environment*, 40(4):762–770.

Liang, X., Kankare, V., Hyyppä, J., Wang, Y., Kukko, A., Haggrén, H., Yu, X., Kaartinen, H., Jaakkola, A., Guan, F., Holopainen, M., and Vastaranta, M. (2016). Terrestrial laser scanning in forest inventories. *ISPRS Journal of Photogrammetry and Remote Sensing*, 115:63–77.

Livny, Y., Pirk, S., Cheng, Z., Yan, F., Deussen, O., Cohen-Or, D., and Chen, B. (2011). Texture-lobes for tree modelling. *ACM Transactions on Graphics*, 30(4):53.

Maldonado, J. M. (2012). MODELLING WIND FLOW THROUGH CANOPIES SYSTEMS USING OPENFOAM.

Manickathan, L., Defraeye, T., Allegrini, J., Derome, D., and Carmeliet, J. (2018). Parametric study of the influence of environmental factors and tree properties on the transpirative cooling effect of trees. *Agricultural and Forest Meteorology*, 248:259–274.

Mohamed, M. A. and Wood, D. H. (2015). Computational study of the effect of trees on wind flow over a building. *Renewables: Wind, Water, and Solar 2015 2:1*, 2(1):1–8.

Moradpour, M., Afshin, H., and Farhanieh, B. (2017). A numerical investigation of reactive air pollutant dispersion in urban street canyons with tree planting. *Atmospheric Pollution Research*, 8(2):253–266.

Moukalled, F., Mangani, L., and Darwish, M. (2016). Mathematical Description of Physical Phenomena. In *The Finite Volume Method in Computational Fluid Dynamics. Fluid Mechanics and Its Applications*, volume 113, pages 43–83. Springer, Cham.

of London Corporation, C. (2019). City of London Wind Microclimate Guidelines.

Ortega-Córdova, L. (2018). Urban Vegetation Modeling 3D Levels of Detail.

Oshio, H., Asawa, T., Hoyano, A., and Miyasaka, S. (2015). Estimation of the leaf area density distribution of individual trees using high-resolution and multi-return airborne LiDAR data. *Remote Sensing of Environment*, 166:116–125.

Parker, G. G. (2020). Tamm review: Leaf Area Index (LAI) is both a determinant and a consequence of important processes in vegetation canopies. *Forest Ecology and Management*, 477.

Pourteimouri, P., Campmans, G., Wijnberg, K., and Hulscher, S. (2020). The impact of buildings' characteristics on airflow patterns and bed morphology at beaches, using CFD modelling. In Patrick, L., editor, *Proceedings of virtual Conference on Coastal Engineering*, volume 36, page 4. American Society of Civil Engineers.

Salmond, J. A., Tadaki, M., Vardoulakis, S., Arbuthnott, K., Coutts, A., Demuzere, M., Dirks, K. N., Heaviside, C., Lim, S., MacIntyre, H., McInnes, R. N., and Wheeler, B. W. (2016). Health and climate related ecosystem services provided by street trees in the urban environment. *Environmental Health: A Global Access Science Source*, 15.

Santiago, J. L., Buccolieri, R., Rivas, E., Calvete-Sogo, H., Sanchez, B., Martilli, A., Alonso, R., Elustondo, D., Santamaría, J. M., and Martin, F. (2019). CFD modelling of vegetation barrier effects on the reduction of traffic-related pollutant concentration in an avenue of Pamplona, Spain. *Sustainable Cities and Society*, 48:101559.

Segersson, D. (2017). A tutorial to urban wind flow using OpenFOAM. In Nilsson, H., editor, *Proceedings of CFD with OpenSource Software*.

Shaw, R. H. and Schumann, U. (1992). Large-eddy simulation of turbulent flow above and within a forest. *Boundary-Layer Meteorology*, 61(1-2):47–64.

*Bibliography*

Szkordilisz, F. and Zöld, A. (2016). Effect of Vegetation on Wind-Comfort. *Applied Mechanics and Materials*, 824:811–818.

Tominaga, Y., Mochida, A., Yoshie, R., Kataoka, H., Nozu, T., Yoshikawa, M., and Shirasawa, T. (2008). AIJ guidelines for practical applications of CFD to pedestrian wind environment around buildings. *Journal of Wind Engineering and Industrial Aerodynamics*, 96(10-11):1749–1761.

Von Der Grün, M., Zamre, P., Chen, Y., Lutz, T., Voß, U., and Kramer, E. (2020). Numerical study and LiDAR based validation of the wind field in urban sites. *Journal of Physics: Conference Series*, 1618(4).

Vos, P. E., Maiheu, B., Vankerkom, J., and Janssen, S. (2013). Improving local air quality in cities: To tree or not to tree? *Environmental Pollution*, 183:113–122.

Vranckx, S., Vos, P., Maiheu, B., and Janssen, S. (2015). Impact of trees on pollutant dispersion in street canyons: A numerical study of the annual average effects in Antwerp, Belgium. *Science of The Total Environment*, 532:474–483.

Wang, L., Su, J., Gu, Z., and Tang, L. (2021). Numerical study on flow field and pollutant dispersion in an ideal street canyon within a real tree model at different wind velocities. *Computers and Mathematics with Applications*, 81:679–692.

## Colophon

This document was typeset using LaTeX, using the KOMA-Script class scrbook. The main font is Palatino.